UNIVERSITA' DEGLI STUDI DI PADOVA

**Dipartimento di Ingegneria Industriale DII**

Master of Science in Mechanical Engineering

# Functional evaluation of an instrumented biofidelic neck surrogate for the assessment of neck protectors

Supervisor: Prof. Nicola Petrone

Co-supervisor: Eng. Giuseppe Zullo

Student: Federico Guidolin

Mat: 1241859

Academic Year 2021/2022

# ABSTRACT

Neck injuries resulting from motorcycle accidents is a recurrent problem.
To prevent the injury risks, companies have started to develop specific personal protective equipment for the protection of the cervical spine.
Neck braces are part of PPE for neck protection developed to reduce the chance of neck injury by reducing range of motion and load on the neck.
However, the efficiency of these devices is still under discussion since a standardized test method for their assessment still doesn't exist.
This thesis work focuses on the prototyping and validation of an instrumented biofidelic neck surrogate for the assessment of neck protectors.
The components of the new biofidelic neck surrogate were obtained by additive Selective Laser Sintering (SLS) technology and the neck vertebras were manufactured by casting a silicon rubber on the neck components in a proper mould.
The overall stiffness of the neck can be modulated by means of stiffening components.
Static and dynamic tests were carried out for the evaluation of the mechanical properties of the neck and comparison with previous prototypes and cadaveric data were made when possible.
A second goal of this work was the instrumentation of the new neck surrogate to measure bending movements and loads acting on the neck.
A six-axis load cell was placed on the top of the neck to measure loads at the Occipital condyles level. An instrumented base was developed to measure bending movements of the neck in frontal and sagittal plane by mean of rotary potentiometers, moreover, this base allows to fix the new neck surrogate on the Hybrid III torso.
Finally, pilot tests were conducted to evaluate the neck braces effectiveness.
A pendulum was used to induce a rotational motion of the Hybrid III dummy neck.
Tests were conducted with two different neck surrogates, the stiff Hybrid III neck and the instrumented biofidelic neck surrogate developed in this thesis. Peak neck angles reached as a result of the impacts were considered to compare tests with and without neck brace and with the two different neck surrogates.
Results highlight that the Hybrid III neck requires very high energies to reach a range of motion that engages the neck brace while the biofidelic neck requires much lower energies.
However, the biofidelic neck has proved to be still too brittle to perform significant impact tests.
Further development will improve the current neck prototype and other test method for the assessment of neck protectors will be proposed.

# ACKNOWLEDGEMENTS

Volevo dedicare questo spazio del mio elaborato alle persone che hanno contribuito, con il loro supporto, alla realizzazione dello stesso.
Un ringraziamento speciale al professor Petrone, per la sua disponibilità, per i suoi indispensabili consigli, per le conoscenze trasmesse durante tutto il percorso.
Un grazie di cuore al mio tutor Giuseppe Zullo, compagno di successi e delusioni, che mi ha guidato in questo percorso. È grazie a lui che ho superato i momenti più difficili. Senza la sua esperienza e i suoi consigli, non ce l'avrei mai fatta.
Un ringraziamento a tutti i ragazzi del laboratorio con cui ho condiviso questi 6 mesi di lavoro, in particolare Nicola, Gregorio e Pierluigi con i quali era un piacere parlare e confrontarsi, mi avete sempre sostenuto e siete sempre stati pronti ad aiutarmi.
Ringrazio infinitamente i miei genitori che mi hanno sempre sostenuto, appoggiando ogni mia decisione.
Infine, ringrazio i miei amici, fondamentali nei momenti in cui avevo bisogno di staccare la spina, vi ringrazio per la pazienza e il supporto che mi avete dato.

# CONTENTS

# LIST OF TABLES

# LIST OF FIGURES

# CHAPTER 1

## 1 INTRODUCTION

Cervical spine injury resulting from high impact loading is a critical issue. The cervical spine is the main location of serious injuries due to Motor Vehicle Crashes (MVCs). A statistical study showed that around 40 to 65% of all spine related injuries are associated with MVCs, where cervical spine is being the most frequently affected injury site [1].

Motorcycles, particularly so, are by their nature far less crashworthy than closed vehicles.

In 2019, 5014 motorcyclists died in motorcycle crashes, according to the National Highway Traffic Safety Administration (NHTSA). In the same year, motorcyclists were nearly 29 times more likely than passenger car occupants to die in a crash per vehicle miles traveled.

A study on motorcycle road crash has indicated that the neck injury is one of the major single causes of death in Malaysian motorcyclists [2].

Flexion and extension movements due to frontal and rear crash impact are the most frequent neck injury mechanisms while side impact and skidding motorcyclists were found to have a high frequency of uncinate process fractures [3].

There are several experimental and numerical studies about motorcycle rider's safety( [4], [5], [6], [7] and [8]) and most of them have studied the helmet and its effect in reducing the risk of brain injury. Some studies about the neck injuries in motorcycle accidents have been done, as well. Dowdell et al. [9] studied 200 cases of helmeted rider crashes and stated that almost 20 percent of cases had neck injuries due to impacts on the helmet. Ramil et al. [10] studied 177 cases with fatal injuries due to motorcycle involved accidents and reported that the majority of neck injuries were related to cervical fractures with the most severe form involving transection of the spinal cord. Ouellet et al. [11] studied crashes of helmeted and unhelmeted riders and reported that helmeted riders have more sublaxation/dislocation injuries in lower cervical region (C3-C7) and more frequent hemorrhage in the carotid sheath.

To improve the safety of motorcyclists, several personal protective equipment (PPE) have been developed such as helmets, neck protectors, protecting clothing, impact protectors, gloves, boots, etc.

Considering the neck protectors, even if we can easily find on the markets various models of these PPE, currently a standardized test method for their assessment still does not exist.

Neck braces are designed to restrict the head motion relative to the rider's torso to prevent excessive motion and therefore prevent traumatic injuries of the cervical spine by transferring the forces occurring at the head and spine to adjacent body structures.

Figure 1.1: Example of neck brace and its operating principle

In order to define a common regulation of those protective devices, the development of specific test methods is needed.
Currently, physical models and Finite Element Models are the two direction that scientists are pursuing.
The growth of the computational power of computers allows to develop increasingly complex FEM making helmet and neck brace interaction models a useful tool for the assessment of neck protectors [12].
Despite the vast potentiality of the simulations, a lack of experimental data on injury mechanics limits the potential of the standard development research.
For that reason, in parallel with the Finite Element models the scientists are focusing their research also to the development of physical replicas in order to evaluate the human behavior in domains, where the data are unavailable and limited to extract.
Currently, the regulation standards in several fields like automotive or sports helmets, are using Anthropometric Test Devices (ATDs) which can be used to evaluate the human kinematics and injury potential in a variety of accident modes.
The Hybrid III is one of most widespread surrogate used as crash test dummy. This surrogate, originally developed to assure reproducibility and repeatability of the measurements as well as high robustness, presents strong lacks in terms of biofidelity, in particular the Hybrid III neck is too stiff to simulate a real interaction between the helmet and the neck brace after a head impact.
Therefore, for the assessment of the neck protectors, a more biofidelic neck surrogate is needed.
The University of Padua (Padua, Italy), and the Mid Sweden University (Östersund, Sweden), have collaborated in the recent past to the development of head and neck prototypes with high biofidelic properties.
This thesis work focused on the manufacture and study of the last neck surrogate developed but also on its instrumentation with the implementation of embedded sensors.
The aim is to have a neck surrogate with biofidelic characteristic to carry out experimental tests for the assessment of the neck protectors.

# CHAPTER 2

# 2 BACKGROUND AND AIMS OF THE WORK

In this chapter an overview on human neck is presented starting from a brief anatomy notion followed by an introduction on the principal neck injury mechanisms and corresponding neck injury criteria.
Finally, a short description of the current state of art on neck surrogates is proposed.

## 2.1 ANATOMY

### 2.1.1 The Spine

The Vertebral Column consists of 33 vertebrae with intervertebral discs among most of them.
It performs different functions:

- Support the head and the trunk but also provides attachments for the limbs, for the chest and for the muscles.
- Allows mobility.
- Protects the spinal cord and the transmission of nervous signals.
- Absorbs the loads.

The vertebras are divided into five groups:

- 7 cervical vertebrae
- 12 thoracic vertebrae
- 5 sacral vertebrae
- 4 coccygeal vertebrae

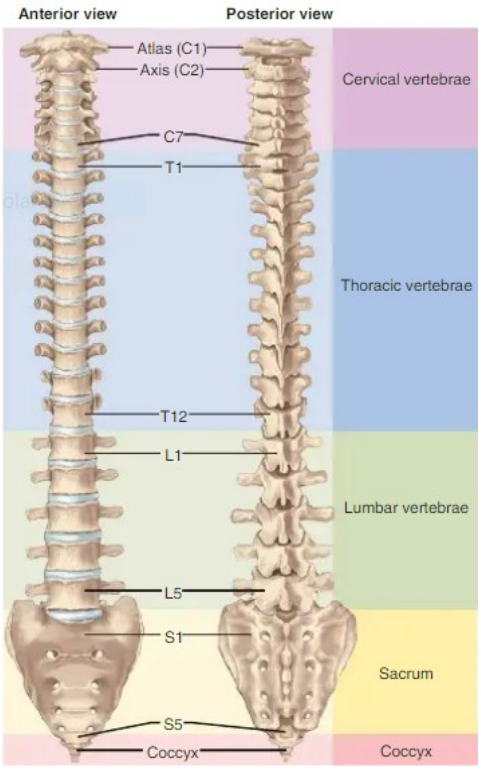

Figure 2.1: The Spine

### 2.1.2 General structure of a Vertebra

The main feature of a vertebra is the body, a mass of spongy bone and red bone marrow covered with a thin layer of compact bone.

Posteriorly to the body there is a canal called vertebral foramen. Collectively the foramina form the vertebral canal in which the spinal cord pass.

The vertebra presents different processes, the spinous and transvers processes provide points of attachment for spinal muscles and ligaments, while the superior articular processes of a vertebra meet the inferior articular processes of a vertebra just above by means of the articular facets restricting twisting of the vertebral column.

Figure 2.2 shows an example of lumbar vertebra, while figure 2.3 shows an example of cervical vertebra.

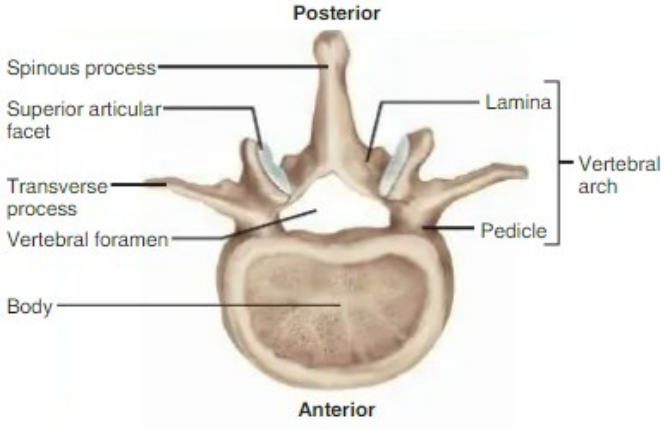


Figure 2.2: Lumbar Vertebra

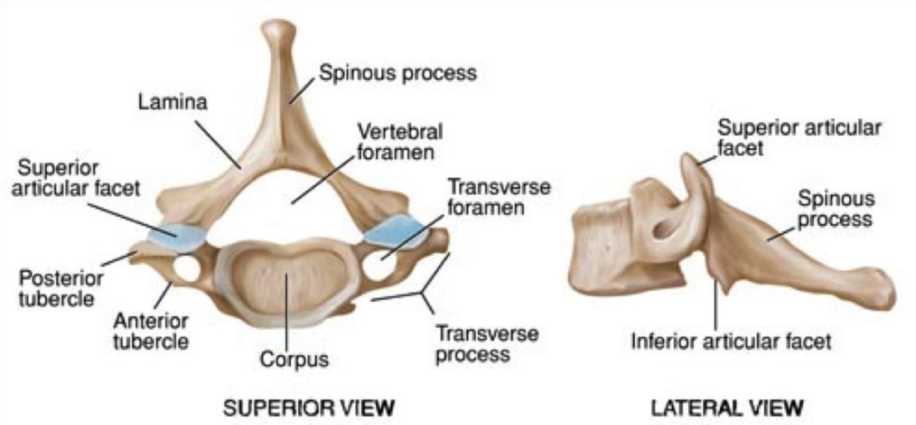


Figure 2.3: Cervical Vertebra (C7)

### 2.1.3 Intervertebral disc

An intervertebral disc (figure 2.4) consists of an external portion with a lamellar structure, the Annulus Fibrosus, and an internal portion, the Nucleus Pulposus, a gel-like structure made of 66% to 86% water that sits at the center of the intervertebral disc and accounts for much of the strength and flexibility of the spine.

The intervertebral discs bind together adjacent vertebrae, enhance spinal flexibility, support the weight of the body and absorb shock.

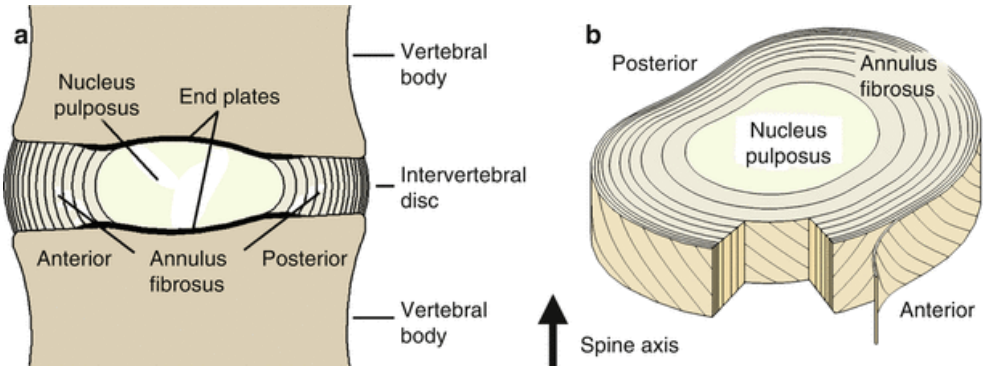


Figure 2.4: Intervertebral disc

### 2.1.4 Fundamental Spinal Unit FSU

A fundamental spinal unit is the smallest physiological motion unit of the spine to exhibit biomechanical characteristic similar to those of the entire spine [13].
A FSU consists of two adjacent vertebrae, the intervertebral disc and all adjoining ligaments between them and excludes other connecting tissues such as muscles.
In vitro studies of isolated or multiple FSUs are often used to measure biomechanical properties of the spine [14].
The typical load-displacement behavior of a cadaveric FSU specimen is nonlinear. Within the total range of passive motion of any FSU, the typical load-displacement curve consists of 2 zones. Near the resting neutral position of the FSU, load-displacement behavior is highly flexible, this zone is called *neutral zone*. The remaining region of FSU motion that continues from the end of the neutral zone to the point of maximum resistance is called *elastic zone*.

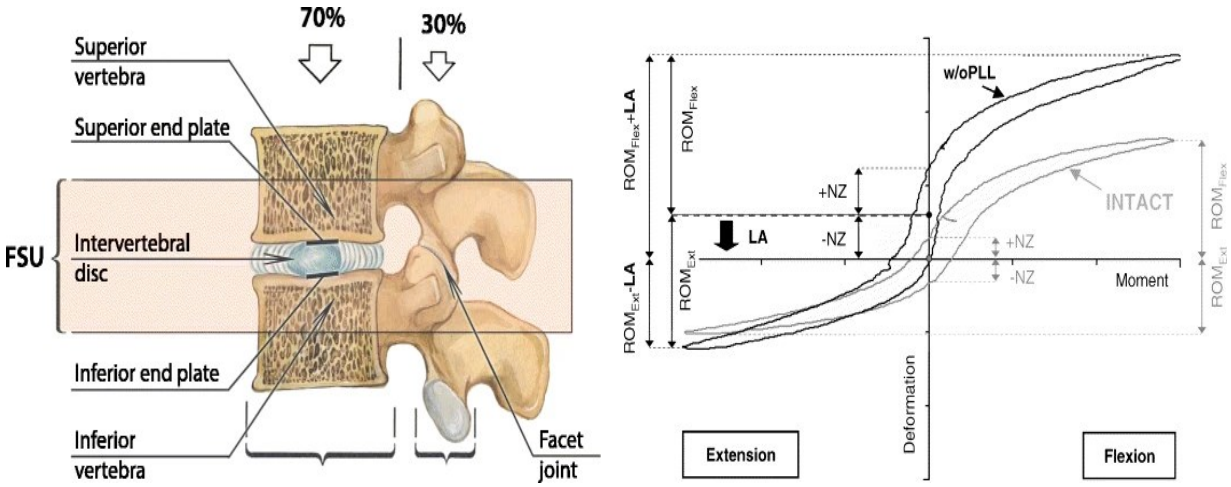


Figure 2.5: On the left an example of Fundamental Spinal Unit, on the right moment-angle curves obtained from intact spine complex after progressive dissection of structural ligaments, in order to evaluate the single % contribution of each ligament structure [15]

### 2.1.5 Cervical spine

The cervical spine is the uppermost part of the spinal column, it is comprised of seven vertebrae, labeled C1 through C7, that range from the base of the skull to the top of the shoulders.
These vertebrae are uniquely shaped and are the smallest within the entire spinal column.
The cervical spine provides support for the head, protect the spinal cord and supports head and neck movements.
Flexion, extension, lateral bending and rotation, schematized in fig. 2.6, are the main head and neck movements permitted by the cervical spine that make it the most mobile region of the spine.

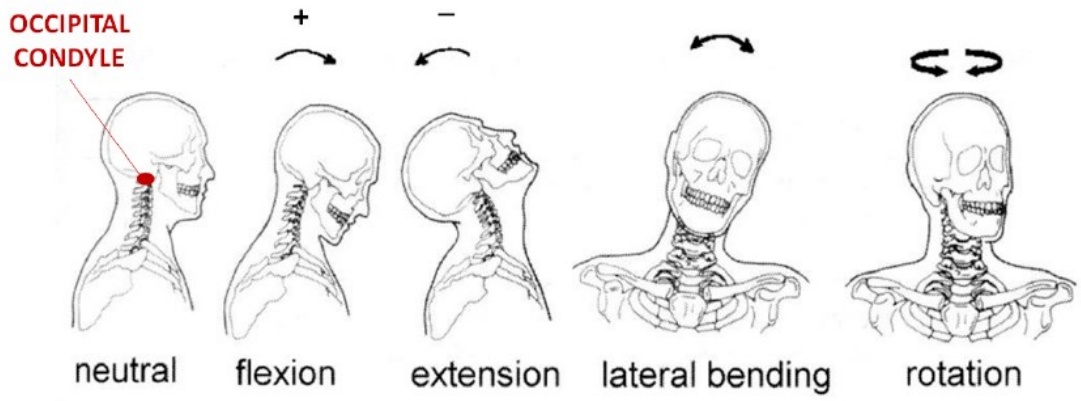


Figure 2.6: Representation of the four main head and neck movements

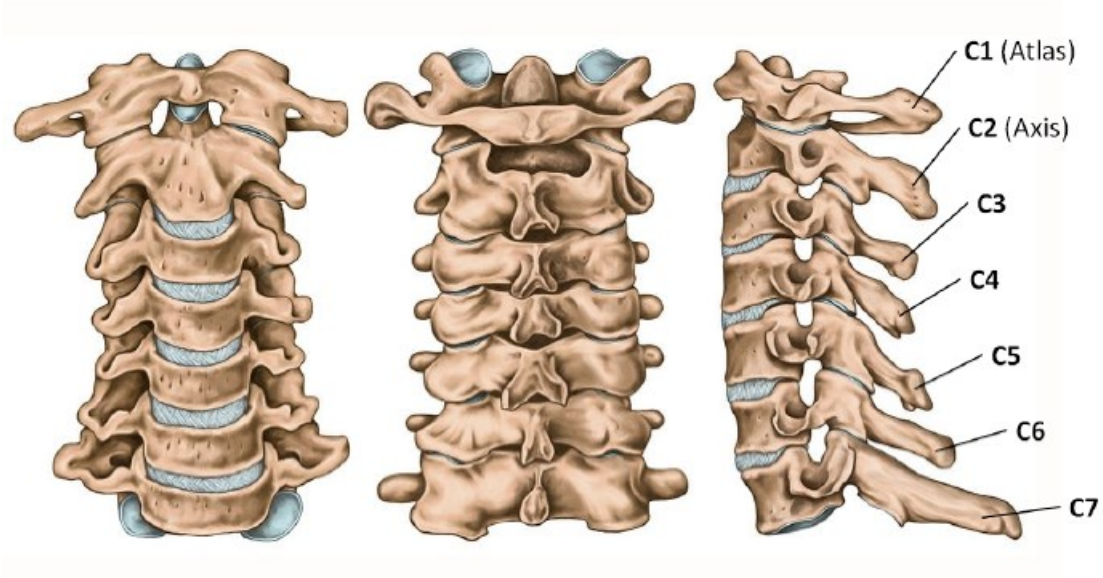


Figure 2.7: Frontal, rear and lateral view of the Cervical spine segment (C1-C7)

## 2.2 INJURY MECHANISMS AND NECK INJURY CRITERIA

Neck injuries follow two main possible injury mechanisms: i) direct impact contacting with a surface or an still object; ii) transmission of an impact coming from other parts of the body (head, thorax, etc).

A complete classification of neck injuries based on the force and its eccentricity for the injured motion segment is shown in Table 2.2 [16].

AIS (Abbreviated Injury Scale) is widely used to assess the severity of several cervical spine injuries (Table 2.1).

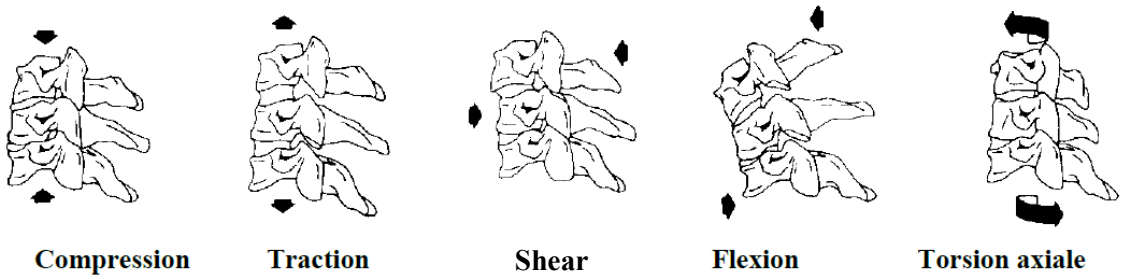


Figure 2.8: Example of possible loading condition for the neck

| AIS score | Injury |
|---|---|
| 1 | Minor |
| 2 | Moderate |
| 3 | Serious |
| 4 | Severe |
| 5 | Critical |
| 6 | Fatal |

Table 2.1: AIS scale

| Loading modes | Injury Types |
|---|---|
| Compression | Jefferson's fracture |
| | Comminuted fracture of atlas |
| | Compression fracture |
| | Teardrop fracture |
| Compression and flexion | Anterior wedge fracture |
| | Cervical sprain |
| | Unilateral facet dislocation |
| | Bilateral facet dislocation |
| | Burst fracture |
| | Teardrop fracture |
| Compression and extension | Fracture of Posterior element |
| | Clay-shoveler's fracture |
| | Hangman's fracture |
| | Anterior disc rupture |
| | Horizontal vertebral body fracture |
| | Teardrop fracture |
| Tension | Atlanto-occipital dislocation |
| Tension and flexion | Bilateral facet dislocation |
| | Unilateral facet dislocation |
| Tension and extension | Whiplash |
| | Tear of facet joint |
| | Tear of intervertebral disc |
| | Chip fracture |
| | Hangman's fracture |
| | Teardrop fracture |
| Torsion | Atlanto-axial dislocation |
| Shear | Atlanto-axial subluxation |
| | Odontoid fracture |
| | Fracture of articular process |
| Bending | Narrowing of intervertebral foramen |
| | Compression of articular process |

Table 2.2: Load condition and different types of cervical spine injuries

PIONEERS [17] has reported the results of tests carried out by several authors on volunteers and cadavers to determine the tolerance limits for neck injury. Table 2.3 summarizes the thresholds value for different load condition (moments evaluated at the Occipital Condyles level).

| Loading | Tested items | Tolerance criteria | Tolerance limit |
|---|---|---|---|
| **Flexion** | Volunteers | Pain | 59.4 Nm |
| | | Maximum load | 87.8 Nm |
| | Cadavers | AIS2 without fracture | 189 Nm |
| **Extension** | Volunteers | No injury | 23.7 Nm |
| | | Pain | 47.3 Nm |
| | Cadavers | AIS2 Ligament injury | 56.7 Nm |
| **Compression** | Cadavers | Bilateral facet dislocation | 1.72 kN |
| | | Injury in compression | 4.8 kN |
| **Tension** | Volunteers | No injury | 1.1 kN |
| | Cadavers | Fracture | 3.1 kN |
| **Shear (antero-posterior)** | Volunteers | No injury | 845 N |
| | Cadavers | Irreversible damage | 2 kN |
| | Functional unit | Ligament rupture | 824 N |

Table 2.3: Tolerance limit for neck injuries for different load condition

From these results PIONEERS has defined the neck range of motions to not exceed to prevent neck injuries.
These threshold angles are reported in table 2.4 and will be used as reference for the preliminary development of the test method for the assessment of neck protectors.

| | ROM [deg] |
|---|---|
| **Flexion** | 72 |
| **Extension** | 64 |
| **Axial Rotation** | 77 |
| **Lateral Bending** | 61 |

Table 2.4: Neck threshold ROM to prevent neck injuries (AIS 0)

Several neck injury metrics have been proposed to evaluate possible neck injury risks.
Usually, force, moment, displacement and acceleration are the parameters taken into account in neck injury criteria.
These neck injury criteria are usually meant for the assessment of automotive crash tests using anthropomorphic test devices so they are not very appropriate for the study of motorcycle crashes.
Some criteria are here reported:

- **$N_{ij}$ criteria**
  $N_{ij}$ is the Normalized Neck Injury Criterion, i index defines the axial load (T tension, C compression), j index defines the sagittal plane bending moment (F flexion, E extension), the equation to calculate this parameter is:

$$N_{ij} = \frac{F_z}{F_{zc}} + \frac{M_{ocy}}{M_{yc}} \tag{2.1}$$

  where $F_z$ is the force at the point of transition head to neck, $F_{zc}$ is the critical force, $M_{OCy}$ is the total moment about occipital condyle, and $M_{yc}$ is the critical moment. The critical values depend on the tested dummy (table 2.4).

| Dummy type | $F_{zc}$ [N] Tension | $F_{zc}$ [N] Compression | $M_{yc}$ [Nm] Flexion | $M_{yc}$ [Nm] Extension |
|---|---|---|---|---|
| **Hybrid III, male 50%** | 6806 | -6160 | 310 | -135 |
| **Hybrid III, female 50%** | 4287 | -3880 | 155 | -67 |
| **Hybrid III, 6YOD** | 2800 | -2800 | 93 | -37 |

Table 2.5: Critical value of Force and Moment for different Hybrid III dummies

Figure 2.9 shows the neck injury risk curves corresponding to $N_{ij}$ criteria.

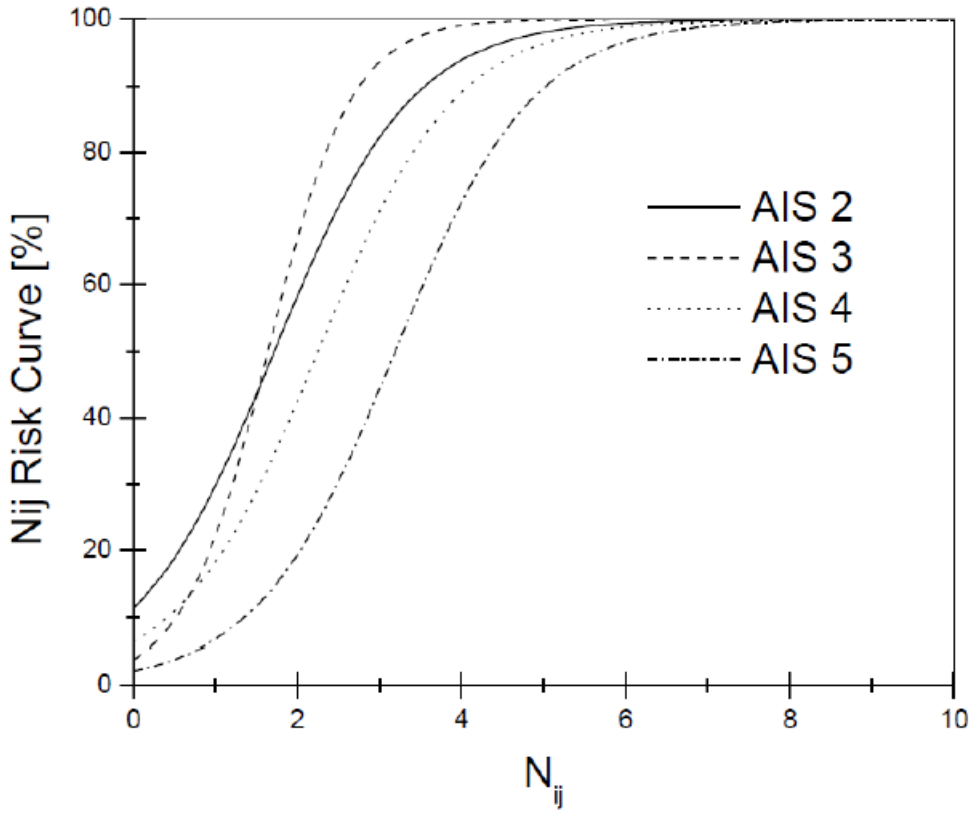


Figure 2.9: Representation of neck injury risk curves corresponding to Nij criteria

The probability for different AIS score can be estimated with the following equations.

$$AIS2\ Nij = 100 * (1 + e^{2,0536-1,1955*Nij})^{-1} \quad (2.2)$$

$$AIS3\ Nij = 100 * (1 + e^{3,227-1,969*Nij})^{-1} \quad (2.3)$$

$$AIS4\ Nij = 100 * (1 + e^{2,693-1,196*Nij})^{-1} \quad (2.4)$$

$$AIS5\ Nij = 100 * (1 + e^{3,817-1,196*Nij})^{-1} \quad (2.5)$$

- **NIC**
  This criterion is used to predicts neck injuries in low-speed rear-end automobile collisions and is based on the relative acceleration and velocity between the top and the bottom of the cervical spine.
  Boström, et al. [18] proposed the Neck Injury Criterion with the equation:

$$NIC = a_{rel} * L + v_{rel}{}^2 \tag{2.6}$$

  where $a_{rel}$ and $v_{rel}$ are the relative horizontal acceleration and velocity between the bottom (T1) and top (C1) of the cervical spine (T1-C1) while the term L represents the length of the cervical spine.

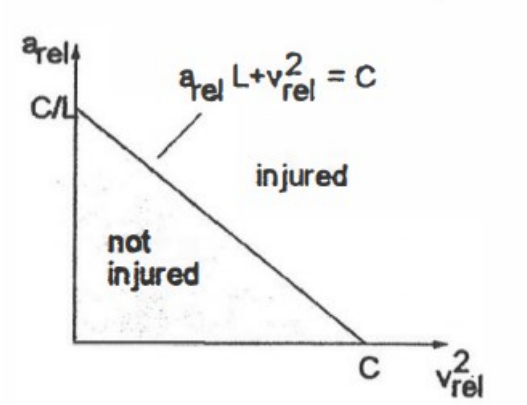


Figure 2.10: In this diagram, a straight line defined by NIC splits up the injured from the not injured

- **BC**
  This neck injury criterion is used in frontal crashed [19].
  BC is based on a beam model of the lower cervical spine and is expressed as:

$$BC = \frac{F_z}{F_{zc}} + \frac{M_y}{M_{yc}} \tag{2.7}$$

  where Fz is the axial compression/tension force, and My is the flexion/extension moment, both at the C7/T1 intervertebral disc.
  Fzc is 5660 in axial tension and 5430 in axial compression, while Myc is 141 Nm in flexion/extension.
  BC of 1.0 correspond to a 50% risk of an AIS ≥ 2 injury in the human cervical spine.

## 2.3 NECK SURROGATE STATE OF ART

In this paragraph some examples of neck surrogate developed in research, including those currently developed by the University of Padova, are reported.

### 2.3.1 Hybrid III Neck

The neck of the 50$^{th}$ percentile Hybrid III dummy is the most used neck surrogate in research.

It's composed by five 6061-T6 aluminum discs that provide the correct mass: the upper one allows the connection with the nodding joint for mounting the Hybrid III dummy head form, the three discs in the central part replicate the vertebral bodies, and finally the lower one is connected to the trunk.

The aluminum plates are connected by means of four different butyl elastomer discs. These discs present a horizontal cut on the anterior side to differentiate the behavior in flexion and extension in the sagittal plane, in fact the Hybrid III neck is stiffer in flexion than in extension also due to the asymmetric distribution of the rubber material.

The Hybrid III neck also has a steel cable that runs through its center and acts to limit the rotation of the neck at large angles.

Table 2.5 shows the stiffness value for the Hybrid III neck estimated by different authors [20], [21], [22].

| REFERENCE | YEAR | $K_{flex}$ [Nm/°] | $K_{ext}$ [Nm/°] |
|---|---|---|---|
| **White et al.** | 1988 | 3,83 | |
| **Spittle et al** | 1992 | 2,45 | |
| **Baughn et al.** | 1993 | 2,56 | 2,08 |
| **Padua University** | 2019 | 2,54 | 1,17 |
| **Nightingale** | 2002/2007 | 0,045 | 0,058 |

Table 2.6: Comparison of the different stiffness values of the Hybrid III neck, the last row shows the value of $k_{flex}$ and $k_{ext}$ evaluated from cadaveric data from Nightingale [23], [24]

From these data is clear how far the Hybrid III neck is from biofidelity in terms of stiffness property.

Figure 2.11: Hybrid III neck and head form assembly

### 2.3.2 University of Alberta

This neck surrogate has been developed and characterized for be used in helmet certification applications [25].
The characterization in flexion, extension, bending and direct impact has been done and compared to existent cadaveric literature.
Figure 2.12 shows the design of this prototype that presents vertebral bodies, intervertebral discs, facet joints, and soft tissue.

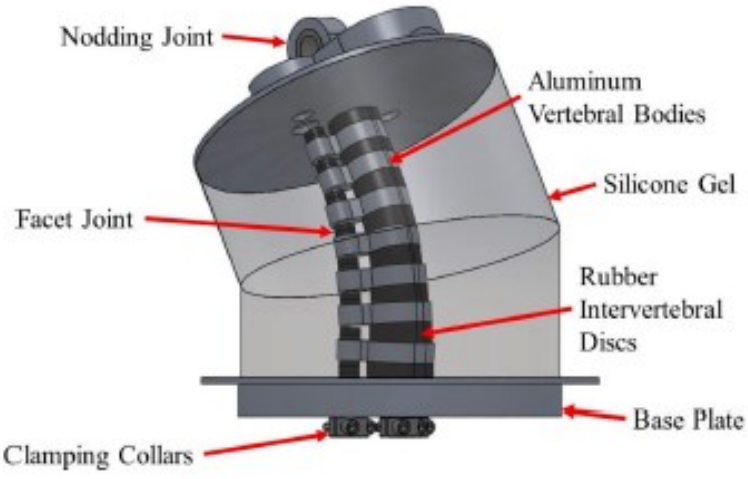


Figure 2.12: CAD model of the neck prototype developed by University of Alberta

The vertebral bodies were obtained from a waterjet cut of aluminum 6061-T6, intervertebral discs were manufactured using 3D printing in a rubber-like material (Tango Black). The entire spinal column of the prototype was encased in silicone rubber 00-30.
An aluminum 6061-T6 nodding joint with a similar design to the Hybrid III neck one allows the dummy head assembly.
Quasi-static bending tests had been carried out to evaluate the flexural stiffness of the neck. A six-degree of freedom robotic platform was used for the purpose.
Forces and moments are collected by a six-axis load cell fastened to one end of the neck, while the other end of the neck was held stationary.

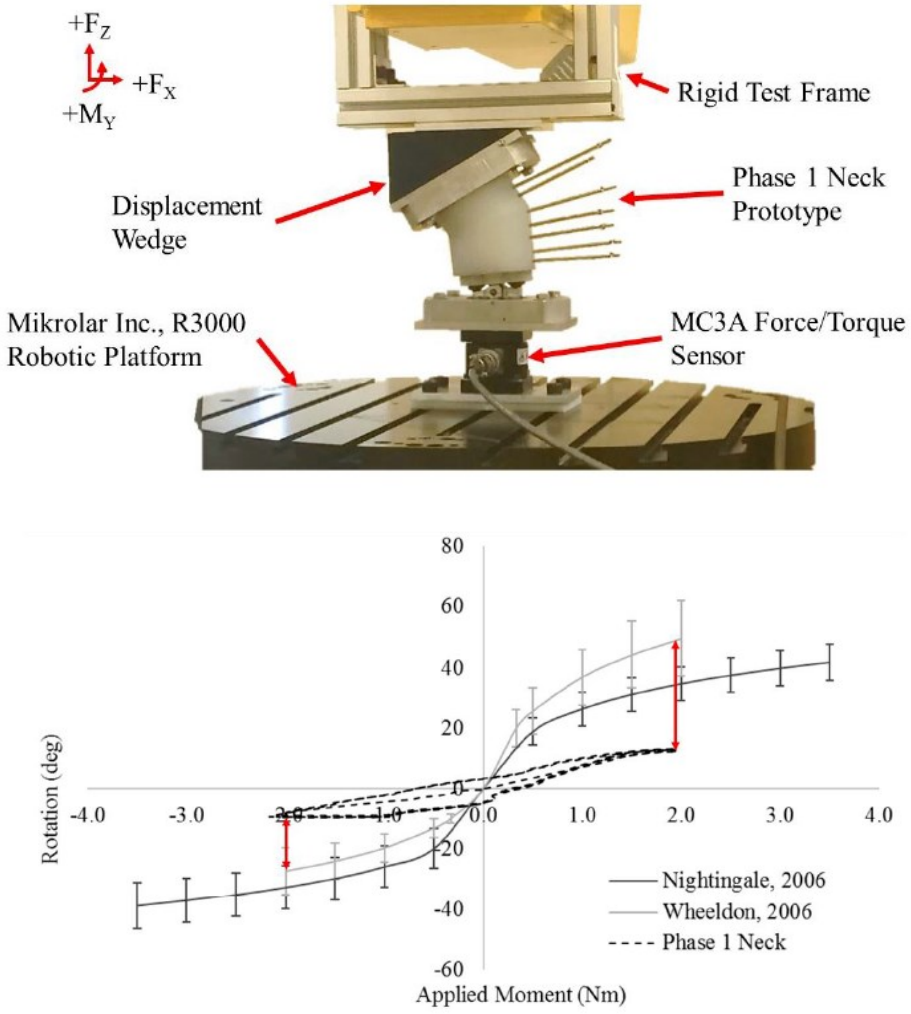


Figure 2.13: On the top the test setup, on the bottom the comparison between experimental results and cadaveric literature data

The results underline a stiffer behavior of the prototype with respect to cadaveric data but anyway closer than the Hybrid III neck one.

### 2.3.3 University of British Columbia (2010)

This neck surrogate model was designed to provide a biofidelic response to head-first impacts with a straightened cervical posture [26].
The neck design incorporates eight vertebrae, T1 to C1. The neck geometry was designed to match the average sagittal centers of rotation (COR) for each vertebra, sagittal vertebral body size, axial displacement, sagittal bending range of motion, and the ratio of flexion to extension bending stiffness at each intervertebral level.
The neck is connected to the head through a pivot joint representing the atlanto-occipittal joint (C0/C1) that allowed only sagittal rotation. At all other levels, both sagittal rotation and pure compression between adjacent vertebrae were allowed.
The neck was tested in a series of head-first impacts on a drop tower to investigate the temporal aspects of the kinetic axial force response for the head and neck and appears suitable for studying the scenario of sagittal plane, aligned column impacts.

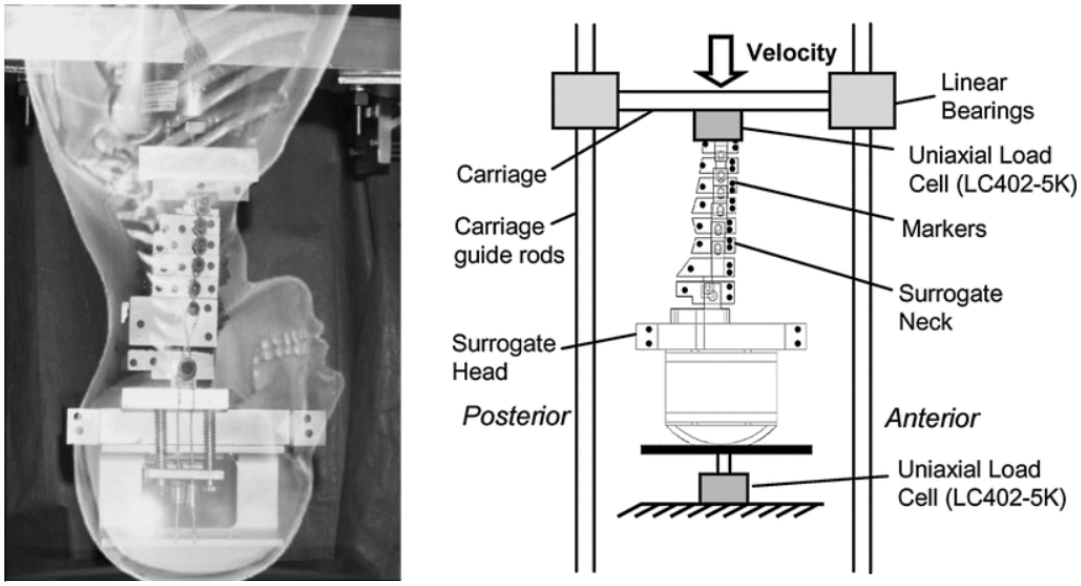


Figure 2.14: On the left the inverted profile of the head and neck surrogate with human anatomy overlain, on the right the test apparatus for the drop tests

The flexibility of the spine was tested as well showing a highly nonlinear response with a characteristic neutral zone and logarithmic shaped flexibility curve as shown in figure 2.15.
The range of motion and the neutral zone data generally have indicated that the bending stiffness increased with incremental increases in follower load and that the neck was stiffer in extension than in flexion.

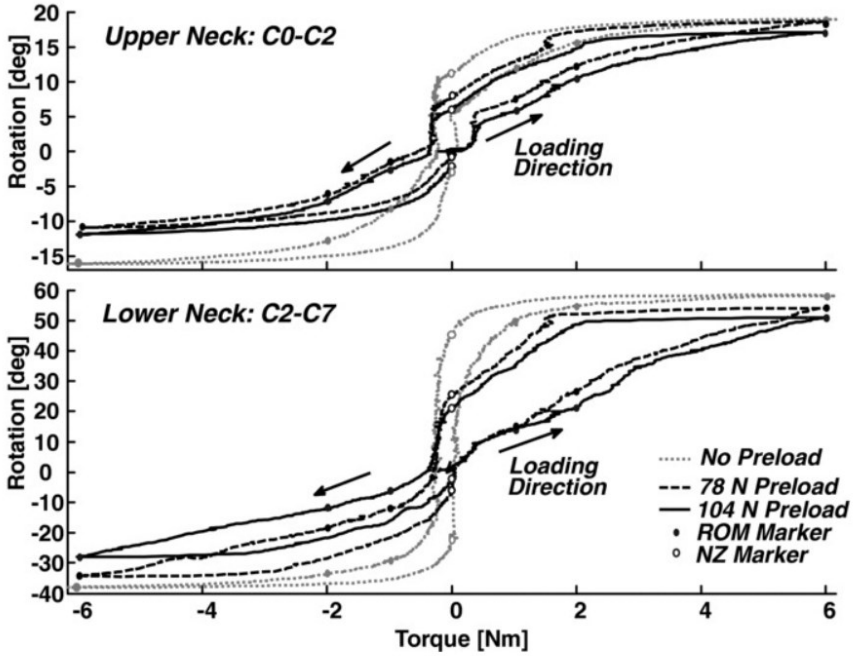


Figure 2.15: Upper neck (C0-C2) and lower neck (C2-C7) flexion–extension moment-rotation response at 0,78, and 104 N follower loads

### 2.3.4 University of British Columbia (2019)

The University of British Columbia has carried out another research on the development of a biofidelic neck surrogate [27]. This research was focused on the designing and constructing of a portion of the neck with high biofidelic characteristics in terms of geometry.

A very detailed vertebrae modeling reproduces the kinematic response of a cervical functional spinal unit (FSU).

The vertebrae were 3D-printed in polyactic acid (PLA), checkered rubber sheets in place of intervertebral discs were used and finally the whole system was placed between two mounting brackets (figure 2.16).

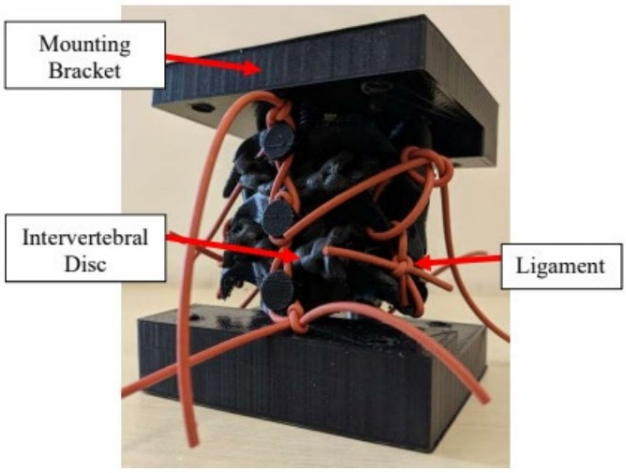


Figure 2.16: FSU with detailed vertebrae modeling developed by University of British Columbia

### 2.3.5 Imperial College of London

M. Ghajari and F. Abayazid have proposed a 3D printable surrogate neck in order to represent the response of the cervical spine in head-first impact [28].
The 3D printable rubbers, which allow to simulate the function of energy absorption, have been characterized using Dynamic Mechanical Analysis.
This model has been patented [29].

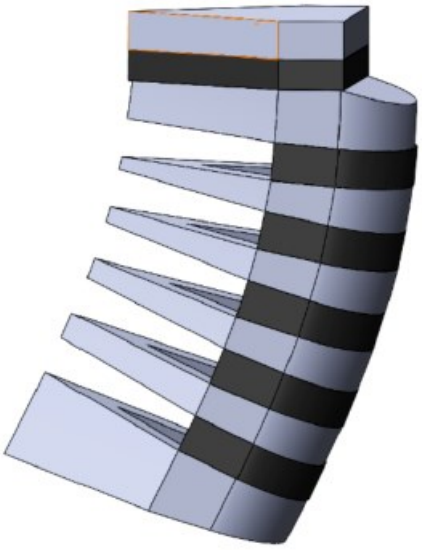

Figure 2.17: CAD model of the neck surrogate proposed by the Imperial College of London

### 2.3.6 Padua and Mid-Sweden Universities

The University of Padua, in collaboration with the University of Mid-Sweden, has been developing a neck surrogate which has been constantly updated over the last few years. Three successive iterations of the Biofidelic Neck Prototype (BNP), as today, was designed, manufactured and characterized: BNP0, BNP1 and BNP2 [30], [31], [32].
These prototypes have been designed following these guidelines:

- Fast prototyping: 3D printing technology was used for the manufacture of the components; this technology allows to obtain a high number of specimens even with a complex structure in a short time.
- Structural simplification: only the vertebrae and the intervertebral disc were taken into account.
- Modularity: single identical FSU were manufacture and assembled together to form the neck assembly, giving it a modular structure that allowed to simplify the design phase and the replacement of a single FSU in case of damage.
- External hooks: these features were taken into in consideration in the design phase in order to replicate the different stiffness of the neck along the four main anatomical direction with elastic components applied on these outer vertebrae hooks.
- Inner cable: an axial cable, passing through each FSU, was used to increase the flexural stiffness of the neck

**BNP0**

The reference value for the BNP0 in terms of stiffness in flexion and extension was equal to the one from the stiffer human neck cervical segment (C6-C7), namely 494,1 Nmm/°. The overall neck flexional equivalent stiffness of 6 identical FSUs, calculated as a series of stiffness, had a value of 82.35 Nmm/°.

The material used to replicate the vertebrae was ABS (Acrylonitrile Butadiene Styrene).

The intervertebral discs of the BNP0 were casted with a Silicone rubber PlatSil 73-60, manufactured by Politek Development Corp., with a hardness 60 on the Shore A scale. The overall length of the prototype had been set to 135 mm (same as Hybrid III neck), while a value of 35 mm for the diameter of the intervertebral disc was suggested by FEM analysis.

Since the ABS material doesn't bond itself with the type of rubber used, different interface surfaces were designed and 3D printed.

The final choice was a grid pattern that traps the rubber disc, as shown in Figure 2.18.

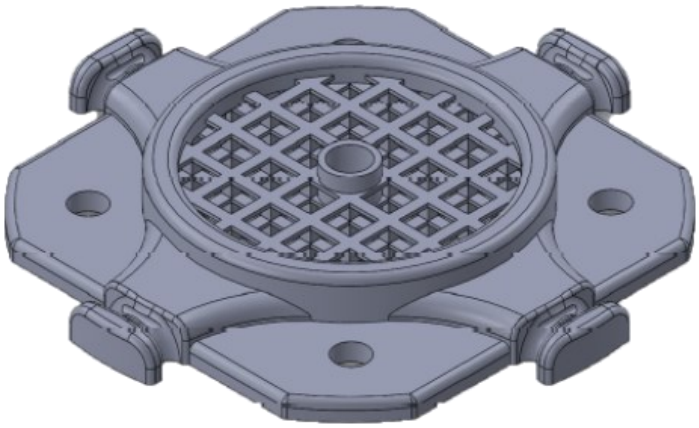

Figure 2.18: Final design of the vertebra for the BNP0 [30]

The whole neck (6 FSUs) was tested in pure bending showing a flexural stiffness of 36,08 Nmm/°, calculated considering the slope of the initial linear behavior (figure 2.19).

The plot shows a too compliant behavior with respect to the design target, represented by the C6-C7 intervertebral level analyzed by Nightingale in 2007 [23]. The possibility to increase the flexural stiffness with elastic bands and the inner cable allowed to reach the target value with a flexural stiffness of 77,21 Nmm/°.

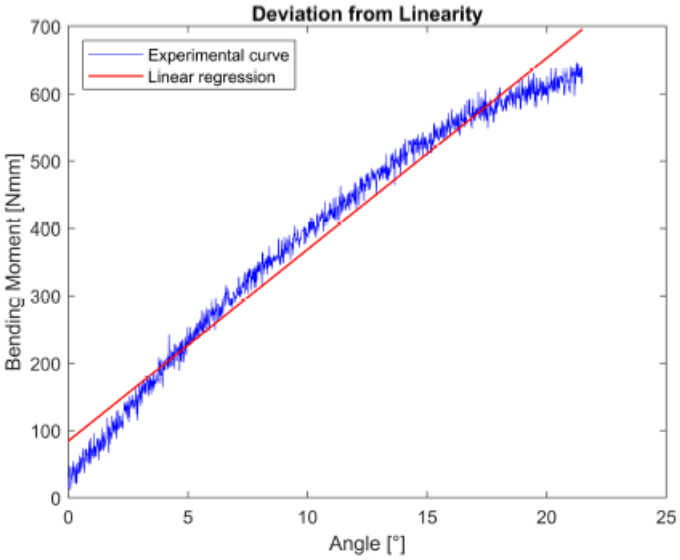


Figure 2.19: Results of the pure bending test performed on the BNP0 [30]

**BNP1**

When the stiffer BNP0 configuration was assembled with the head surrogate, the whole system resulted too compliant.

A second bigger and stiffer design of the neck was achieved by scaling the first geometry to obtain the Biofidelic Neck Prototype 1 with a rubber disc diameter of 50 mm (figure 2.20).

The BNP1, tested in pure bending, showed a flexural stiffness of 261,17 Nmm/°, the application of the elastic components and the inner cable in this prototype conferred to the neck a flexural stiffness of 584,52 Nmm/°.

These results underline a too stiff behavior of the neck even in its softest configuration.

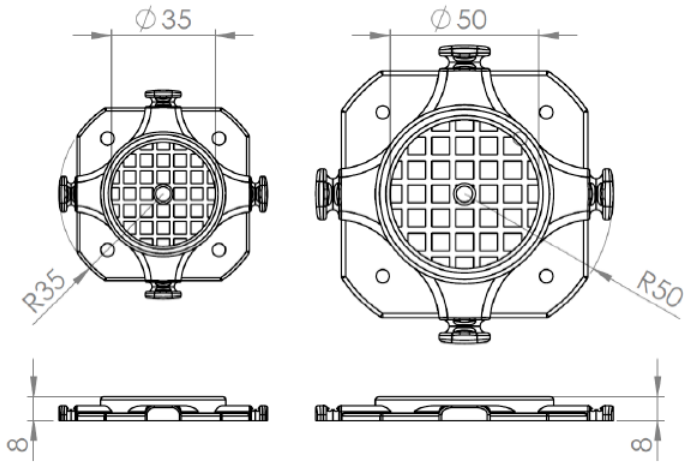


Figure 2.20: BNP1 vertebra design, obtained by scaling the geometry of the one of the BNP0 [30]

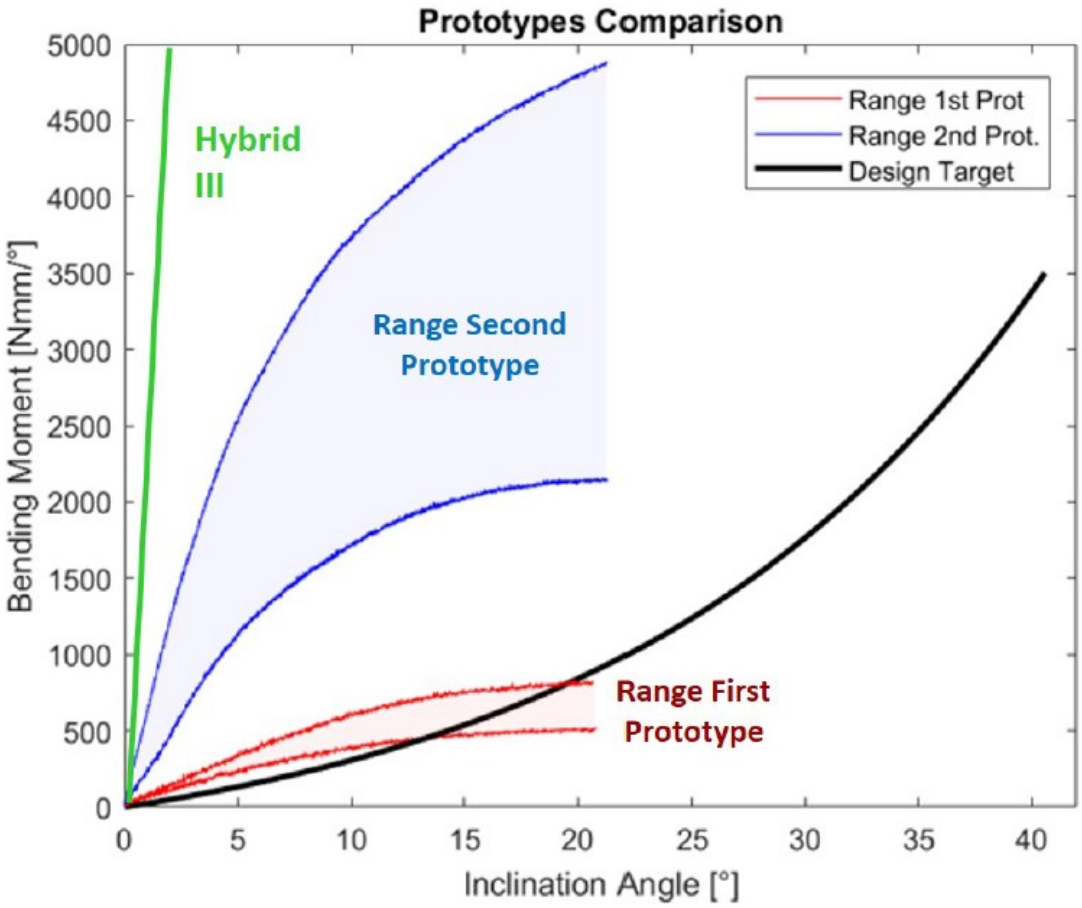


Figure 2.21 :Comparison plot of the experimental bending test, showing the flexional behavior of the first prototype (BNP0) and the second prototype (BNP1) with respect to the Hybrid III neck and the chosen design target [30]

**BNP2**

The aim of this prototype was to reduce the BNP1 flexural stiffness by using a different rubber type for the intervertebral discs.

Three PlatSil Gel compounds available in Sports Tech Research Centre, Mid-Sweden University, were taken into account. To obtain a wider stiffness variability, the Deadener component, which softens the rubber, was introduced.

The casted FSUs with precise mix definition in terms of component A, B and D (Deadener) are listed below:

- PlatSil Gel 01-30 1A:1B
- PlatSil Gel OO 1A:1B, 1A:1B:1D and 1A:1B:2D
- PlatSil Gel 25 1A:1B and 1A:1B:2D

The rubber choice was suggested by a FEM analysis which suggested to adopt the PlatSil Gel 01-30 to get an average flexional behavior between the range of specimen.

Similar to the previous prototypes, the BNP2 was tested in pure bending, showing a flexural stiffness of 29 Nmm/°.

Elastic bands, inner cable and cylindrical rubbers were used to enhance the stiffness of the neck which was not able to bear the weight of the Hybrid III head without their contribution.
The stiffer configuration of this prototype reaches the value of 139 Nmm/° in flexural stiffness.

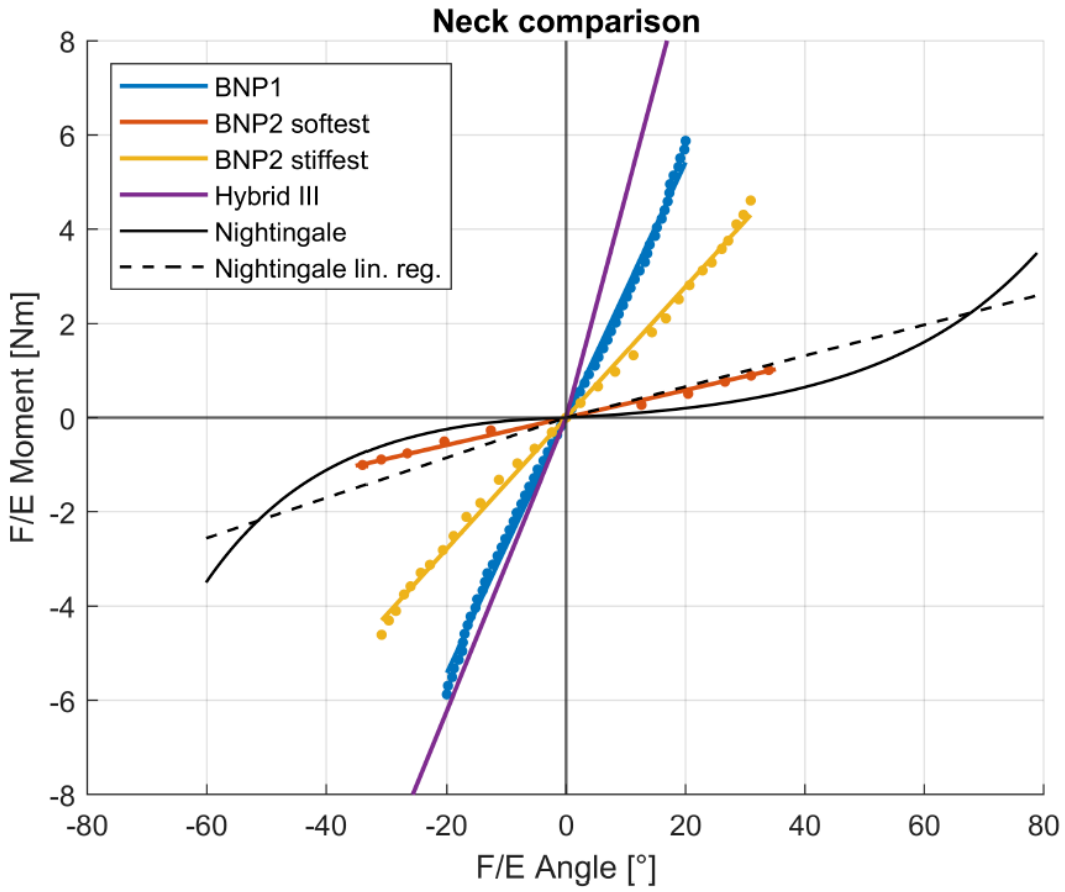


Figure 2.22: Neck comparison plot for static flexion tests [32]

**SUMMARY**
Table 2.6 summarizes the results obtained with the different BNP neck prototypes in terms of flexural stiffness while figure 2.23 shows their final design.

| Neck | Min $K_{flex}$ [Nmm/°] | Max $k_{flex}$ [Nmm/°] |
|---|---|---|
| **BNP0** | 36,08 | 77,21 |
| **BNP1** | 261,17 | 584,52 |
| **BNP2** | 29 | 139 |

Table 2.7: Minimum and maximum flexural stiffness for the BNP neck prototypes

Figure 2.23: From the left to the right, BNP0 assembly, BNP1 assembly, BNP2 assembly

### 2.3.7 Aims of the work

This thesis work focuses on two aspects: on the development of the new biofidelic neck surrogate and on the preliminary study of a possible test method for neck braces effectiveness evaluation.
The aims of this thesis can be summarized as follow:

1. Prototyping and re-design of the new biofidelic neck surrogate.

2. Validation of the new prototype with static and dynamic characterization tests.

3. Instrumentation of the neck for the evaluation of neck bending angles and loads acting on the neck.

4. Development of a test method for the assessment of neck protectors.

5. Carrying out of pilot tests with two different neck surrogates: the stiffer Hybrid III neck and the new more biofidelic neck prototype.

# CHAPTER 3

# 3 BIOFIDELIC NECK PROTOTYPE 3 (BNP3)

In this chapter is presented the development of the new biofidelic neck prototype, as well as the modifications introduced for its instrumentation.
A first test to evaluate the biofidelity of the new prototype was done by evaluating its passive range of motion ROM and comparing it with in vivo data.

## 3.1 OVERVIEW

The design of the biofidelic neck prototype 3 started during the Master Thesis of Marco Rango [32].
This new prototype aimed to improve the critical aspects of the previous necks surrogates in order to create a more biofidelic and more robust neck surrogate.
The BNP3 presents some changes in terms of geometrical features, the outer shape of the neck was brought from a square to a cylinder. The circumscribing circle diameter was reduced to ϕ85 mm to improve the compatibility with the Hybrid III head form.
About the external hooks, thickening and filling measures were taken to increase the overall structural properties.
The new vertebras feature 4 additional holes of ϕ2.5 mm around the ϕ5.5 mm hole for the inner cable. These holes will allow for the passage of 4 fishing line that will be used for the instrumentation of the neck (figure 3.1).
The grid of the vertebra was thickened, and the edges were smoothed to increase the breaking loads.

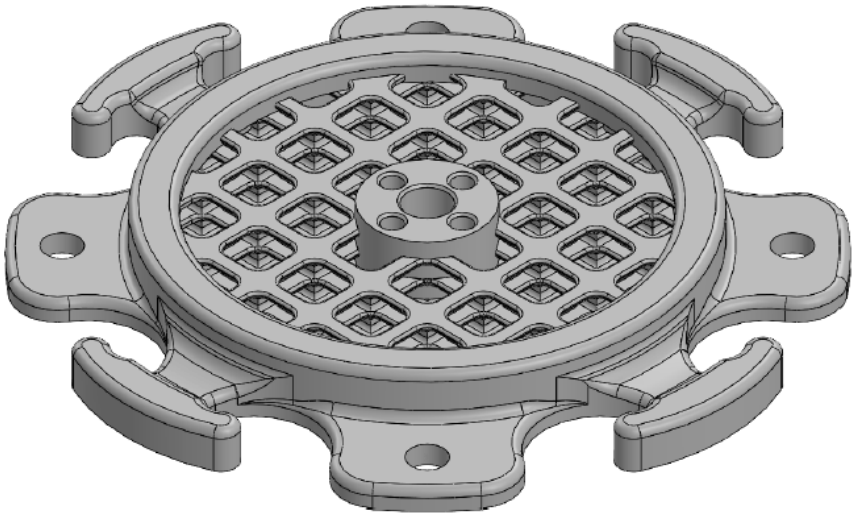

Figure 3.1: BNP3 vertebra

The upper vertebra base was thickened from 2,5 mm to 4,5 mm to sustain the axial compression loads while the bottom vertebra has the four vertical holes for the neck

instrumentation tilted by 65° in order to avoid the contact with the washer of the inner cable (figure 3.2).

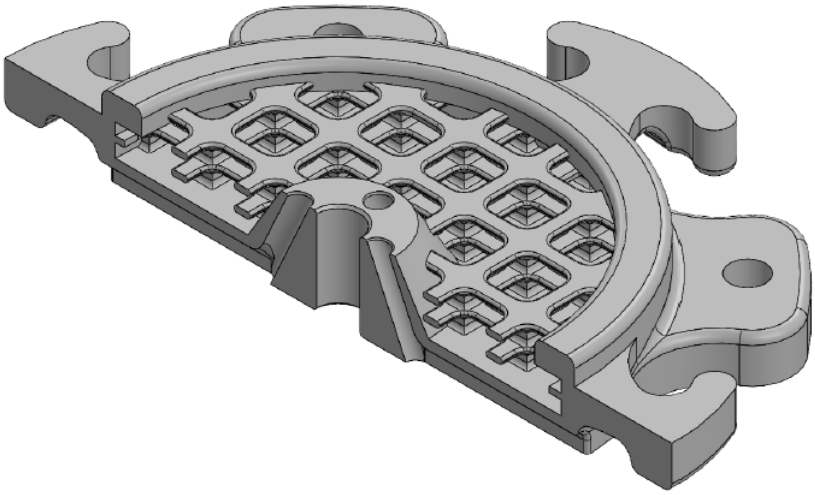

Figure 3.2: BNP3 bottom vertebra

The nodding joint follows the design of the vertebra geometry in terms of hook shape and external diameter (figure 3.3).

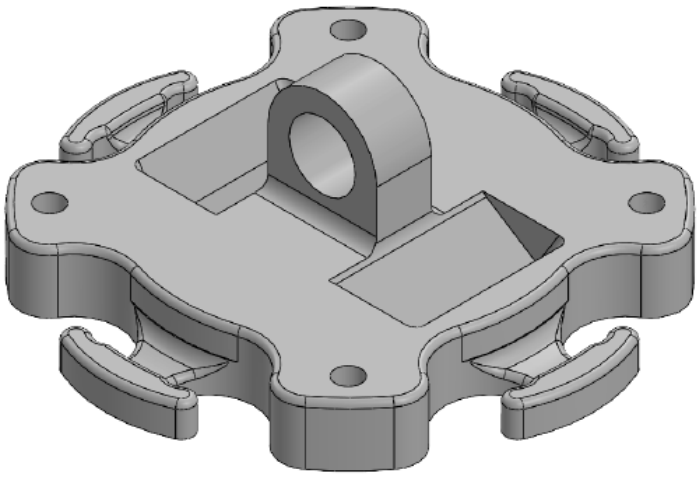

Figure 3.3: BNP3 Nodding Joint

For each component of the new prototype a structural simulation in Ansys has been carried out to give a quantification of the benefits.
The chosen material for the manufacture of the vertebras by 3D printing technology is Nylon Pa12, which has a tensile yield strength between 13.0 MPa and 170.0 MPa [33].
The material of the intervertebral discs, chosen for this prototype, is the same of the previous one (BNP2), that is Platsil Gel 01-30.
This choice was taken to guarantee the stability of the neck while it bears the weight of the head.

In figure 3.4 is shown the final assembly of the BNP3

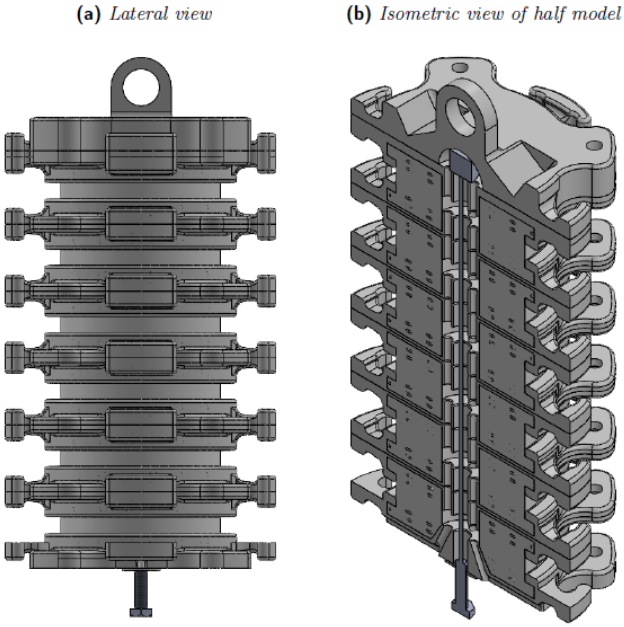


Figure 3.4: BNP3 assembly

## 3.2 BNP3 MANUFACTURE

The first goal of this thesis work was the manufacture of the BNP3.
The neck components introduced in the previous paragraph were obtained by additive Selective Laser Sintering (SLS) technology.
For the assembly of the neck, the single FSUs must be manufactured by casting the Platsil Gel 01-30 in a proper mould.
This mould was modeled to accommodate the shape of the vertebras as is shown in figure 3.5, and it was always obtained by additive technology in Nylon Pa12.
The process to manufacture an FSU is the follow:
A release agent is smeared on the two pieces of the mould in order to ease the extraction of the finished component.
The lower vertebra is positioned under the moulds and kept in position with screws on the four connection holes. Then, four PTFE tubes ($\theta_E$ 2.5 mm $\theta_I$ 1.5mm) are positioned in their sit and will allow a low friction movement of the fishing lines used for angular sensors.
To obtain the intervertebral disk, a PlatSil Gel 01-30 silicone rubber is mixed adding its A and B components in a 1:1 ratio. After the mixing, the gel cures within six minutes.
The gel, thanks to its viscosity, can be poured on the two vertebras and finally, the upper vertebra could be placed over the mould which is then secured with nuts.
After about 1 hour the polymer has completely reticulated and the FSU can be extracted from the mould, the vertical central pin is removed while the four pieces of Teflon pipe must remain inside of the FSU for their functional task.
6 FSUs were produced and assembled one over the other giving the modular structure of the neck as shown in figure 3.7.

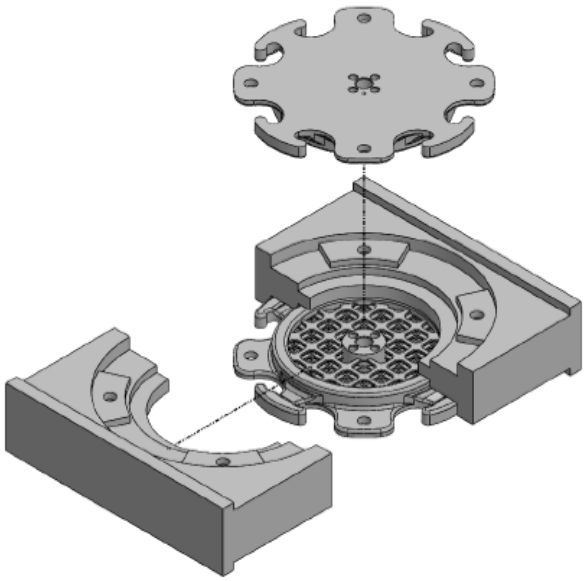

Figure 3.5: Mould assembly

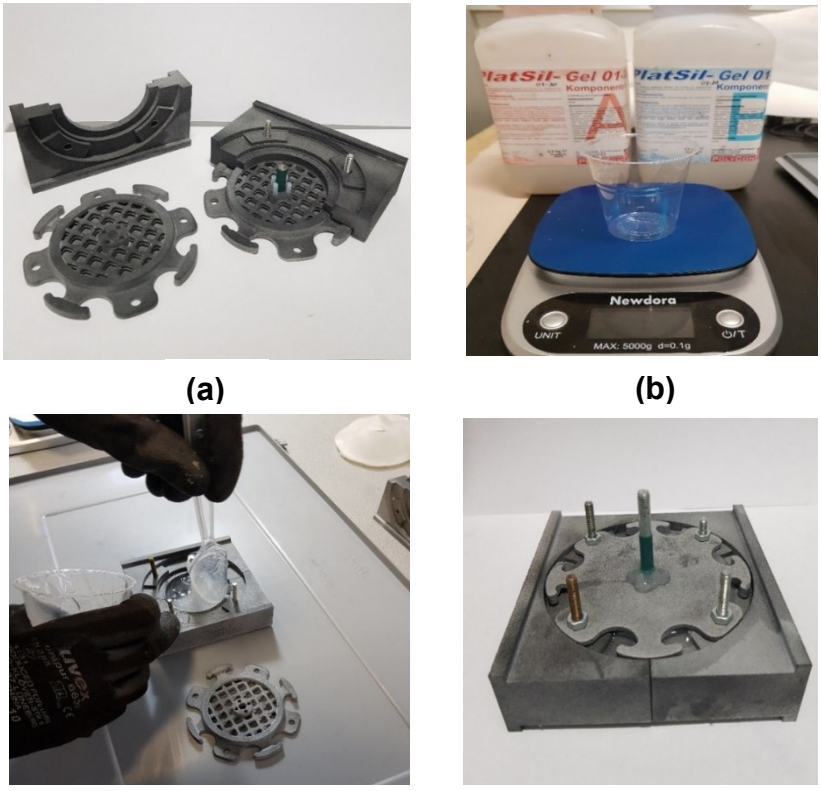


**(a)** **(b)**

**(c)** **(d)**

Figure 3.6: Manufacture of the FSUs: **(a)** Set up, **(b)** Preparation of the Platsil-Gel, **(c)** Gel pouring **(d)** Demoulding phase

Figure 3.7: BNP3 assembly

## 3.3 BNP3 STIFFENING

The BNP3 as it is, is not able to bear the weight of the Hybrid III head.
This can be considered a biofidelic behavior of the neck surrogate since our head is sustained by the activation of the neck muscles while if we neglect their contribution, the head wouldn't maintain its elevated position, indeed this is what happen considering a human that lose consciousness.
Despite that, a neck that is able to sustain the head of the Hybrid III is necessary to carry out our tests so some measures to make the BNP3 less compliant were adopted.
The measure taken into account take their cue from the previous works and their contribution in the neck stiffening was studied and reported in chapter 4.

### 3.3.1 Inner cable:

This simple idea was taken from the Hybrid III neck, where a steel rod permits to give certain compression to the surrogate, changing its mechanical response.
This system has been replicated with a steel cable, whose extremity was welded on one side to a M5 screw and on the other side to a flat screw head with a braze welding technique. The flat screw head presses the upper part of the neck and assures the centering of the cable along the neck while on the other side a nut is being fastened along the screw.
The inner cable acts as a tie rod, one rotation of the nut correspond to an axial displacement in compression of the neck equal to the M5 screw pitch (0,8 mm).
To withstand the load generated by the axial compression of the neck a washer is placed under the nut, in addition a counternut is fastened along with the first nut to avoid unscrewing.

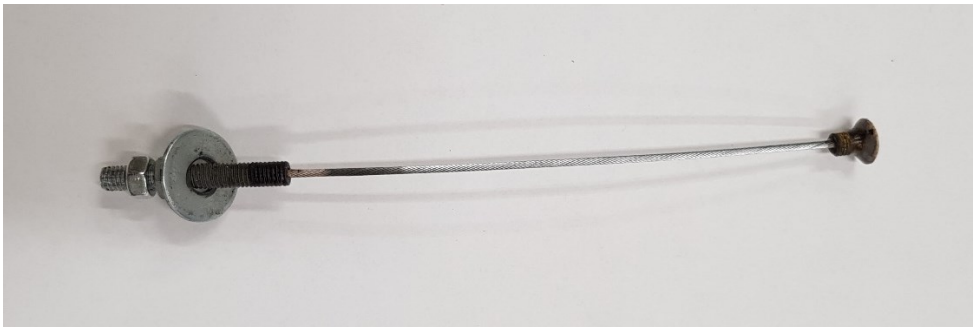

Figure 3.8: BNP3 Inner cable

### 3.3.2 O-Rings:

The hooks of each vertebra allow to install elastic components along the neck and modify its flexural stiffness, there is also the possibility to give an asymmetry behavior to the system just changing the arrangement and the number of the elastic components along the four directions (front, laterals, back).
For the BNP2 elastic bands 90 mm long and 6 mm thick were used as elastic component instead of the O-Rings used previously.
For the current prototype the O-Rings were reconsidered for their stronger mechanical properties and for their more engineering applications.
In this case O-Rings with 20,22 mm inner diameter and 3,53 mm thick, made out of Nitrile rubber were used.
The dimensions of the O-Rings were chosen considering the space between two consecutive vertebras hooks in order to generate a preload on the O-Ring when the O-Ring is inserted.
We know that the O-Rings are not manufactured for be used in such a way, for this reason we carried out a characterization of this component in order to better understand their behavior for our applications.
A static test was carried out to evaluate the stiffness of the O-Ring.
We are interested in a component that is elastic but also presents a stiffening behavior that can simulate the stiffening behavior of the human neck for high angles of flexion and extension.

### 3.3.3 O-Rings static test

A static test was done to estimate the stiffness of the O-Ring under axial load and its trend along the displacement.
For the tests the servo hydraulic machine Minibionix for axial tests, available at the University's laboratory was used.
The O-ring was inserted between two hooks fixed on the machine clamps.
The test was carried out in displacement control, 70 mm of displacement were set from the starting distance between the hooks that was set to 23 mm.
The figure 3.10 shows the trend of the force along the imposed displacement.
A first stiffening response is observed after 4 mm of displacement followed by a second stronger stiffening in correspondence of a displacement equal to 36 mm.
If we consider two consecutive hooks, the bottom surface of the first hook is 27 mm from the upper surface of the second hook.

That means the stiffness of the O-Ring when is inserted between two consecutive hooks is equal to the slope of the curve between the two stiffening responses and can be calculated as:

$$k_{OR} = \frac{\Delta Force}{\Delta Displacement} = 1{,}44\ \frac{N}{mm} \tag{3.1}$$


Figure 3.9: O-Ring static test set-up

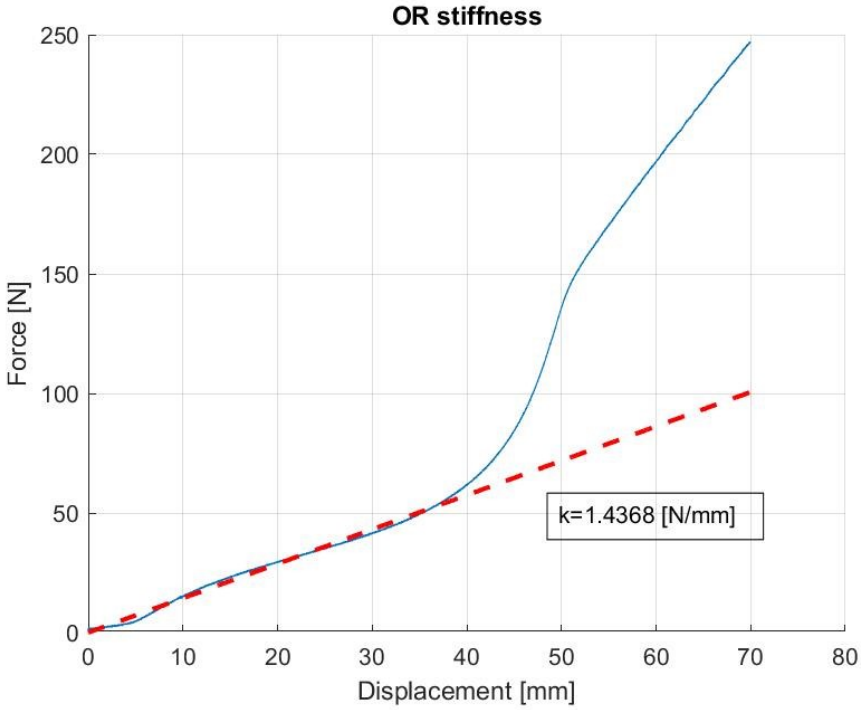


Figure 3.10: Force vs Displacement curve

When a O-Ring is placed between two consecutive hooks, it exerts a preload force that can be estimated by knowing the stiffness just measured.
The undeformed O-Ring has a circular shape, its inner circumference is:

$$C = \pi \cdot \emptyset = \pi \cdot 20{,}22 = 63{,}52\ mm \tag{3.2}$$

When the O-Ring is inserted, it follows the geometry of the hooks and its deformed shape can be approximated with a rectangle which perimeter is:

$$P = (2a + 2b) = (2 \cdot 8) + (2 \cdot 27) = 70\ mm \tag{3.3}$$

where *a* and *b* are the sides of the rectangle defined by two consecutive hooks (fig. 3.11).
The difference between the perimeter of the rectangle and the starting circumference defines the total elongation of the O-Ring that can be split mainly to the two longer sides.

$$\Delta L = P - C = 6{,}48\ mm \tag{3.4}$$

Finally, the preload exerted by the O-Ring is:

$$F_{OR} = \frac{\Delta L}{2} \cdot k_{OR} = 4{,}66\ N \tag{3.5}$$

If a FSU has one O-Ring inserted on each side, the O-Rings, that work as parallel springs, exerts an overall preload to the FSU equal to:

$$F_{FSU} = 4 \cdot F_{OR} = 18{,}64\ N \tag{3.6}$$

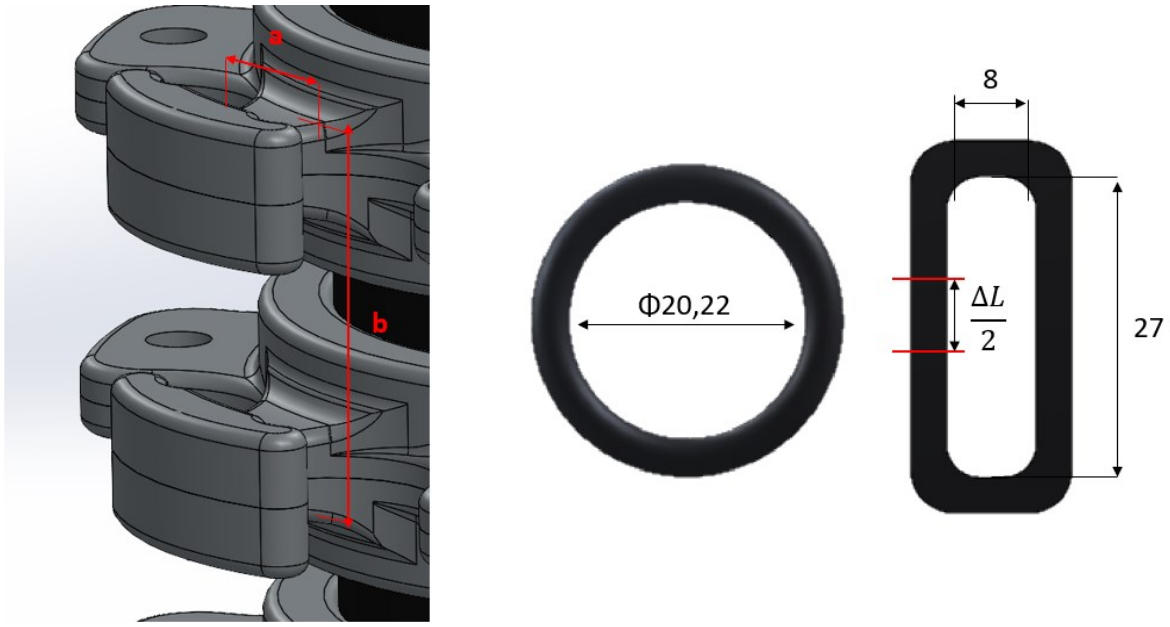


(a) (b)

Figure 3.11: **(a)** Space between two consecutive hooks, **(b)** undeformed and deformed O-Ring

## 3.4 BNP3 REDESIGN

Another purpose of this thesis is the instrumentation of the neck surrogate.
The idea is to implement sensors for the data acquisition of loads acting on the neck and displacements/rotations movements.
For loads acquisition a load cell will be installed between the nodding joint and the upper FSU, while for the displacements/rotations acquisition, 4 cable passing through the neck and insert into an instrumented base will be used (Chapter 5).
In order to make the BNP3 neck surrogate suitable for the implementation of those sensors, adjustment to some components of the BNP3 has been done.

### 3.4.1 Nodding joint V2

The new nodding joint presents four ϕ5 mm holes with countersinking to accommodate the heads of the screws for the load cell fastening.
This component will be manufacture in aluminum so the two slots for the rubber blocks for the head self-centering are plane to make easier the future manufacturing with machine tools. Two other slots have been added to reduce the overall weight of the component.
The hooks in the previous model have been removed as no longer necessary in this part, as also the semi-spherical cavity on the bottom and the four holes for the old nodding joint fixation.
The new model is thinner (4 mm) to reduce the axial dimension of the overall assembly having regard to the addition of the load cell and the flange described subsequently.
The outer diameter is the same of the old model (70 mm).

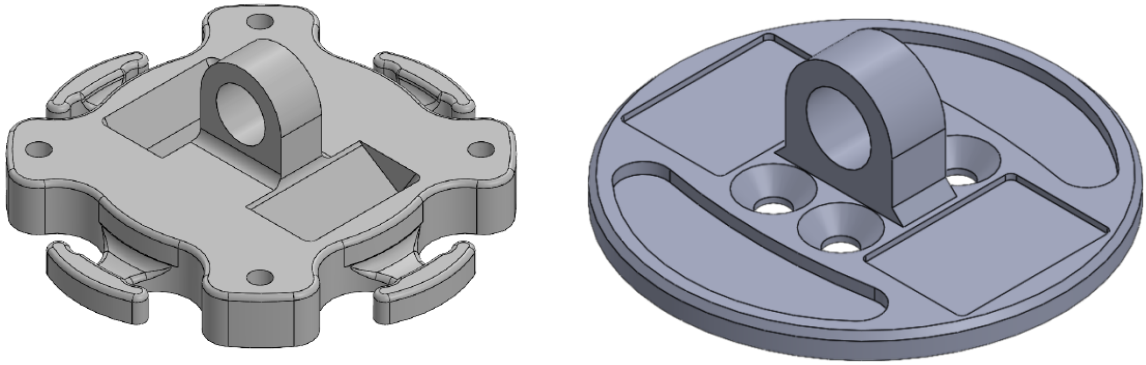

**(a)** Old model **(b)** New model

Figure 3.12: Old and new model of the Nodding joint

### 3.4.2 Flange

This new component has been designed to fix the load cell on the neck.
It has six ϕ5 mm holes with countersinking to accommodate the heads of the screws for the load cell fastening and four external holes for the neck side fastening.
A central hole of ϕ40 mm has been made to reduce the weight of the part.

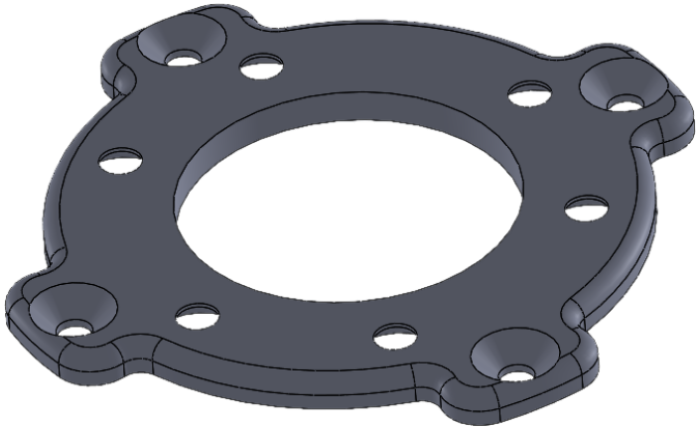

Figure 3.13: Flange model

### 3.4.3 Bottom vertebra and Upper vertebra V2

The main changes on these two components have been made to adapt the neck to the use of the four cables used for the instrumentation.
On the bottom vertebra the four hollows digged on the base have been removed as no longer necessary and the four tilted holes have been made completely vertical to allow the insertion of the cables into an instrumented base.
The upper surface of the upper vertebra has been redesigned to allow the accommodation and fixation of the four cables. The four hooks have been turned upside down as they replace the hooks removed from the Nodding joint. The four vertical holes for the PTFE tubes have been tilted by 65° in order to avoid the contact with the head of the inner cable.

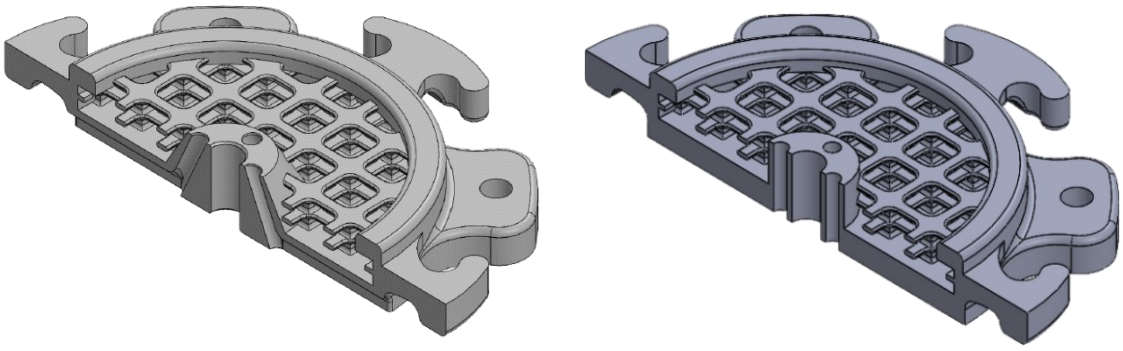

a) Old model **(b)** New model

Figure 3.14: Old and new model of the Bottom vertebra

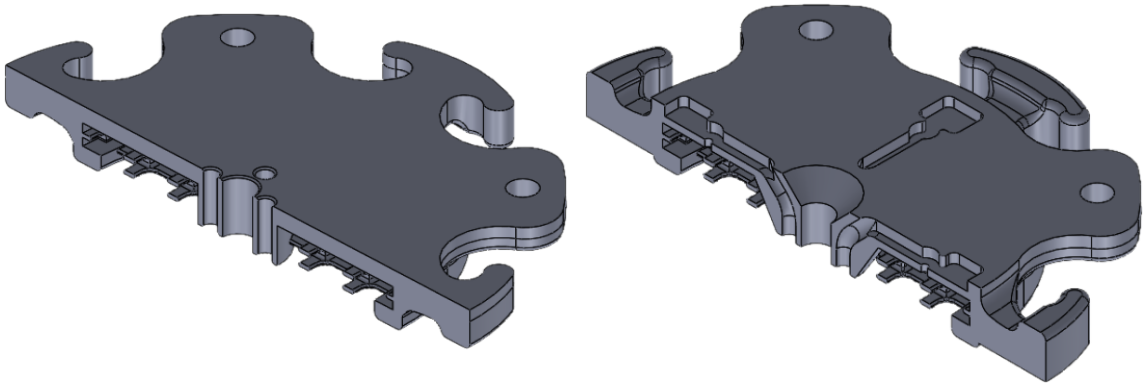

**(a)** Old model **(b)** New model

Figure 3.15: Old and new model of the Upper vertebra

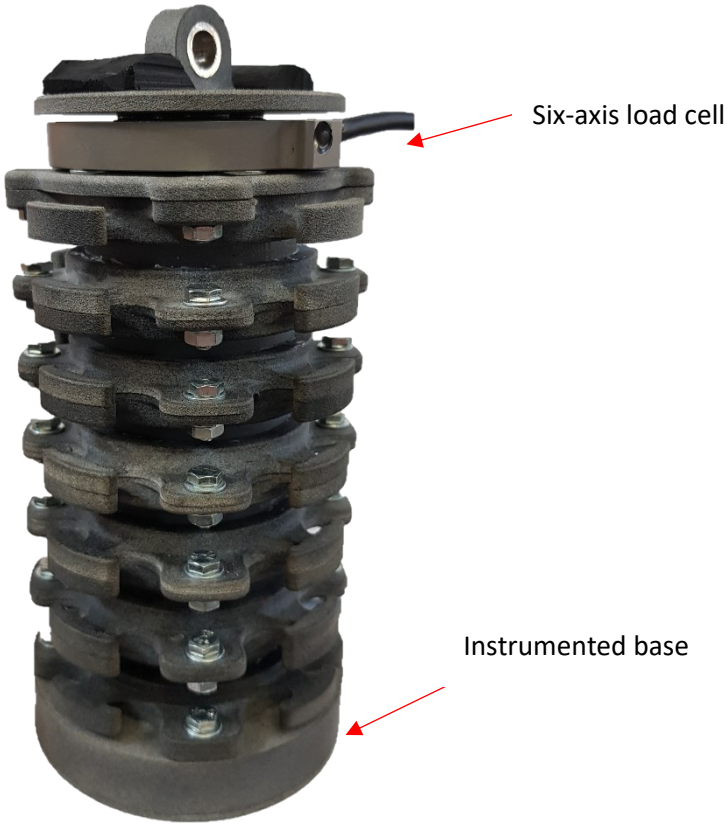


Figure 3.16: Second version of the BNP3 prototype adapted for the instrumentation of the neck

## 3.5 BNP3 Range Of Motion (ROM)

A first test on the new prototype was done to verify its biofidelity.
The range of motion (ROM) in flexion, extension and lateral bending of the BNP3 was compared with the ROM obtained by in vivo test.
Range of motion is the capability of a joint to go through its complete spectrum of movements and it can be passive or active.
Active range of motion is the range of motion that can be achieved when opposing muscles contract and relax, resulting in joint movement.
Passive range of motion can be defined as the range of motion that is achieved when an outside force causes movement of a joint and is usually the maximum range of motion that a joint can move.
The muscles system of the neck has not been implemented in this prototype yet.
Therefore, the BNP3 as it is (without any stiffening element) is not able to bear the weight of the Hybrid III head and the movements that it performs due to gravity when the head is mounted can be consider passive movements.
Hence, passive movements were considered for in vivo test.
In vivo data were obtained experimentally by capturing the passive movements of the head of a subject with a motion capture system. These data were then compared with the ones obtained from in vitro test where the BNP3, which mounted the Hybrid III head, performed the same movements done during in vivo test.

### 3.5.1 In vivo test

For this test three participants were chosen.
Subjects were seated on a chair keeping the trunk straight against the back of the chair and performed flexion, extension and lateral bending movements just relaxing the neck and letting the head fall in the different directions.
Each position was maintained for 10 seconds and the mean value of the angle reached in each phase was considered.
A motion capture system (SMART DX), tracked reflective markers placed on the head (3) and torso (5). The range of motion in flexion, extension and lateral bending was estimated by evaluating the maximum angle of the head relative to the fixed torso reached for each movement.

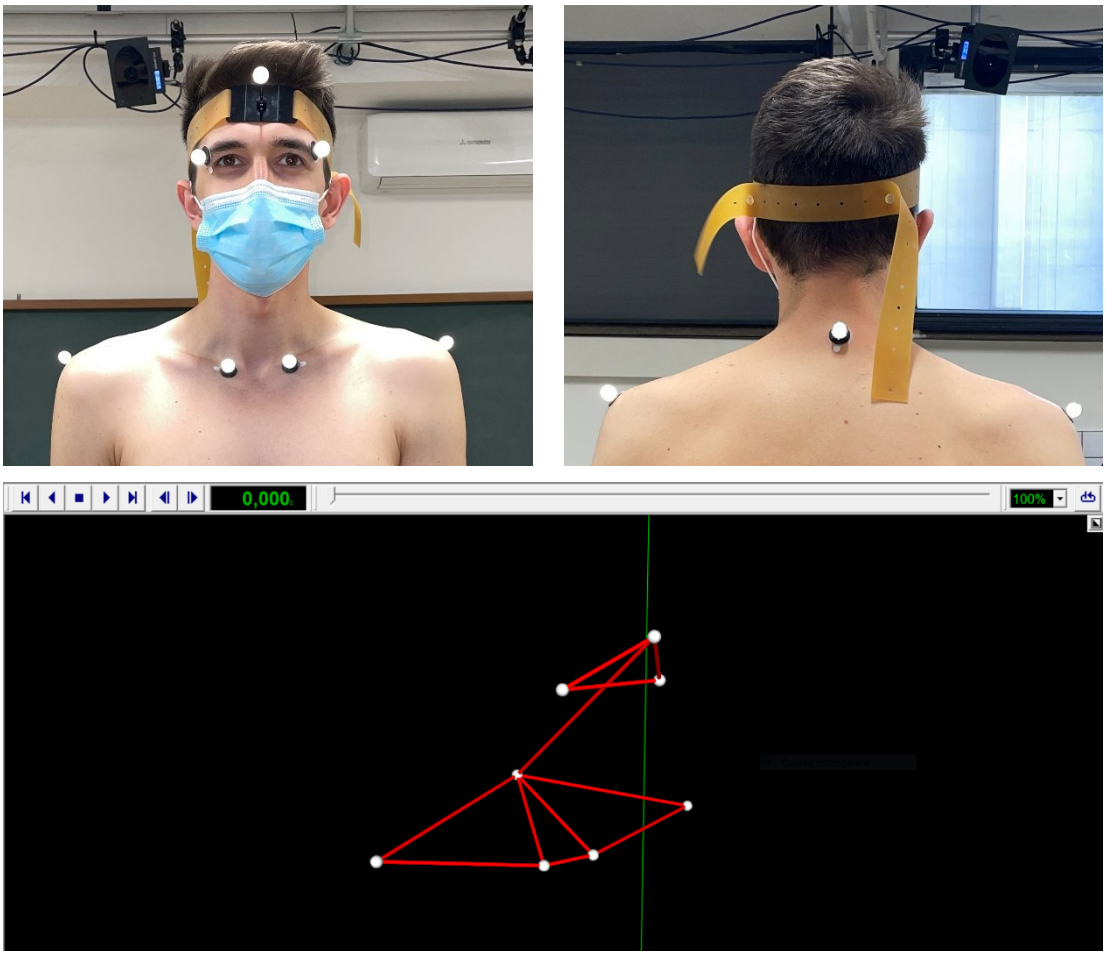


Figure 3.17: On the top the configuration of markers adopted for the test, on the bottom the tracking of the markers in SMART Analyzer environment

The relative angle between the head and torso should match with the absolute angle between the head and the reference frame of the laboratory since it was placed with the axes coincident with the three anatomical planes of the human body (frontal, sagittal and transverse) during the calibration phase of the motion capture system.
Figure 3.18 shows instead how there were discrepancies between the absolute (green curves) and relative angles (red curves) of the head.

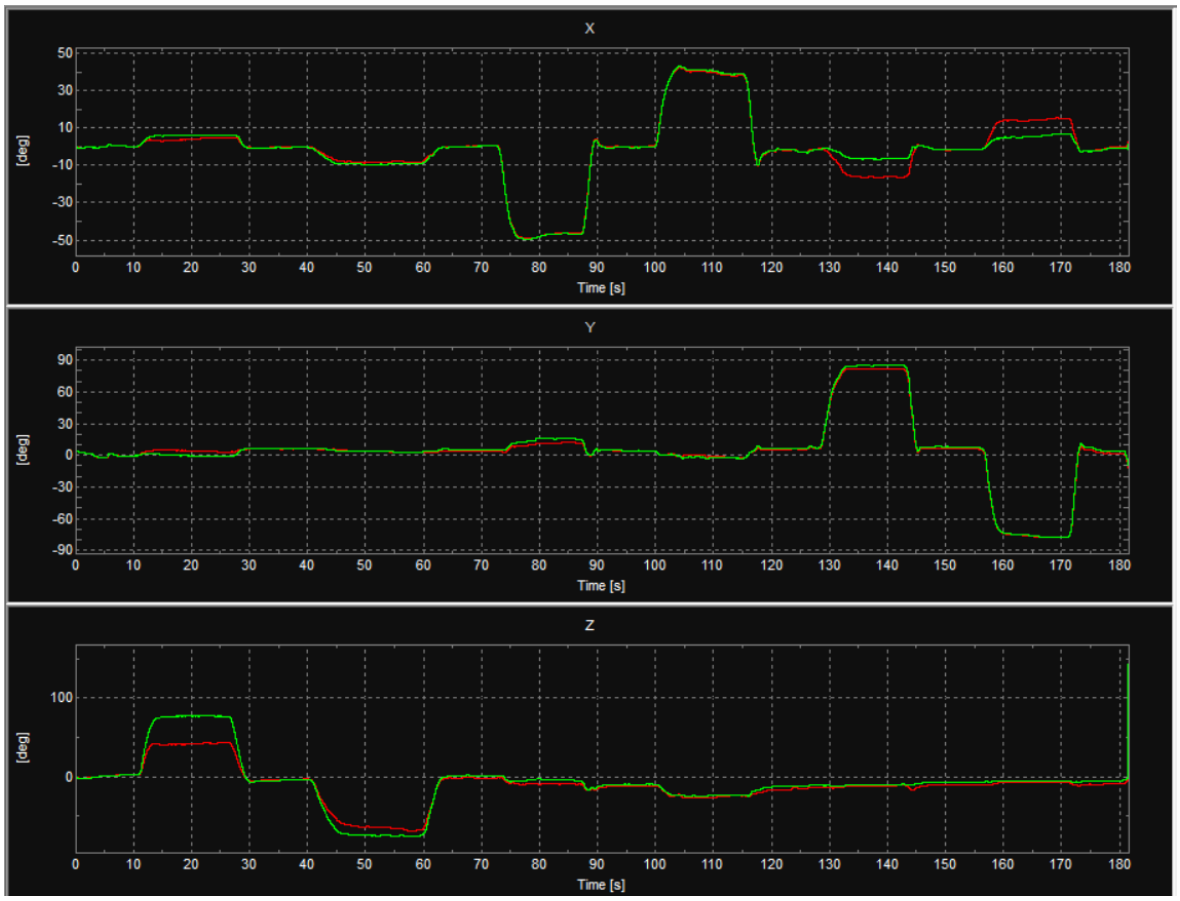


Figure 3.18: Absolute (green curves) and relative (red curves) angles of the head along X, Y and Z axis

The markers on the torso were supposed to be fixed in order to define the orientation of the fixed torso but the movements of the head stretch and relax the skin where the markers were placed causing their displacement and this caused the discrepancies just observed.
Considering another configuration of markers on the torso, placing three markers on the chest as shown in figure 3.19, these discrepancies between absolute and relative angle were reduced as the skin on the chest doesn't slide during head movements and the markers don't move.

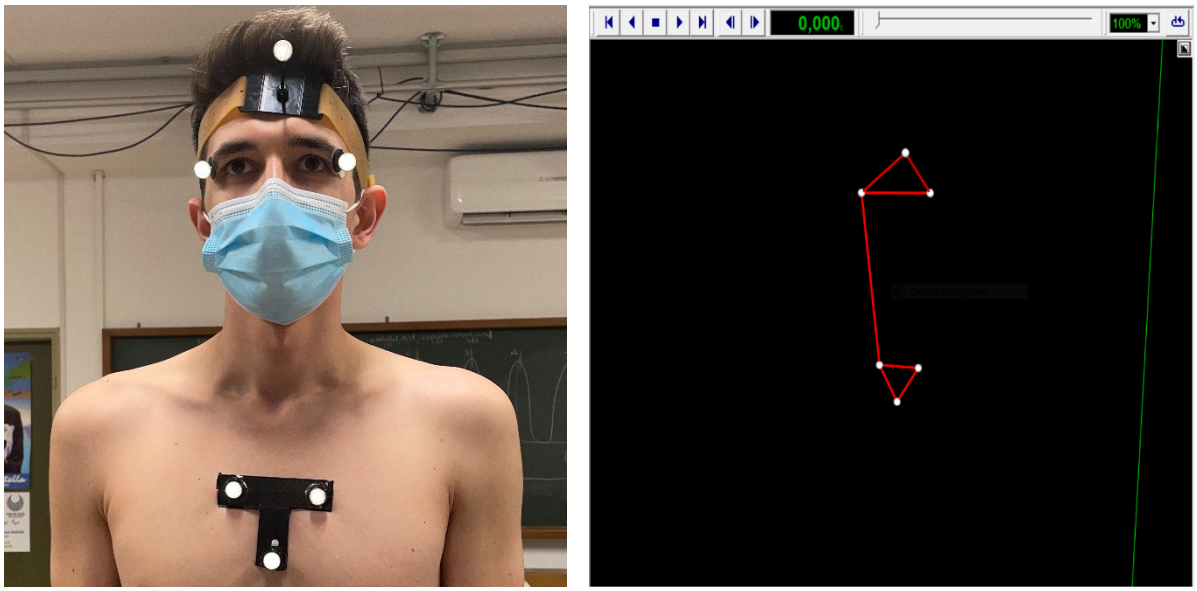


Figure 3.19: On the left the second configuration of markers with triad of markers on the chest, on the right the tracking of the markers in SMART analyzer environment

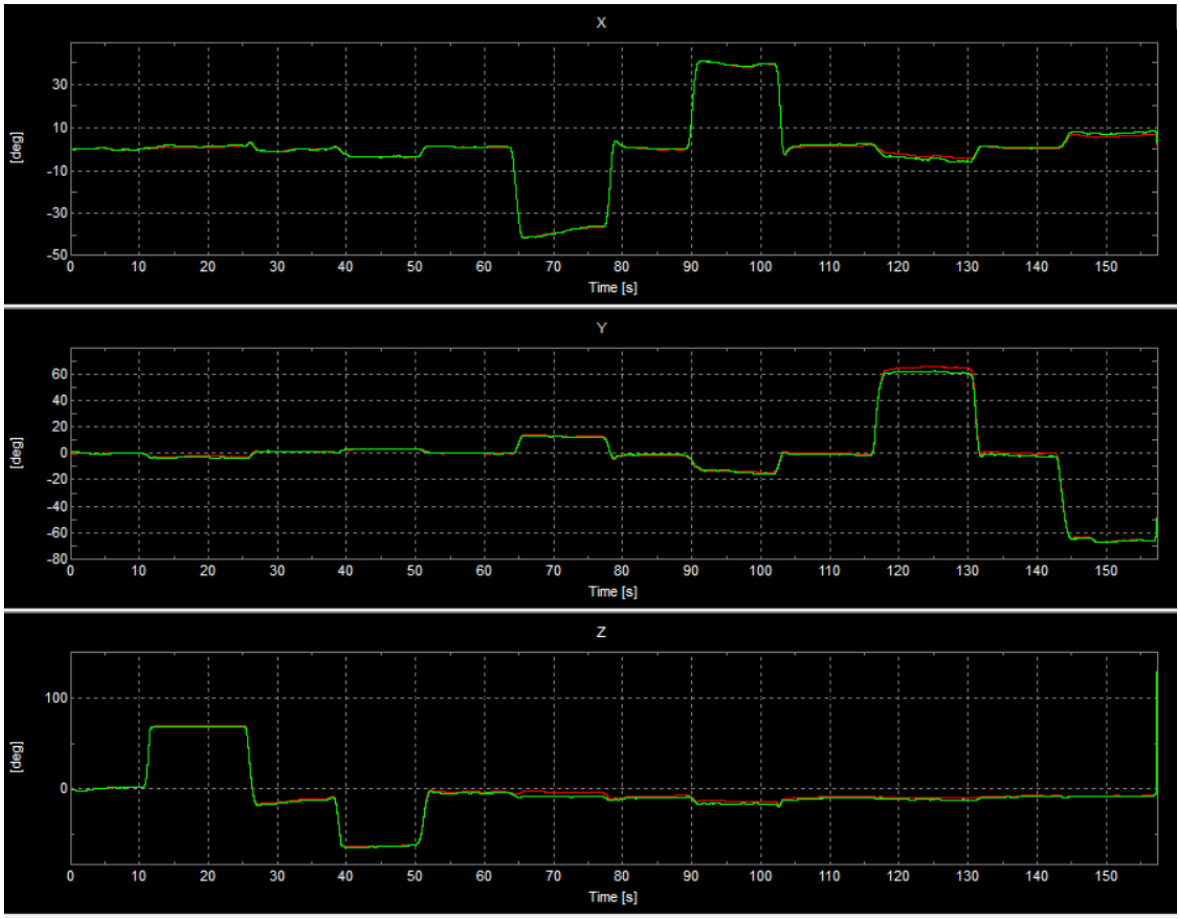


Figure 3.20: Absolute (green curves) and relative (red curves) angles of the head along X, Y and Z axis with the second configuration of markers on the torso

Proved that the absolute and relative angle of the head match, without repeat the whole test for each subject, the absolute angles of the head obtained with the first configuration of markers were considered to evaluate the range of motion of the human neck.
The results are reported in table 3.1.

| | Subject #1 | Subject #2 | Subject #3 | Mean | |
|---|---|---|---|---|---|
| | $\theta_H$ [deg] | $\theta_H$ [deg] | $\theta_H$ [deg] | $\theta_H$ [deg] | St. Dev. [deg] |
| **Flexion** | 76,67 | 73,2 | 62,66 | 70,84 | 7,3 |
| **Extension** | -74,85 | -59,68 | -63,48 | -66 | 7,89 |
| **Flex-Ext ROM** | 151,52 | 132,88 | 126,14 | 136,85 | 13,15 |
| **Lateral right** | 47,8 | 43,53 | 33,47 | 41,6 | 7,36 |
| **Lateral left** | -40,56 | -42,72 | -44,02 | -42,43 | 1,74 |
| **Lateral ROM** | 88,36 | 86,25 | 77,49 | 84,03 | 5,76 |

Table 3.1: Range of Motion of the human neck highlighted by in vivo test.

### 3.5.2 In vitro test

In vitro test was carried out with the BNP3 neck mounting the Hybrid III head.
The BNP3 was too compliant and reaching a stable position of the head during the test was not possible so it was installed the inner cable at 0 turns to confer a minimum stiffness to the neck.
For the test the Hybrid III head was manually placed in such a way that the neck reached the maximum configuration in flexion, extension and lateral bending.
As well as in vivo test, each position was maintained for 10 seconds and the mean value of the angle reached in each phase was considered, the motion capture system tracked three reflective markers placed on the Hybrid III head.
The range of motion in flexion, extension and lateral bending was estimated by evaluating the maximum absolute angle of the head relative to the laboratory frame.
The results of in vitro test are shown in table 3.2.

| | BNP3 + Hybrid III head + Inner cable |
|---|---|
| | $\theta_H$ [deg] |
| **Flexion** | 41,7 |
| **Extension** | -55,1 |
| **Flex-Ext ROM** | 96,8 |
| **Lateral right** | 52,5 |
| **Lateral left** | -33,9 |
| **Lateral ROM** | 86,4 |

Table 3.2: Range of Motion of the BNP3 neck highlighted by in vitro test

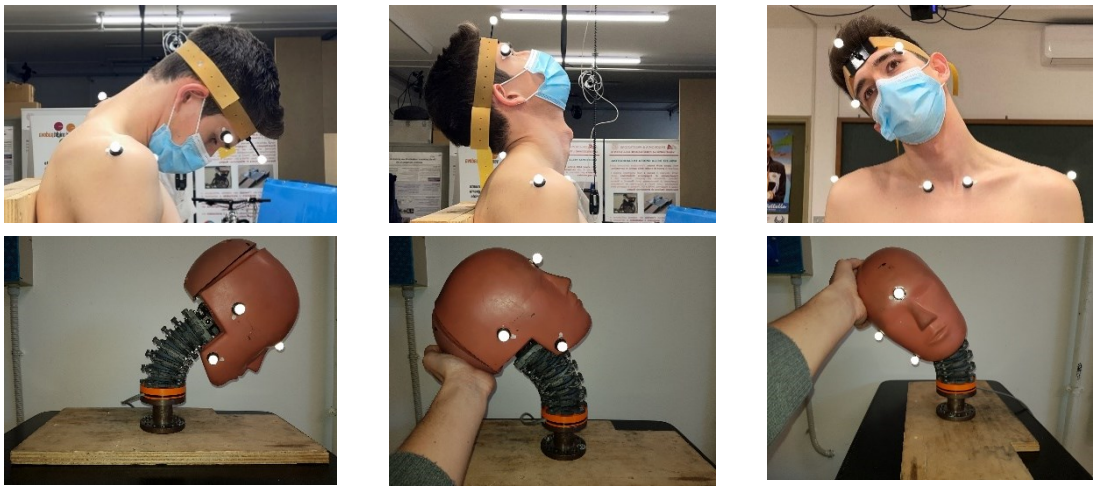

a) Flexion b) Extension c) Lateral Bending

Figure 3.21: Comparison between in vivo and in vitro range of motion in flexion, extension and lateral bending

### 3.5.3 Discussion

The new neck prototype range of motion is close to the real human neck one in lateral bending while in flexion and extension the difference is higher.
The difference observed in flexion and extension could be reduced by removing the inner cable that seem to restrict too much the maximum range of motion of the BNP3, in favor of two rows of O-Ring placed frontally and posteriorly.
Since the BNP3 has a symmetric geometry the lateral bending ROM in the two directions should be symmetric. The results showed in table 3.2 underline how the right lateral bending reach higher values than the left lateral bending.
This is due to the fact that the starting position of the head, corresponding to a 0° of flexion, extension and lateral bending was maintained manually without consider any kind of reference which could be for example a line drawn on the Hybrid III head that define the Frankfurt plane which is the anatomical position of the human skull, based on a plane passing through the inferior margin of the left orbit and the upper margin of each ear canal or external auditory meatus [34].

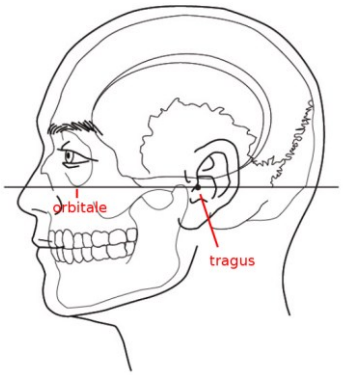


Figure 3.22: Head alignment according to the Frankfurt plane

# CHAPTER 4

# 4 BNP3 CHARACTERIZATION

This chapter focuses on the characterization of the new neck prototype.
Static and dynamic tests were carried out to evaluate the mechanical properties of the BNP3. Comparison with previous prototypes have been reported when possible.

## 4.1 STATIC FLEXION TESTS

Static tests were performed to evaluate the behavior of the BNP3 in static flexion in order to have a comparison with the previous surrogates and to check how far is this new prototype from biofidelity.
The main variable taken into account to compare the neck prototypes is the bending stiffness in flexion and extension evaluated as the slope of the linear regressions of the curves obtained from the tests.
Several configurations of the neck were tested considering the possibility to implement the stiffening measurements described in chapter 3 to evaluate how they contribute to the overall neck stiffness.

### 4.1.1 Test setup

To carry out the tests, a test bench that works on the same principle of the one employed by Rango M. [32] was used.
This test bench allows to apply a pure bending moment to the specimen under investigation and makes possible a comparison with cadaver literature data under the same load conditions [34], [35].
Two forces, with same magnitude and direction but opposite sign, are applied each at one end of an M10 bar fixed to the upper vertebra, while the lower one is fixed.
The force comes from known weight equally divided for each bar end. At one extremity, a pulley allows to change the direction of the force, which is now upwards.
A six-axis load cell measures the moments applied and ensures that the moment remains pure while the flexion/extension angle data are collected by an Inertial Measurement Unit (IMU), wireless connected to a pc and mounted on the top of the upper vertebra.
The base consists of four aluminum profiles and, at the center of it, the load cell is fixed.
Before mounting the neck, a flange is interposed as a spacer. A vertical M12 bar with a pulley on the top is used to counterweight the M10 bar.

Figure 4.1: Static test bench for bending stiffness evaluation employed by Rango M [32].

The test bench used for the current study has some differences with respect to the ones employed by Rango M.
The M10 bar was replaced with two L shaped aluminum bars and the base constituted of four aluminum profiles was replaced with a heavy steel plate.
The vertical M12 bar for the counterweighting of the M10 bar was removed as the weight of the two aluminum bars (200 g) was considered negligible with respect to the weight of the previous M10 bar (800 g).
The two plastic cups were replaced with two plates to make easier the removal of the loads for the unloading phase.
The flexion/extension angle data were acquired using a Motion Capture System (SMART DX).

Figure 4.2: Current static test bench for bending stiffness evaluation

### 4.1.2 Test method

A calibration of the cameras of the motion capture system is needed to define the work space in which the tests are done.
Each test was done by applying known weights to both plates, in this case M12 screws with a weight of 39 g were used, the starting point wants a system completely unloaded with the two L shaped bars horizontal. This configuration defines the neutral position of the neck corresponding to a 0° of flexion/extension movements. After 10 seconds the two plates are applied and the test proceed with eight load steps (the first five with 1 screw of load for each plate while the last 3 with two screws of load for each plate), followed by the unloading steps. After the positioning of each load, the first 5 seconds were neglected in the analysis to allow load stabilization and a repeatable measure given the viscoelasticity of the material. After this time, mean values of moment and angle were considered for the results.
The bending moments applied to the neck are collected by the load cell, to synchronize the data collected by motion capture system a digital input from a trigger box was used as a reference to start the data collection.
SMART Tracker was used for the tracking of the reflective markers. A triad of markers were placed on the top of the neck to capture its rotation, five markers were placed on the right lateral side of the neck in correspondence of C2 C4 C5 C6 and base, two markers were placed on the frontal and back side in correspondence of C5 and C6 to capture the maximum opening and closing of a FSU, two markers were finally placed each at one end of the L shaped bars to evaluate how the lever arm of the forces change during the load steps.
SMART Analyzer was used to create the protocol for the Motion capture data processing.
SoMat is the Data Acquisition System used to collect and post process data from the load cell.
All data have finally been processed in Matlab environment.

.


Figure 4.3: From the left to the right, markers configuration on the neck, samples of screws used as weights, Data Acquisition System

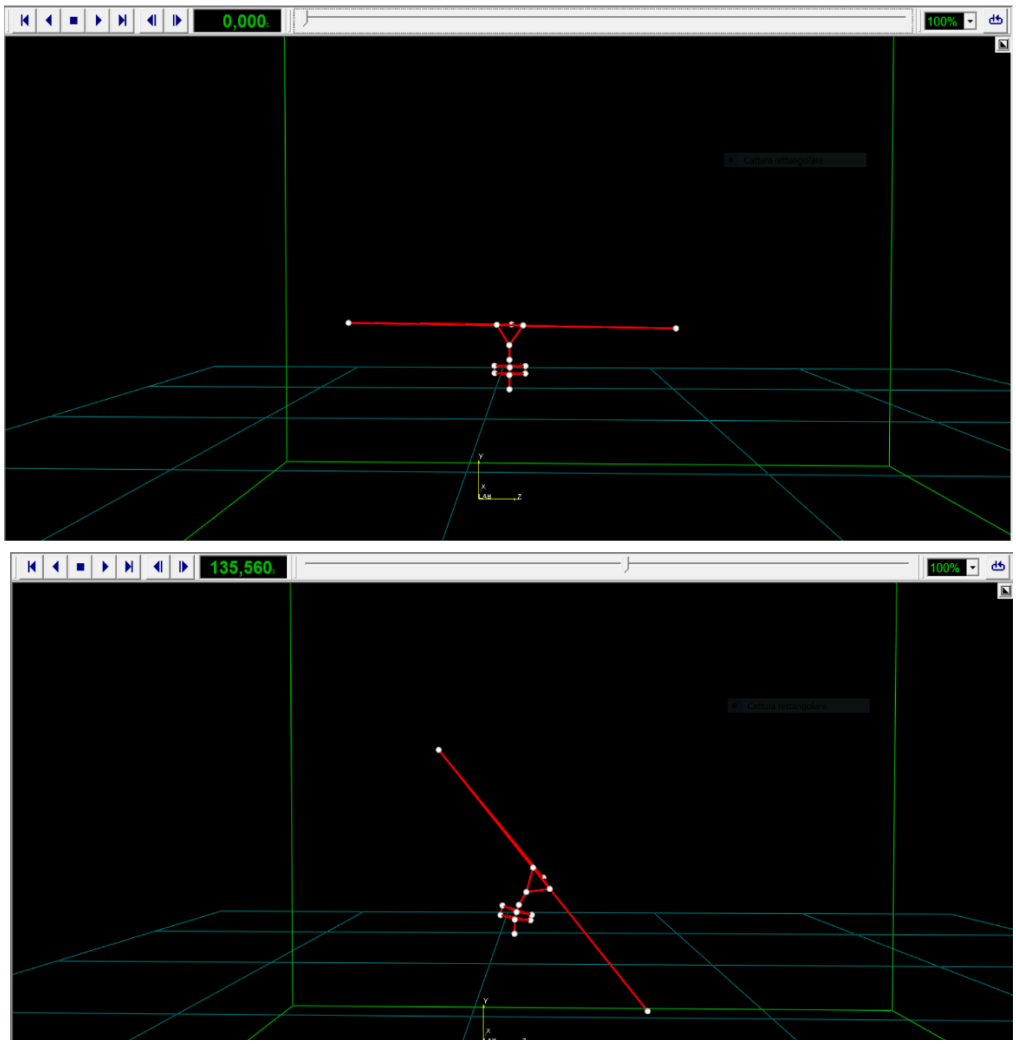


Figure 4.4: Example of tracking in SMART Tracker environment, on the top the figure shows the starting neutral position of the system, on the bottom the system configuration when the maximum load is applied

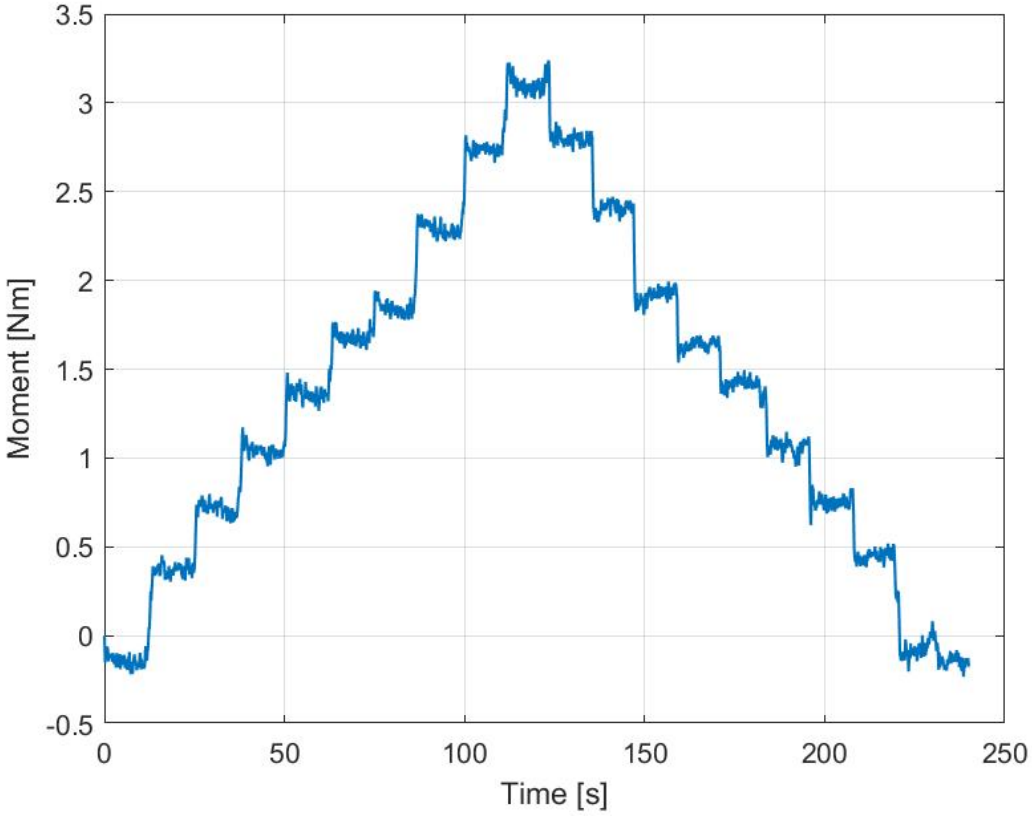


Figure 4.5: Moments over time collected by the load cell in a load and unload run (signals filtered using a second order Butterworth low pass filter having a 2 Hz cutoff frequency)

For the evaluation of bending stiffness of each neck configuration tested, the slope of the linear regression of the curve obtained considering the mean values of moment and angle between the loading and unloading phase was considered. The R-squared value was evaluated to check how far the linear regression from the real curve trend was.
A hysteretic behavior was observed within the loading and unloading phase, the dissipated energy $E_d$ was evaluated considering the area defined by the two curves.

### 4.1.3 Neck configurations tested

Several tests were performed with different neck configuration, the convention used to define the different configurations is explained below and the summary of the tests performed is reported in table 4.1.

- BNP3 is the neck prototype as it is
- OR stands for O-Ring and is followed by the label FBL.
  FBL stands for frontal, back and lateral (considering that the test bench performs a flexion movement to the neck) and states the sides where the O-Rings are applied.
  Example:
  a) F2B2L means that two rows of O-Rings are applied frontally, two rows of O-Rings are applied posteriorly and one row of O-Rings is applied on each of the two laterals side of the neck.
  b) FB means that one row of O-Rings is applied frontally and one row of O-Rings is applied posteriorly, no O-Rings are applied laterally.
- IC stands for Inner cable and is followed by a number that states how many turns of the nut were done when the inner cable is installed.
  Example:
  c) IC3 means that the Inner cable is installed with 3 turns of the nut.

| | **Neck configuration** |
|---|---|
| **New neck surrogate** | BNP3 (base) |
| **O-Rings contribution** | BNP3-OR-FB |
| | BNP3-OR-FBL |
| | BNP3-OR-FB2L |
| | BNP3-OR-F2B2L |
| **Inner cable contribution** | BNP3-IC0 |
| | BNP3-IC3 |
| | BNP3-IC6 |
| **O-Rings + Inner cable contribution** | BNP3-OR-FB-IC3 |
| | BNP3-OR-FBL-IC3 |
| | BNP3-OR-FB2L-IC3 |

Table 4.1: List of the neck configurations tested

### 4.1.4 Results

The results obtained from the tests are reported below for the different neck configurations tested.

- **BNP3 (base)**

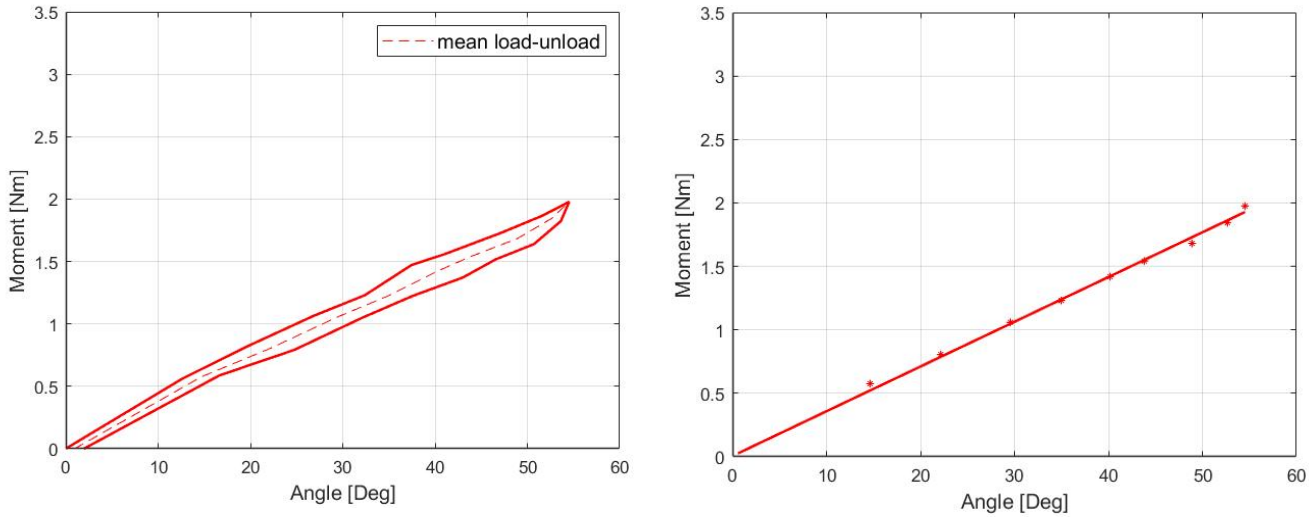


Figure 4.6: On the left the trend of flexion angles of the BNP3 neck in loading and unloading phase, on the right the linear regression of the curve obtained considering the mean values of moment and angle between the loading and unloading phase

| | $K_{flex}$ [Nm/°] | $R^2$ | Ed [J] |
|---|---|---|---|
| **BNP3** | 0,0353 | 0,99 | 0,159 |

Table 4.2: Stiffness and dissipated energy of the BNP3 neck surrogate for static flexion test

- **O-Rings contribution**

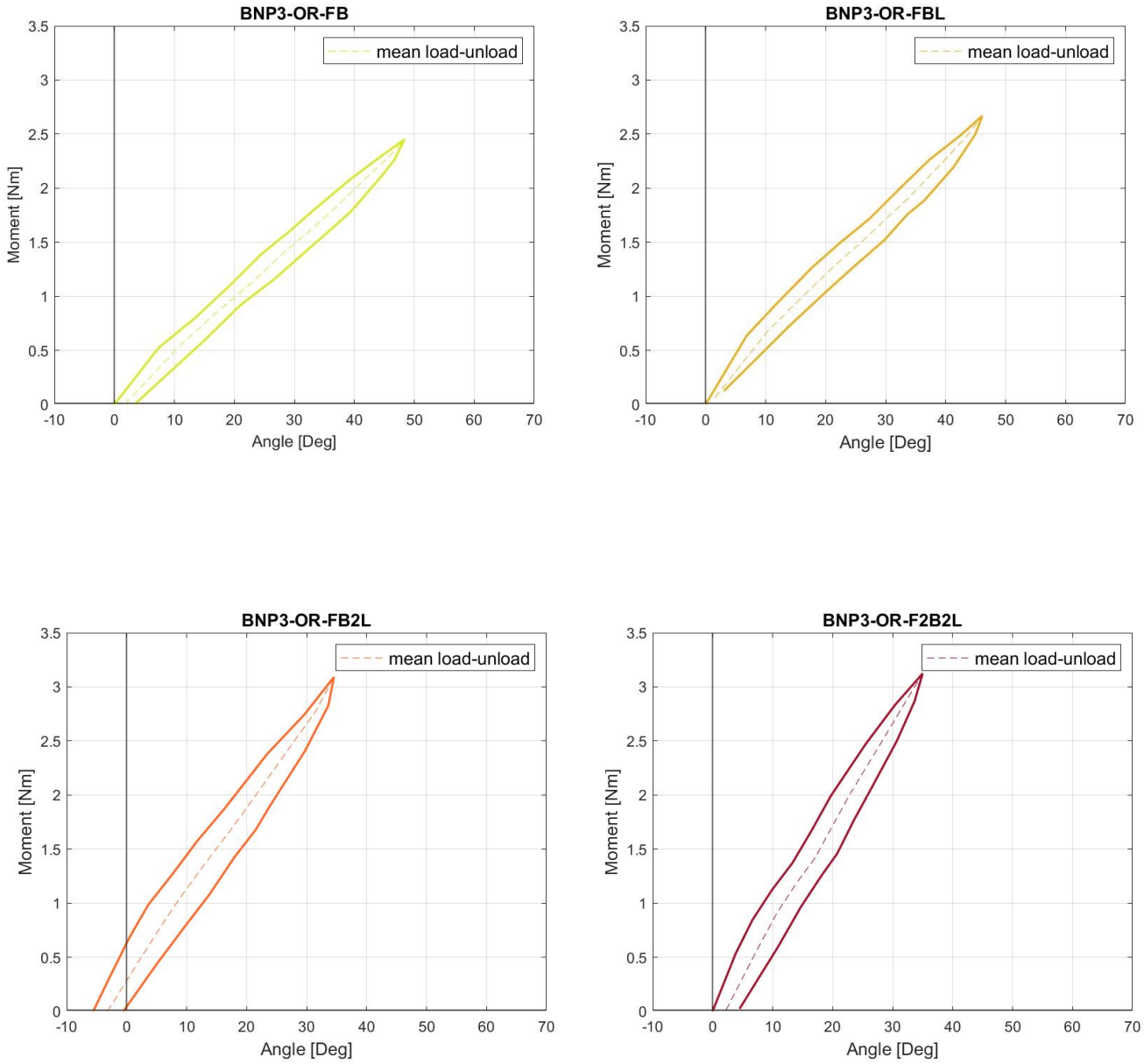


Figure 4.7: Trends of flexion angles in loading and unloading phase of the BNP3 with O-Rings applied in different configurations

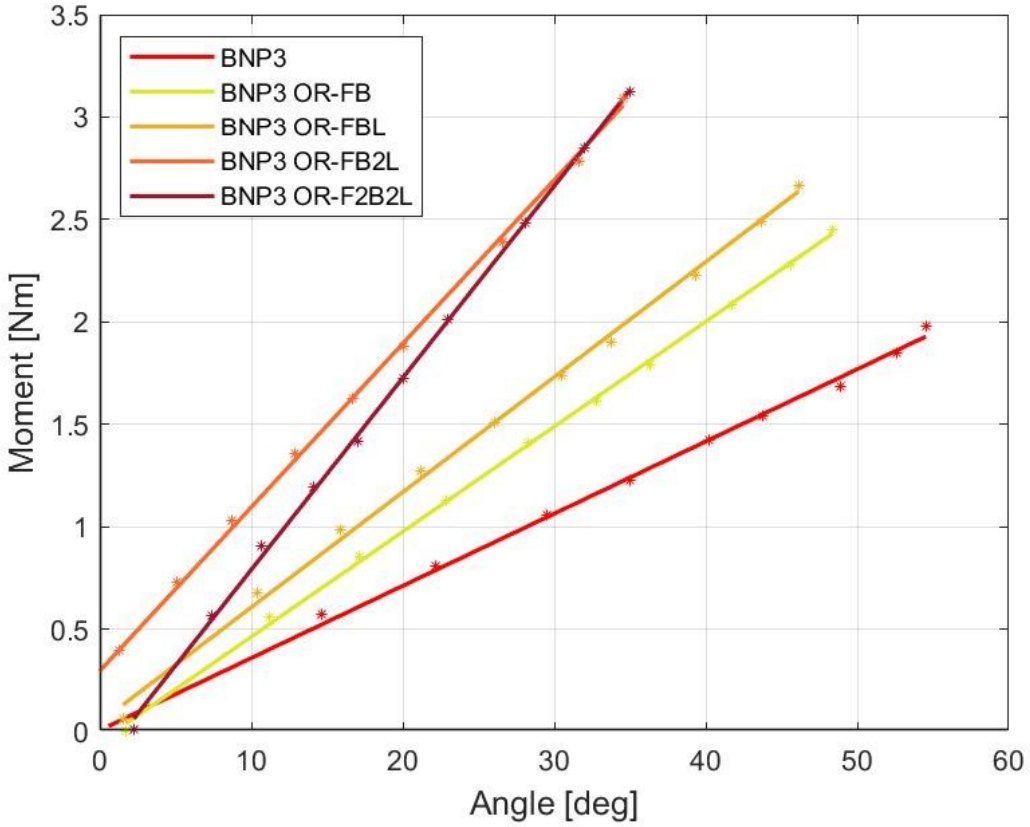


Figure 4.8: Linear regressions of the curves obtained considering the mean values of moment and angle between the loading and unloading phase in “O-Rings contribution” tests

| | $K_{flex}$ [Nm/°] | $K_{flex}/K_{BNP3}$ | $R^2$ | Ed [J] | $Ed/Ed_{BNP3}$ |
|---|---|---|---|---|---|
| **BNP3-OR-FB** | 0,0513 | 1,45 | 0,999 | 0,226 | 1,42 |
| **BNP3-OR-FBL** | 0,0562 | 1,59 | 0,997 | 0,228 | 1,43 |
| **BNP3-OR-FB2L** | 0,0799 | 2,26 | 0,999 | 0,35 | 2,2 |
| **BNP3-OR-F2B2L** | 0,0936 | 2,65 | 0,999 | 0,29 | 1,82 |

Table 4.3: Stiffness and dissipated energy of the BNP3 neck surrogate with O-rings applied in different configurations for static flexion test

- **Inner cable contribution**

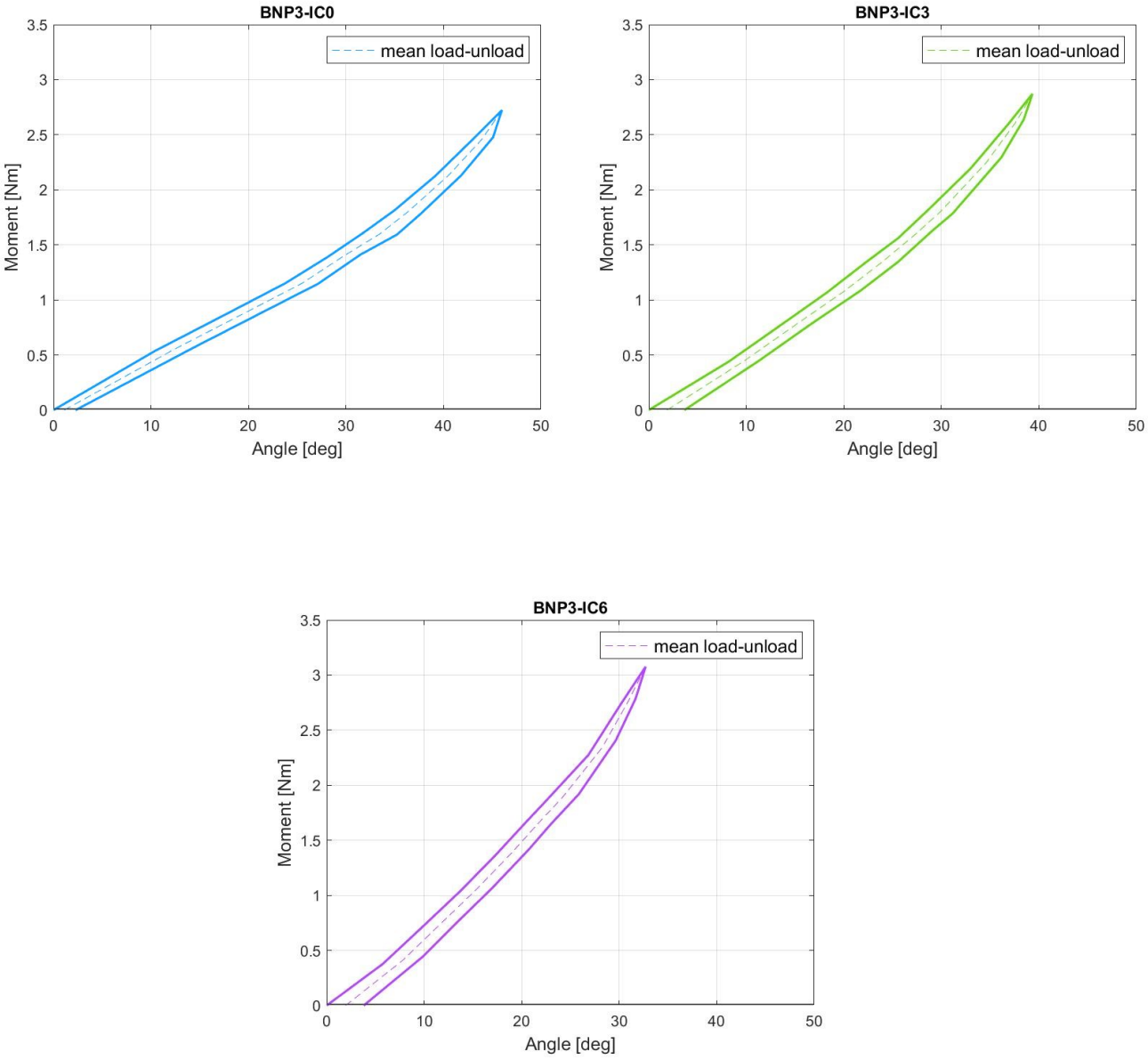


Figure 4.9: Trends of flexion angles in loading and unloading phase of the BNP3 with Inner cable installed with 0, 3 and 6 turns of the nut

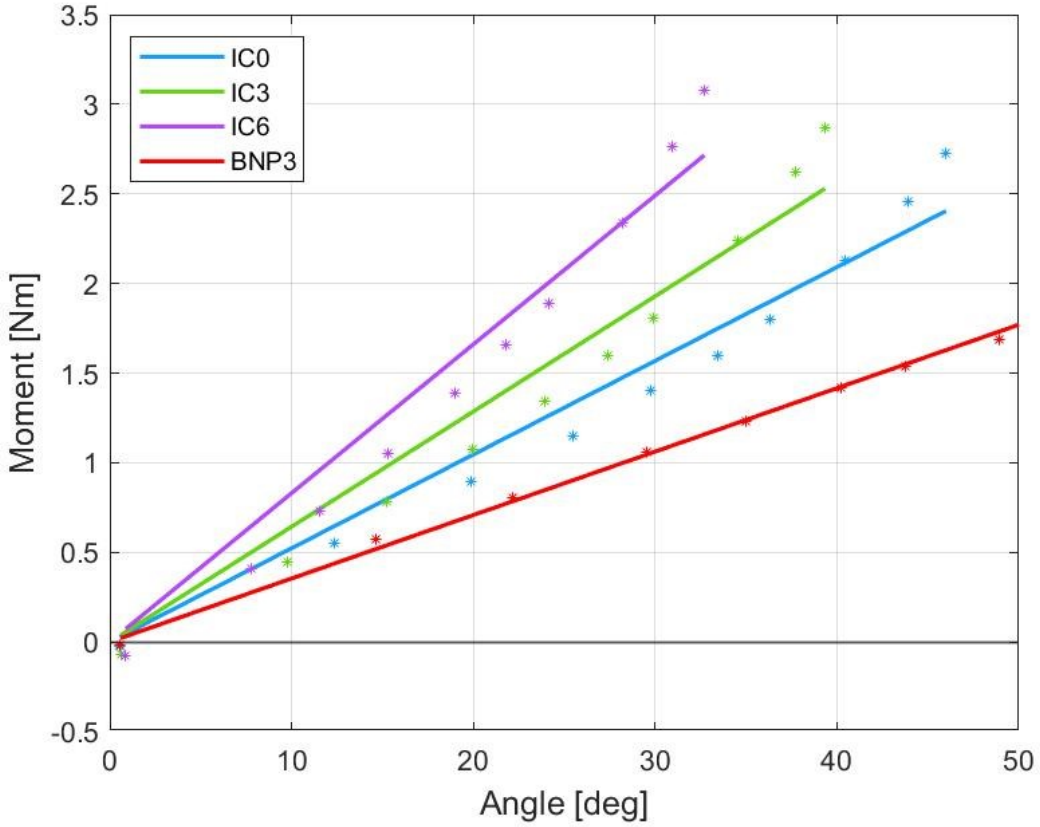


Figure 4.10: Linear regressions of the curves obtained considering the mean values of moment and angle between the loading and unloading phase in “Inner cable contribution” tests

| | $K_{flex}$ [Nm/°] | $K_{flex}/K_{BNP3}$ | $R^2$ | Ed [J] | $Ed/Ed_{BNP3}$ |
|---|---|---|---|---|---|
| **BNP3-IC0** | 0,0523 | 1,48 | 0,962 | 0,134 | 0,842 |
| **BNP3-IC3** | 0.0643 | 1,82 | 0,955 | 0,133 | 0,846 |
| **BNP3-IC6** | 0,083 | 2,35 | 0,955 | 0,136 | 0,855 |

Table 4.4: Stiffness and dissipated energy of the BNP3 neck surrogate with Inner cable installed with 0, 3 and 6 turns of the nut for static flexion test

- **O-Rings + Inner cable contribution**

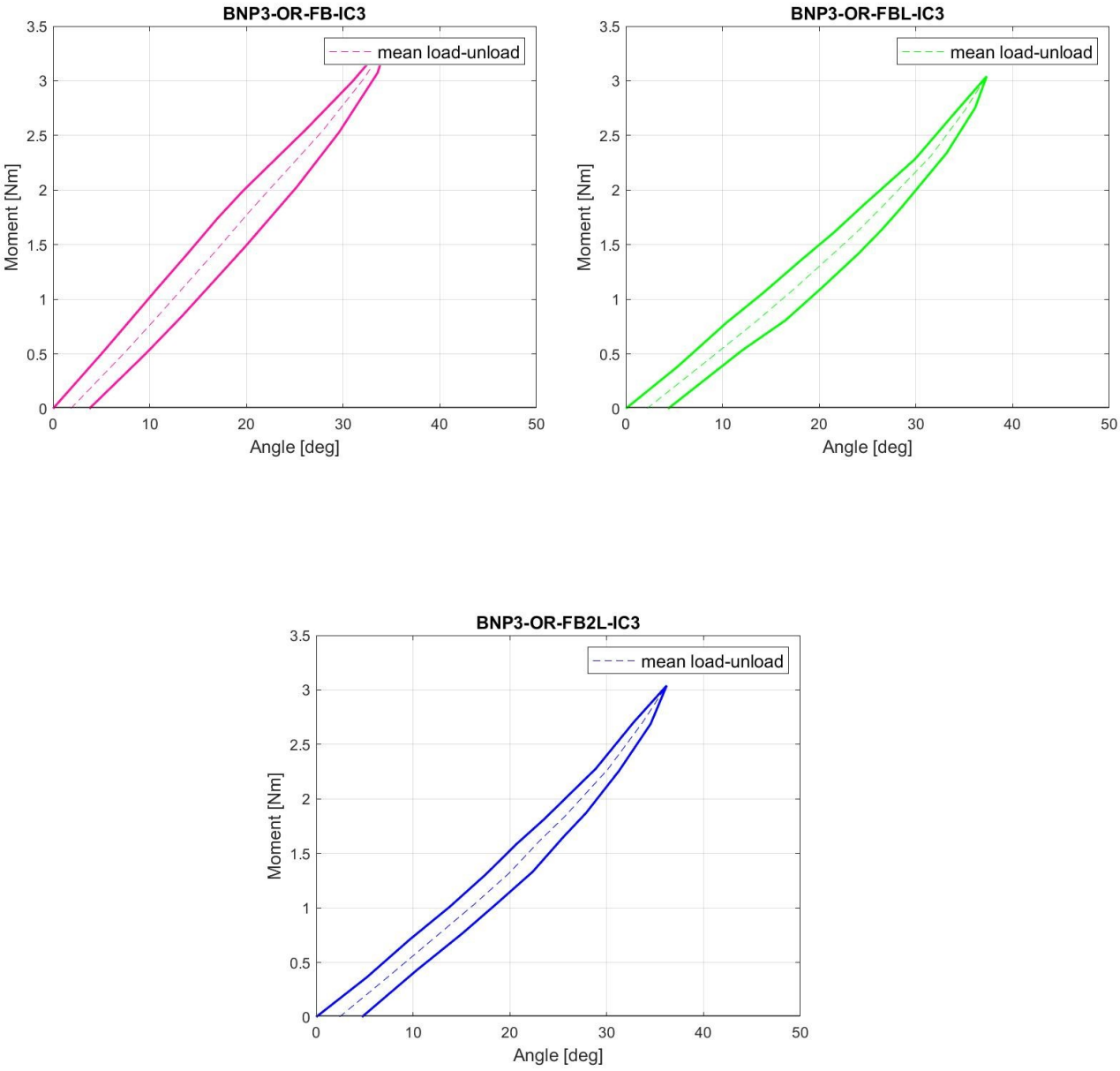


Figure 4.11: Trends of flexion angles in loading and unloading phase of the BNP3 with Inner cable installed and O-Rings applied in different configuration

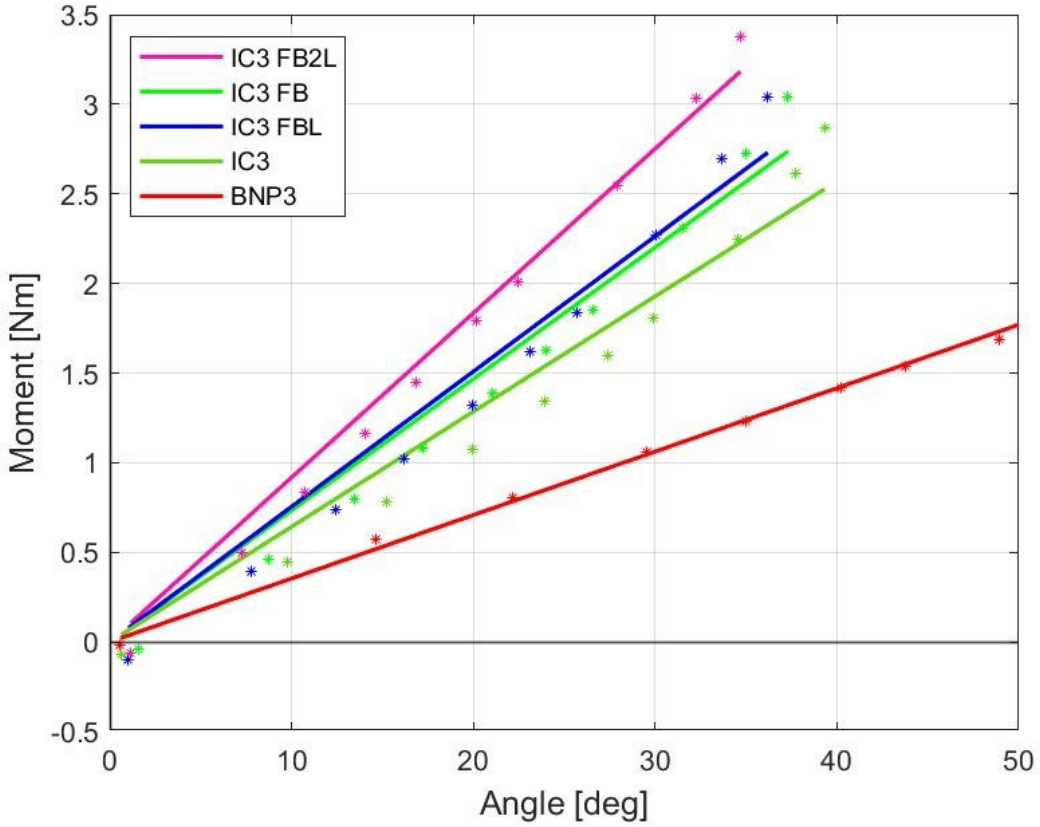


Figure 4.12: Linear regressions of the curves obtained considering the mean values of moment and angle between the loading and unloading phase in “O-Rings + Inner cable contribution” tests

| | $K_{flex}$ [Nm/°] | $K_{flex}/K_{BNP3}$ | $R^2$ | Ed [J] | $Ed/Ed_{BNP3}$ |
|---|---|---|---|---|---|
| **BNP3-OR-FB-IC3** | 0,073 | 2,068 | 0,966 | 0,21 | 1,32 |
| **BNP3-OR-FBL-IC3** | 0.075 | 2,12 | 0,964 | 0,192 | 1,21 |
| **BNP3-OR-FB2L-IC3** | 0,091 | 2,58 | 0,986 | 0,245 | 1,54 |

Table 4.5: Stiffness and dissipated energy of the BNP3 neck surrogate with Inner cable installed and O-Rings applied in different configuration for static flexion test

### 4.1.5 Discussion

The stiffness of the BNP3 neck surrogate is very close to the one of the previous prototype (BNP2), this is an expected result since the rubber used to replicate the intervertebral disc is the same for the two prototypes.
Figure 4.6 shows the maximum flexion angle reached during the test, that is 54,53° for an applied moment of 1,98 Nm.
Figure 4.8 shows how the O-Rings and their distribution influence the stiffness of the neck. O-Rings applied on lateral sides of the neck contribute to neck stiffness in flexion and extension, the stiffness of “BNP3-OR-FBL” configuration is in fact higher than “BNP3-OR-FB” configuration.
For the asymmetric “BNP3-OR-FB2L” configuration a starting moment different to 0 Nm is necessary to keep the neck in a straight initial configuration corresponding to a 0° of flexion and extension.
Two rows of O-Rings for each frontal and back side significantly increase the stiffness of the system, comparing “BNP3-OR-F2B2L” and “BNP3-OR-FBL” configurations, the stiffness increases by 66,54%.
With the application of O-Rings the moment-angle curves maintain a linear trend, but the hysteresis and the dissipated energy Ed increase.
Figure 4.10 shows the contribution of the inner cable in neck stiffening.
Even with 0 turns of the nut, that correspond to 0 N of axial load on the neck, the flexural stiffness of the neck increases by 48,2% since the Inner cable limits the overall movements of the neck as already seen in BNP3 range of motion test (3.5).
The installation of the Inner cable introduces a non-linearity for high flexion angles as shown in figure 4.9, which results in a reduction of the $R^2$ index.
The Inner cable doesn’t introduce further hysteresis to the system; the values of dissipated energy evaluated in “Inner cable contribution” are lower than the dissipated energy evaluated for the BNP3 without Inner cable because the maximum flexion angles reached during the tests with Inner cable are lower.
Finally, Figure 4.12 shows the contribution of O-Rings and Inner cable in neck stiffening when they are applicated at the same time.
Their contribution can be considered additive since starting from the configuration of neck with only Inner cable installed at 3 turns, the flexural stiffness increases when the O-Rings are added. In this case the non-linearity introduced by the Inner cable is less pronounced.
Comparing the results shown by figure 4.8, 4.10 and 4.12, it is noted that the different tests reach different values of maximum flexion moment even if the loads applied are the same in each test. Sketch in figure 4.13 explains how wider angles of flexion produces lower values of moment with the same force applied since the rotation of the bar reduce the lever arm of the forces.
This is a limit of the test bench used to carry out the static test.
Another problem related to the rotation of the bar for wide flexion angles is the development of a horizontal shear component of the upward force that occur due to the no longer vertical orientation of the wire as shown in figure 4.14.

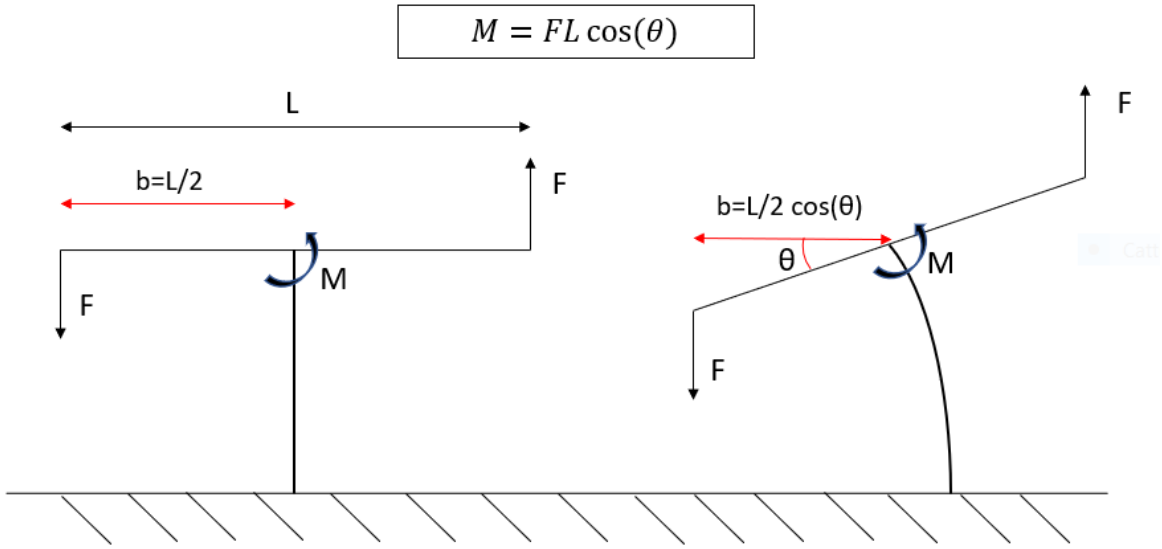


Figure 4.13: Sketch that explains how the lever arm is reduced due to the rotation of the bar

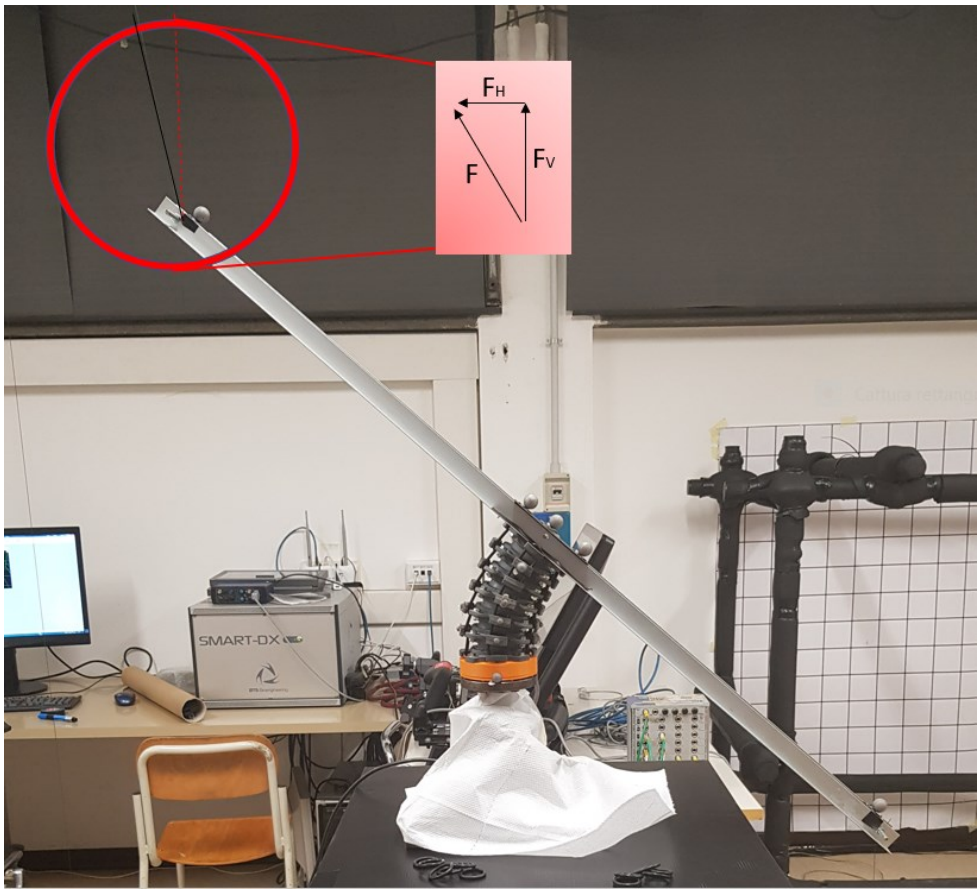


Figure 4.14: Horizontal component of the upward force generated for wide flexion angles

This problem was partially solved by placing the pulley that change the direction of the force as high as possible in order to reduce as much as possible the horizontal component of the force.
Another issue that emerged from the tests is that the effects of stiffening components (O-Rings and Inner cable) are not independent each other, if the Inner cable is installed first, the following addition of O-Rings will discharge the load generated by the Inner cable and vice versa, therefore the order of application of stiffening components is significant.
For that reason, for future tests is suggested to apply first the O-Rings and then the Inner cable.
In conclusion a comparison with the previous prototypes can be made.
Table 4.6 summarize the results obtained so far with the BNP prototypes in terms of flexural behavior and compares these results with the ones obtained testing the Hybrid III neck and the ones evaluated from cadaveric data from Nightingale.
The stiffness in flexion and extension for the BNP prototypes is the same since the necks present a symmetric geometry with respect to the frontal and sagittal plane.
The stiffness values reported has been estimated considering the slope of the linear regressions of the curves obtained from static flexion tests and showed in figure 4.15.

| Neck | $K_{flex}$ [Nm/°] | $K_{ext}$ [Nm/°] |
|---|---|---|
| **BNP1** | 0,261 | 0,261 |
| **BNP2** | 0,029 | 0,029 |
| **BNP3** | 0,035 | 0,035 |
| **Hybrid III** | 2,54 | 1,17 |
| **Nightingale (Linear regression)** | 0,033 | 0,043 |

Table 4.6: Comparison of flexion and extension stiffness of BNP prototypes with Hybrid III neck and cadaveric data from Nightingale for static flexion test.

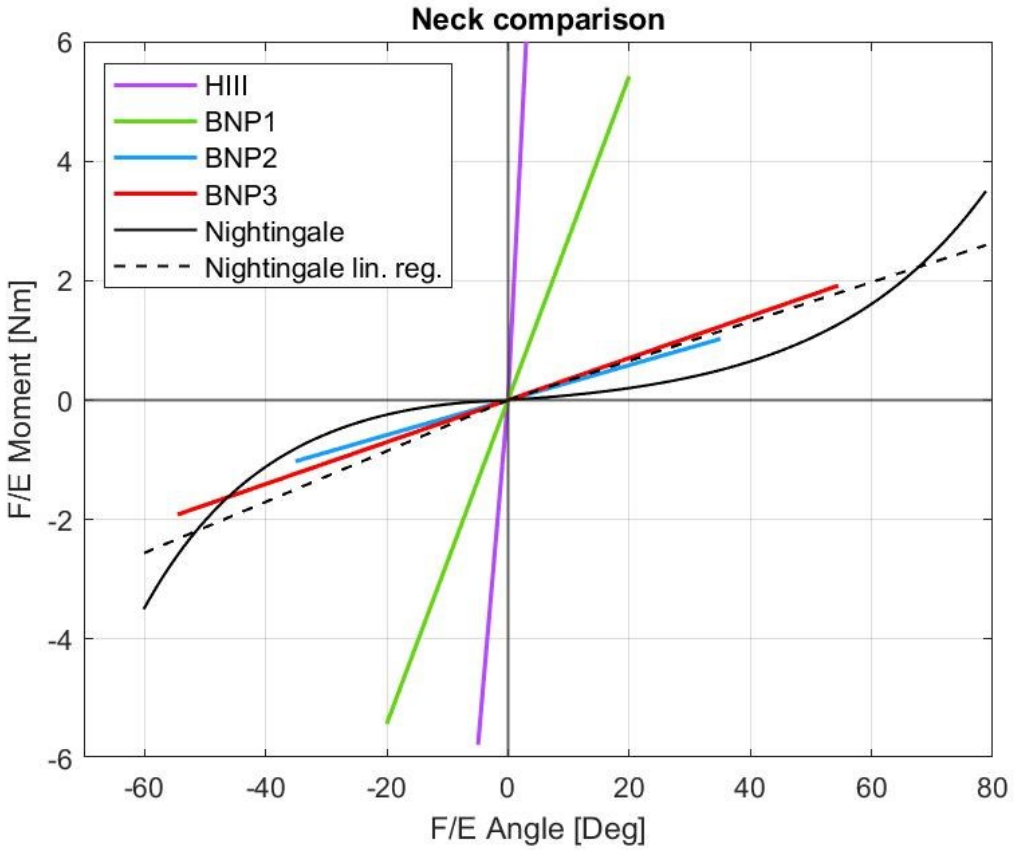


Figure 4.15: Neck overall comparison plot for static flexion test

More effort is needed to reach a more biofidelic behavior; a feature that allow to mimic the initial neutral zone of a real human cervical spine is necessary as also the implementation of elements that introduces stiffening only when the neck reaches wide angles of bending.

## 4.2 AXIAL COMPRESSION TEST

The BNP3 neck was tested in axial compression using a servohydraulic cylinder from “Colossus” test bench available at the University’s laboratory.
As is shown in figure 4.16 a cylindrical tube is fixed to the extremity of the cylinder to uniformly compressing the neck at a specified rate of 0,5 mm/s.
The compression load was acquired by a load cell and then the Load-Displacement curve has been plotted.
From this curve the axial stiffness of the neck has been evaluated.
Load-displacement curve can be also used to estimate the load on the Inner cable when it is installed as stiffening component, for example the compression load for 0,8 mm of axial displacement of the neck, corresponds to the load on the Inner cable when it is installed with 1 turns of the nut since the pitch of the screw is equal to 0.8 mm and 1 turns of the nut corresponds to 0,8 mm of axial displacement of the neck.
The total displacement of the neck was set to 10 mm and the results are shown in figure 4.17.


Figure 4.16: Setup for the axial compression test

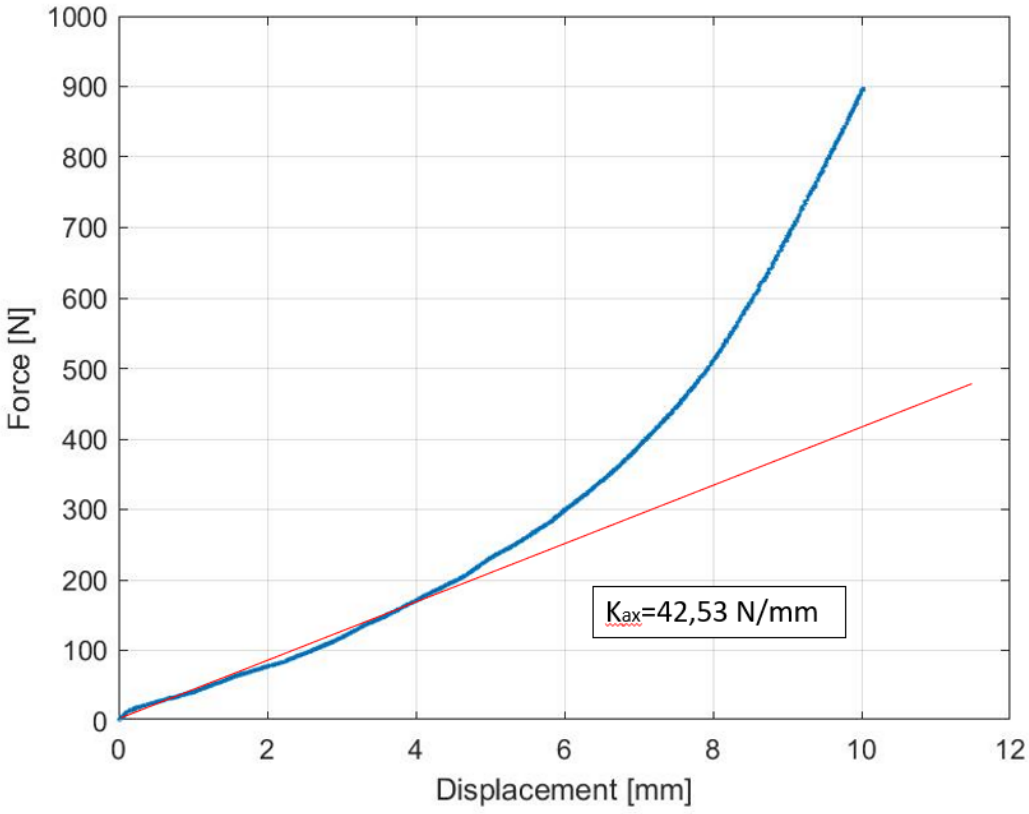


Figure 4.17: Force vs displacement curve for the axial compression test

The behavior of the neck was approximated as linear up to 4 mm of compression while for further displacements it shown a nonlinear stiffening trend.
The axial stiffness of the BNP3 has been evaluated considering the slope of the first linear trend of the curve, this value corresponds to the stiffness of the neck when the Inner cable is installed with 5 turns of the nut.
Table 4.7 reports the axial stiffness of the BNP3 while table 4.8 reports the loads that Inner cable generates at different turns of the nut.

| | **Axial stiffness $K_{ax}$ [N/mm]** |
|---|---|
| **BNP3** | 42,53 |

Table 4.7: BNP3 axial stiffness

| **Inner cable turns** | **Displacement [mm]** | **Force [N]** |
|---|---|---|
| **0** | 0 | 0 |
| **1** | 0,8 | 33,7 |
| **2** | 1,6 | 63,2 |
| **3** | 2,4 | 90,1 |
| **4** | 3,2 | 128,2 |
| **5** | 4 | 170,2 |

Table 4.8: Axial load generated by the Inner cable when is installed for different turns of the nut

## 4.3 DAMPING TESTS

This test was done to evaluate the damping property of the BNP3.
The rubber discs of the FSUs were considered as viscous dampers and from free oscillations of the neck it was possible to evaluate the damping ratio of the system by applying the logarithmic decrement method.
This test allowed also to estimate the flexural stiffness of the neck from a dynamic point of view and it was easily adaptable for the evaluation of the stiffness in torsion.

### 4.3.1 Test method

The system used is the same as the one for the static tests introduced in 4.1.
The neck was flexed manually up to about 25° and then suddenly released and left to swing freely. The neck performed free vibrations until the rubber discs dissipated completely the energy stored from the starting flexed configuration, returning the neck to the undeformed configuration. Similarly, the test was performed in torsion just twisting the neck instead of flexing it.
The free dumping vibrations were captured by motion capture system providing data for the application of the logarithmic decrement method.
The logarithmic decrement $\delta$ is defined as the natural log of the ratio of the amplitudes of any two successive peaks such as x1 and x2 in figure 4.18.

$$\delta = ln\left(\frac{x1}{x2}\right) \tag{4.1}$$

The damping ratio is then found from the logarithmic decrement by:

$$\zeta = \frac{1}{2\pi} \cdot \delta \tag{4.2}$$

From damping ratio, we can estimate the damping coefficient as:

$$c = c_{cr} \cdot \zeta \tag{4.3}$$

where $c_{cr}$ is the critical damping:

$$c_{cr} = 2 \cdot \omega_n \cdot I \tag{4.4}$$

$I$ is the moment of inertia of the system (the moment of inertia of the neck was neglected), while $\omega_n$ is the natural pulsation estimated considering the oscillation period T of the free vibrations.

$$\omega_n = \frac{2\pi}{T} \tag{4.5}$$

Another free vibration parameter that can be evaluated is the damped natural pulsation:

$$q = \omega_n \cdot \sqrt{1 - \zeta^2} \tag{4.6}$$

Finally, we can estimate the stiffness k:

$$K = {\omega_n}^2 \cdot I \tag{4.7}$$

For each test three set of free oscillations were done and for the results the mean values between the set were considered.
A neck configuration tested besides the BNP3 as it is, is the “BNP3-OR-FBL-IC5”, which is the one that allows the neck to support the weight of the Hybrid III head (actually the configuration that ensures a straight alignment of the neck while the Hybrid III head is mounted is “BNP3-OR-FB2L-IC5” but to carry out these tests a symmetric configuration of the neck was needed).

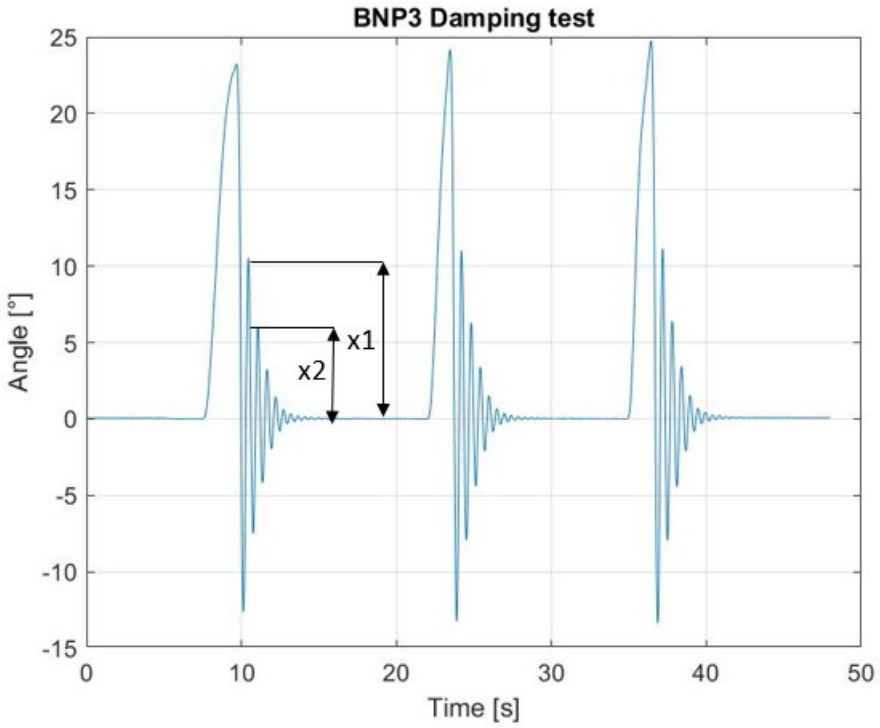


Figure 4.18: Three set of free oscillations performed in a damping test

### 4.3.2 Results

The results obtained from the tests are reported below for flexion/extension and torsion.

| | I [kgm$^2$] | $\omega_n$ [rad/s] | ζ [%] | c [Nm*s/rad] | q [rad/s] | $K_{flex}$ [Nm/°] |
|---|---|---|---|---|---|---|
| **BNP3** | 0,023 | 10,77 | 8,8 | 0,044 | 10,73 | 0,047 |
| **BNP3-OR-FBL-IC5** | 0,023 | 16,15 | 13,1 | 0,097 | 16,01 | 0,106 |

Table 4.9: Free vibrations parameters for flexion/extension damping tests

| | I [kgm$^2$] | $\omega_n$ [rad/s] | ζ [%] | c [Nm*s/rad] | q [rad/s] | $K_{torq}$ [Nm/°] |
|---|---|---|---|---|---|---|
| **BNP3** | 0,023 | 5,55 | 7 | 0,018 | 5,54 | 0,012 |
| **BNP3-OR-FBL-IC5** | 0,023 | 7,46 | 7,9 | 0,027 | 7,44 | 0,023 |

Table 4.10: Free vibrations parameters for torsion damping tests

### 4.3.3 Discussion

From the damping ratios point of view, the O-Rings in the second configuration introduce one more damping component that rise the value of the damping ratio.
A comparison with the previous prototypes can be made in terms of damping ratio in flexion and extension considering the results achieved by Rango M. [32] for BNP1 and BNP2 prototypes.

| | ζ [%] |
|---|---|
| **BNP1** | 5,41 |
| **BNP2** | 5,18 |
| **BNP3** | 8,8 |

Table 4.11: Damping ratios comparison for BNP prototypes

The BNP3 has higher value of damping ratio with respect to previous prototypes.
More interesting is the value of $k_{flex}$ obtained for the BNP3 with this method.
This value differs from the one obtained during static test by 33,1%.
If we fit the angle data obtained from the damping test with the following equation,

$$\theta(t) = \theta_0 e^{-\omega_n \zeta t} \cos\left(\omega_n \left(\sqrt{1-\zeta^2}\right) t\right) \tag{4.8}$$

which is the equation of motion for free damped vibrations, we obtain the plot shown in figure 4.19.
We observe that the fit is good in the amplitude prediction but the frequency of vibration appears to increase for smaller oscillations over time and influences the fit. This could be the reason that explain the different values obtained for flexural stiffness in the two approaches.
The one degree of freedom system considered in this approach (neck rotation θ), may be too approximated; a two degree of freedom system that considers a translational movement of the neck combined to the rotational one could give better results.
For the evaluation of stiffness properties of the neck, the damping test method is faster than the static test but lack in terms of accuracy, however, this method was useful to estimate the stiffness in torsion of the BNP3.

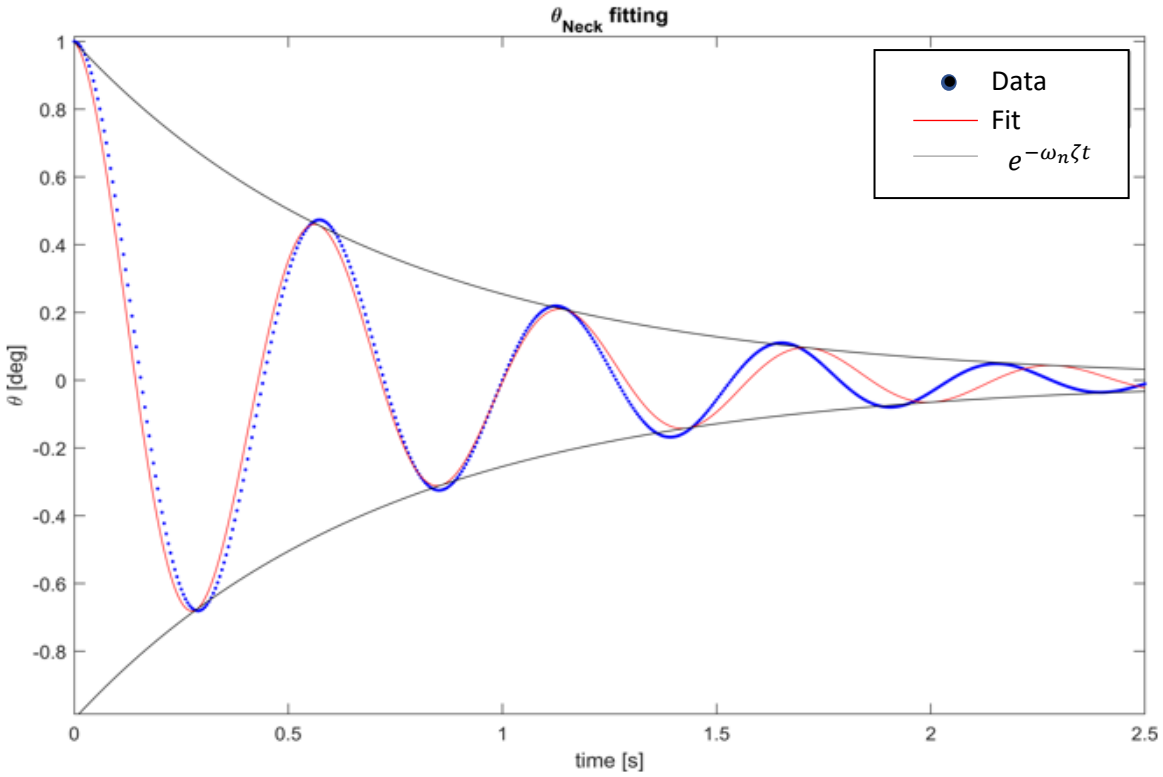


Figure 4.19: Fit of angle data after the perturbation, data was normalized such that $\theta_0=1$

## 4.4 SHAKING TEST

This test was done to evaluate the behavior of the neck from a dynamic point of view.
In particular this test allowed to define a dynamic stiffness of the neck in the sagittal plane.

### 4.4.1 Test method

The test was performed using the servohydraulic cylinder from “Colossus” test bench already used for the axial compression test.
The Hybrid III head was mounted on the BNP3 neck fixed on a sliding platform free to move linearly along a rail.
The configuration of the neck used in this test was the “BNP3-OR-FB2L-IC5” since it is the configuration that ensures a straight alignment of the neck while the Hybrid III head is mounted.
Thanks to the servohydraulic cylinder, it was possible to apply a sine-wave to the sliding platform with a known frequency and amplitude, for a fixed number of cycles.
The linear movement of the sliding platform results in a flexion-extension movement of the neck, thanks to the moments resulting from the inertial properties of the head.
The bending moment that comes from the shaking head is measured by a six-axis load cell placed between the neck and the sliding platform.

Flexion-extension neck angles were acquired using the Motion Capture System (Vicon Bonita). Three markers were placed on the head and three on the sliding platform as shown in figure 4.20.
The angles were obtained from the relative rotation of the reference system defined by the three markers placed on the head with respect to the reference system defined by the three markers placed on the platform.

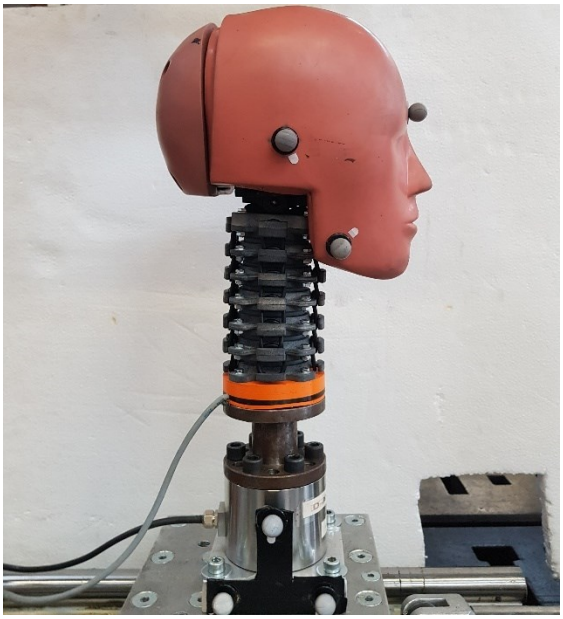

Figure 4.20: Shaking test setup

Table 4.12 reports the amplitudes of the movements imposed to the platform for the different tests and the corresponding maximum flexion ($\theta_{FLEX}$) and extension ($\theta_{EXT}$) angles reached as well as the overall range of motion ($\Delta\theta$).
For each test 20 cycles were set at the frequency of 1 Hz.

| | **Amplitude [mm]** | **MAX $\theta_{FLEX}$ [deg]** | **MAX $\theta_{EXT}$ [deg]** | **ROM $\Delta\theta$ [deg]** |
|---|---|---|---|---|
| **BNP3-OR-FB2L-IC5** | 5 | 2,06 | -1,98 | 4,04 |
| | 10 | 6,15 | -6,17 | 12,32 |
| | 20 | 14,64 | -16,3 | 30,94 |
| | 30 | 22,13 | -26,57 | 48,7 |

Table 4.12: Values of amplitudes and corresponding flexion-extension angles imposed for each shaking test

In order to evaluate the mechanical properties an average cycle of the last 10 cycles performed in each test was considered (the first 10 cycled were neglected to avoid the transitional effects).
For each test, after plotted the bending moments in function of the flexion/extension angles, the dynamic stiffness of the neck $k_D$ has been evaluated in flexion and extension as the slope of the straight line passing through the point corresponding to the starting moment applied before the head starts shaking (0,9 Nm) and the point

corresponding to the maximum moment (flexural stiffness) or the minimum moment (extensional stiffness) reached during the test as shown in figure 4.21.
As well, the dissipated energy $E_d$ has been evaluated, considering the area of the hysteresis cycle and to better compare the different tests, the value of $E_d$ has been normalized with respect to the angular range of motion $\Delta\theta$.

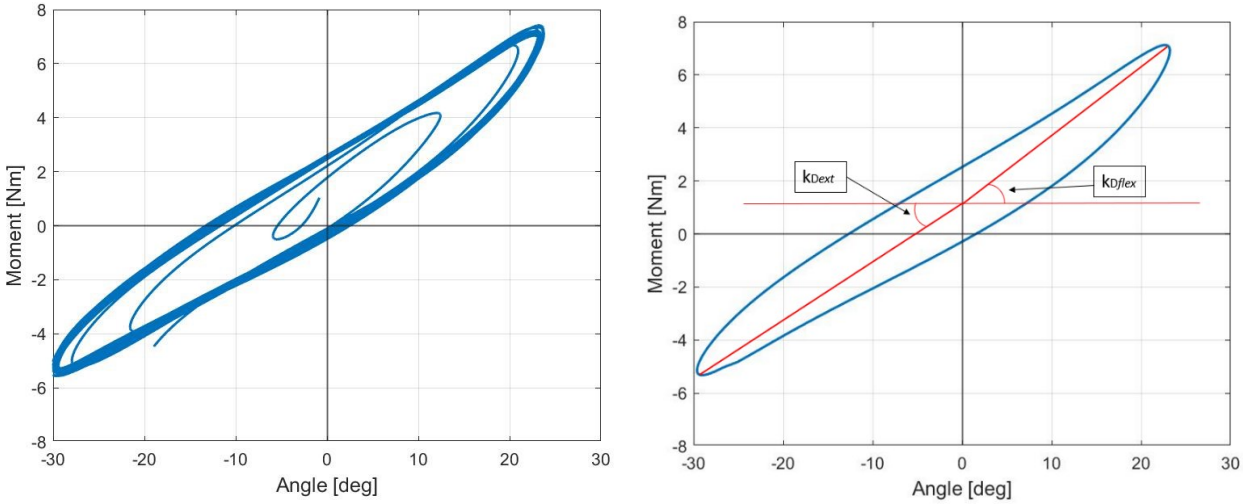


Figure 4.21: On the left an example of the overall angles-moments cyclic plot (signals filtered using a fourth order Butterworth low pass filter having a 5 Hz cutoff frequency), on the right the corresponding average cycle plot and the slopes that define the sagittal stiffnesses

### 4.4.2 Results

The results obtained from the tests are reported below.

| Amplitude [mm] | $k_{Dflex}$ [Nm/°] | $k_{Dext}$ [Nm/°] | $k_{Dflex}/k_{Dext}$ | Ed [J] | Ed/Δθ [J/°] |
|---|---|---|---|---|---|
| **5** | 0,346 | 0,335 | 1,03 | 0,02 | 0,0049 |
| **10** | 0,297 | 0,259 | 1,15 | 0,184 | 0,015 |
| **20** | 0,264 | 0,216 | 1,22 | 0,991 | 0,032 |
| **30** | 0,260 | 0,205 | 1,27 | 2,158 | 0,044 |

Table 4.13: Sagittal neck dynamic stiffness and dissipated energy for shaking test

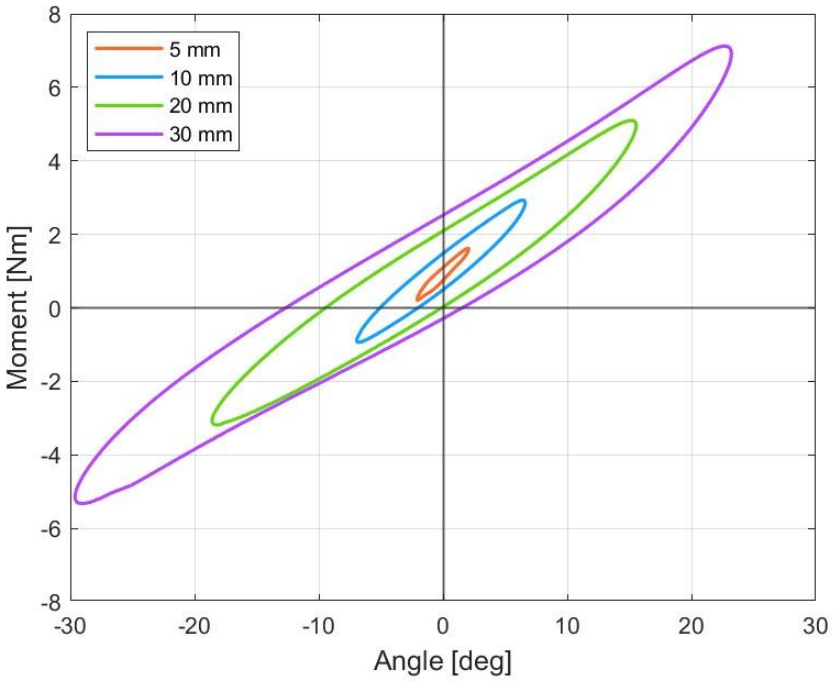


Figure 4.22: Shaking test results

### 4.4.3 Discussion

From table 4.13 it is noted that the flexural stiffness is higher than the extensional one, this is in agreement with the no-symmetric configuration of the neck tested.
In addition, it is observed that an increase of the amplitude results in a reduction of the dynamic stiffness and in an increase of the dissipated energy.
If we compare these dynamic stiffnesses with the static stiffness evaluated in damping test for “BNP3-OR-FBL-IC5” neck configuration (this neck configuration is not the same of the one currently tested but it is very similar) we observe that the dynamic stiffnesses are much higher than the static one.
This test was limited to 30 mm of amplitude to avoid failures of the neck; higher amplitudes would result in higher overall range of motion of the neck and therefore this test could be proposed as possible test method for the assessment of neck protectors just by adding the shoulders to the assembly.

# CHAPTER 5

# 5 NECK INSTRUMENTATION

A parallel goal to the biofidelity is the instrumentation of the neck.
The idea is to implement sensors for data acquisition of loads acting on the neck and displacements/rotations movements.
In this chapter are presented the solutions introduced to embed sensors into the BNP3 prototype.

## 5.1 SIX-AXIS LOAD CELL

As already introduced in chapter 2, the upper part of the BNP3 was modified to allow the installation of a SunRise M3564F1 six-axis load cell.
This load cell will measure loads that will act at the Occipital condyles, which are the references of the neck considered to define the most of neck injuries tolerance limits shown in table 2.3.

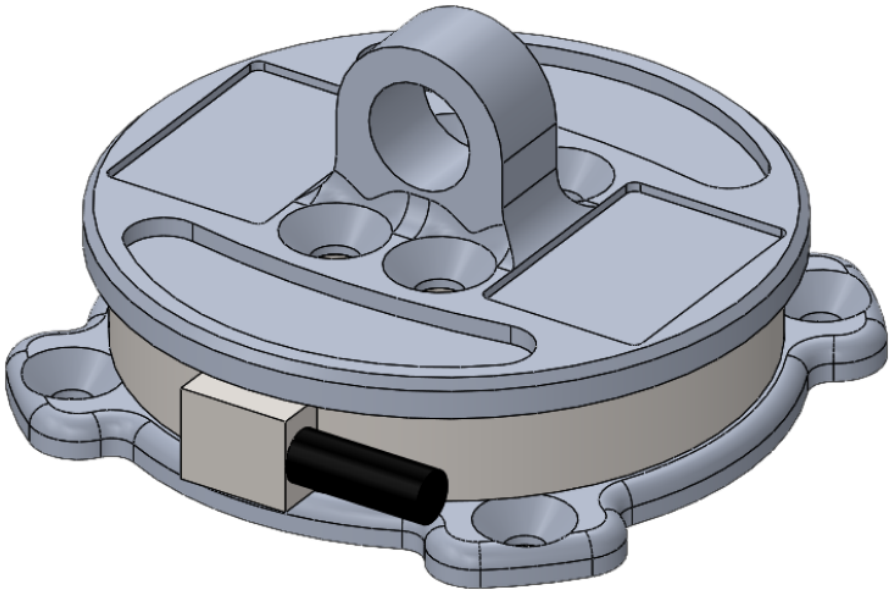

Figure 5.1: Simplified CAD model of the 6-axis load cell installed between the nodding joint and the flange

Figure 5.1 shows how the load cell introduces thickness to the neck which was designed to be as high as the Hybrid III neck.
This effect can be compensated by removing a FSU considering a neck configuration with only 5 FSU.

## 5.2 INSTRUMENTED BASE

A lot of effort was dedicated to design a system that allow to measure the angles of the neck while it performs flexion, extension and lateral bending movements.
These measures are useful for the assessment of neck protectors since these devices are designed to restrict the head motion.
The following embedded system is proposed as an alternative to the use of an external measurement system such as motion capture system that despite the high guaranteed accuracy, it is high time demanding in terms of calibration procedure and it limits the volume in which a test can be carried out.
A first attempt to realize this system was made by Riello L. [31], who used four linear motion potentiometers which converted a mechanical linear motion of a cylindrical shaft into a proportional voltage.
Four fishing line, passing through four holes drilled on the vertebrae, connected the neck to the potentiometers, which were placed symmetrically and allowed to collect data during a flexion-extension movement as well as lateral bending.
A positive aspect of this solution was the internal position of the four cables which doesn't get in touch with a hypothetical external structure during motion.
The limit of the system showed in figure 5.2, is relative to the sensor travel: the 60 mm linear range of the potentiometers is not enough to follow wide ROM of the neck in flexion-extension and lateral bending.
Another critic is the size of the potentiometers used that make the neck prototype uncomfortable to perform tests.
A smarter solution has been developed in this thesis work starting from the idea proposed by Riello L.

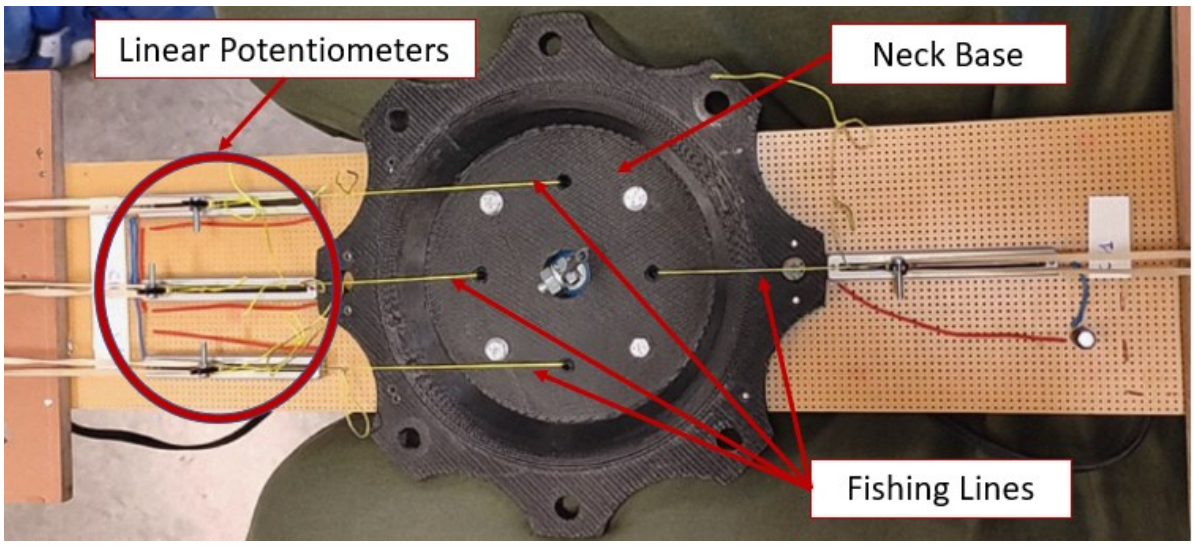

Figure 5.2: Configuration adopted by Riello L. for the addition of the potentiometers

### 5.2.1 Design

The idea was to exploit a flange designed to make the BNP3 compatible to the assembly on the Hybrid III torso. This flange will serve as base for the neck and will accommodate the sensors used to measure the movements of the neck.
The design of the flange was very challenging since its size had to add as little thickness as possible to the neck and therefore the space available to implement the sensors was very limited.
The solution proposed employs four rotary potentiometers that are directly connected to four pulleys by mean of four small shafts.
Four cables, wrapped around the pulleys, are passed through the four small holes present in each FSU and then fixed to the upper part of the neck. The movements of the neck cause the cables to stretch or relax causing the rotation of the pulleys and as a consequence the rotation of the potentiometers rotor that will produce an electrical signal used to estimate the angles reached by the neck while moving.
Figure 5.3 shows the CAD exploded view of the instrumented base realized.
Below is reported the description of each component designed for the assembly of the base.

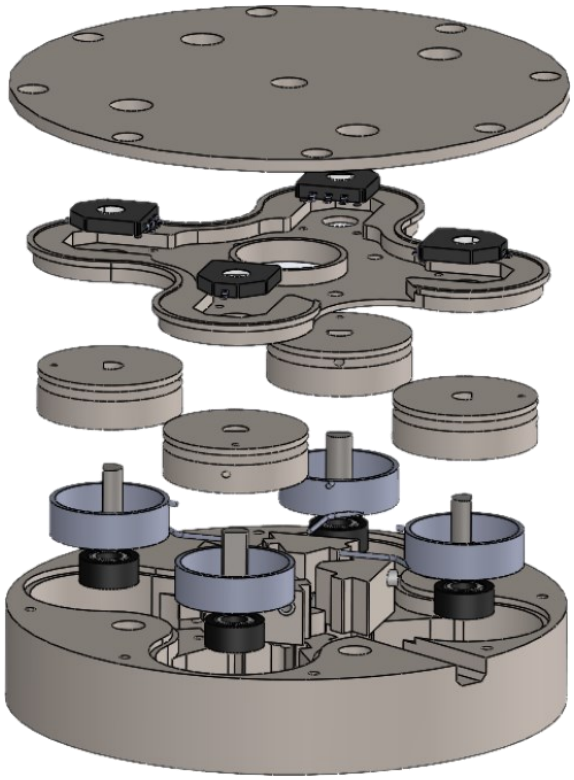

Figure 5.3: CAD exploded view of the instrumented base.

- **Base**

This base serves as a flange and make the BNP3 compatible with the assembly on the Hybrid III torso.
On the upper surface it has four external holes for M4 screws for the assembly of the BNP3, four ϕ2,5 mm holes for the passage of the cables and one ϕ5,5 mm hole for the passage of the Inner cable, while on the bottom surface it has four holes for M8 screws arranged to match with the four holes on Hybrid III upper torso and eight holes for M2 screws for the fastening of the lid.
The external diameter is ϕ85 mm like the external diameter of the BNP3 and the thickness is 15 mm.
The base has been modeled to accommodate the components for the instrumentation.
The optimal design was achieved after several attempts. Some of them are reported in figure 5.4 showing the overall evolution of the component. The third solution proposed in the figure implemented a possible solution to measure the torsion angle of the neck, this solution however was abandoned since not feasible.

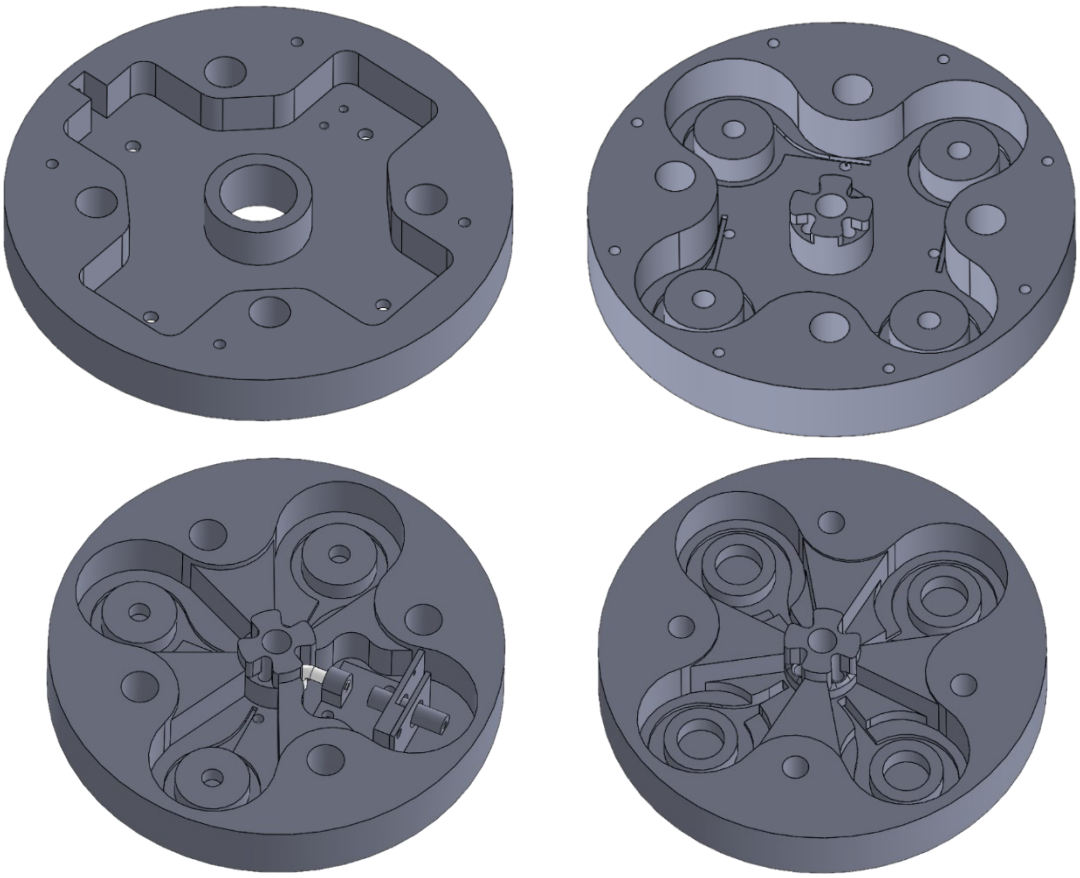

Figure 5.4: Improvement steps of the base component

The optimal design is shown in figure 5.5.
Four bearings are installed inside the four cylindrical structures, externally to these cylindrical structures, four torsional springs are placed following the dig that replicas their shape.
The raised features allow to support and fix the baseplate where the potentiometers are installed.

A channel dug on the lower surface of the base allows the exit of the electrical cables of the potentiometers.

- *Front sectioned view*

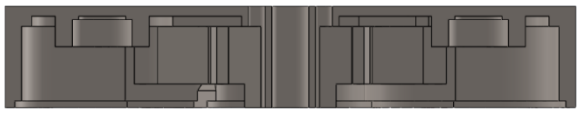

- *Side view*

- *Top view*

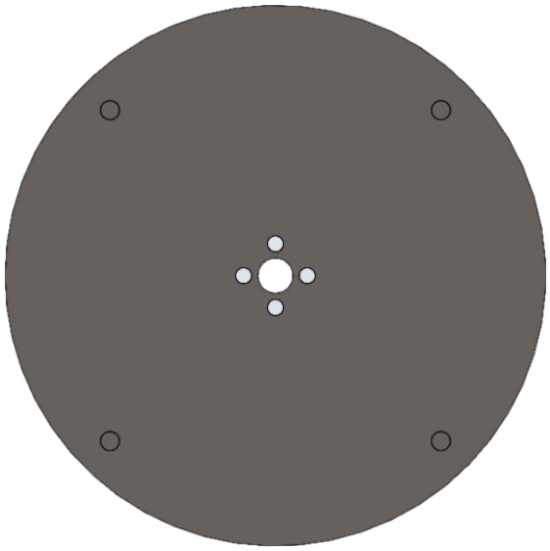

- *Bottom isometric view*

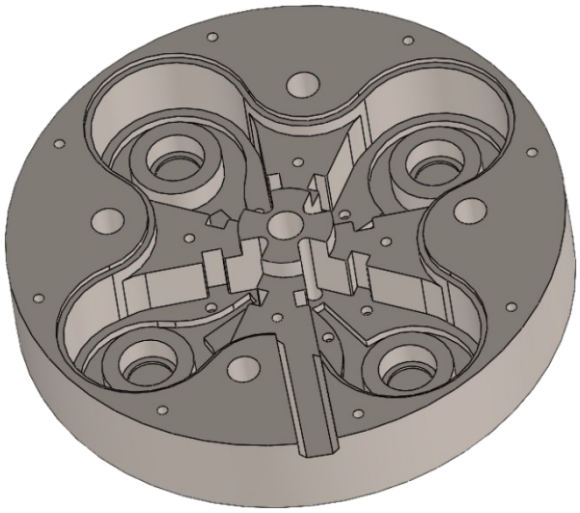

Figure 5.5: Front, side, top and isometric views of the base component

- **Lid**

The lid allows to open and close the instrumented base for eventual operations of assembly, disassembly and maintenances. The closure of base is made by 8 flat M2 screws.

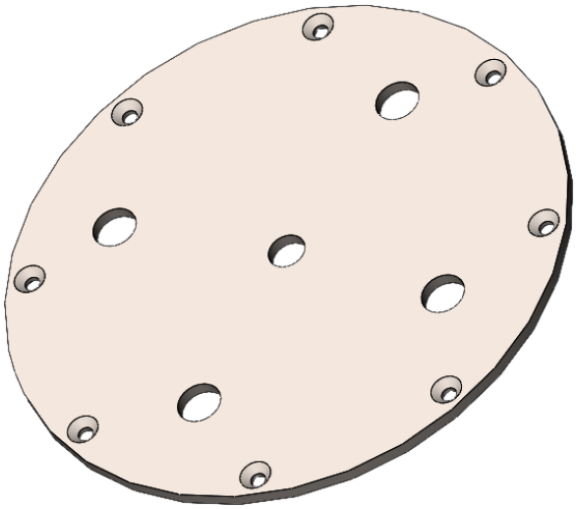

Figure 5.6: Lid component

- **Bearings**

Four bearings 4x9x4 have been used to support the shafts and assist their rotation by minimizing friction.
They are mounted inside the four cylindrical structures of the base by interference.


Figure 5.7: 4x9x4 bearing

- **Pulleys**

The pulleys convert the translational movement of the cables into a rotational movement of the shafts which are coupled to the pulleys through a semicircular seat. The external diameter is ϕ22 mm and the thickness is 7 mm.
The pulley is dug inside to accommodate the torsional spring which engages by mean of a hole on the pulley surface.
Another hole on the pulley allows the passage of one extremity of the cable which is glued to the pulley and then wrapped.
The hole on the upper surface is used as reference to preload the torsional spring.

- *Front sectioned view*

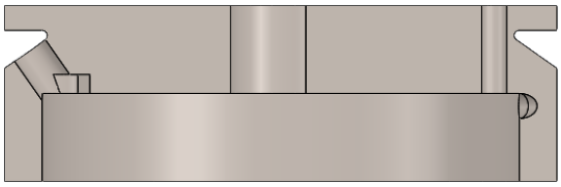

- *Side view*

- *Top view*

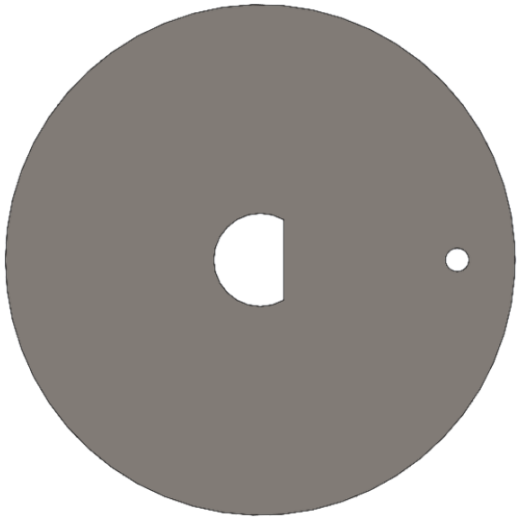

- *Isometric view*

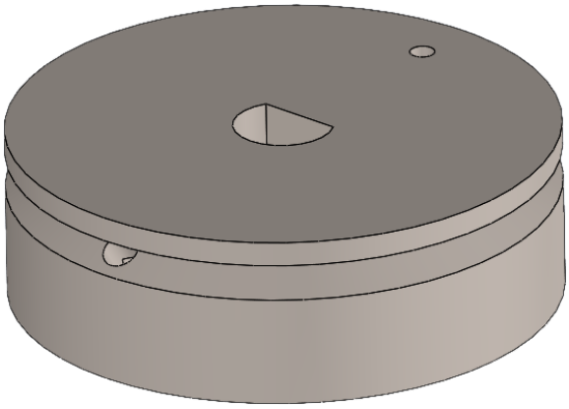

Figure 5.8: Front, side, top and isometric views of the pulley component

- **Torsional spring**

The torsional spring generates an action of preload that is able to turn back the pulley at the starting configuration when the neck performs a movement, keeping the cables always tensioned.
The diameter of the spring wire is ϕ0,75 mm and the external diameter is ϕ18 mm, the spring has 5 loops that become 4 after the spring is modelled to be engaged on the pulley.

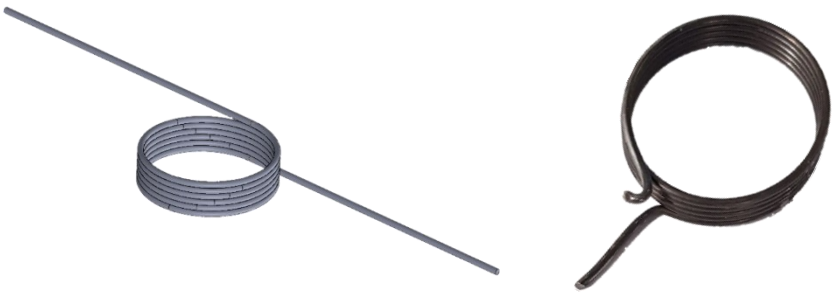

Figure 5.9: On the left the CAD model of the torsional spring, on the right the same torsional spring modelled to be engaged on the pulley

- **Shafts**

The shaft, of ϕ4 mm diameter and 12,5 mm long, transmits the movement of the pulleys to the potentiometers. A milling operation allows the shrink-fit of the pulley and the potentiometer to the shaft.

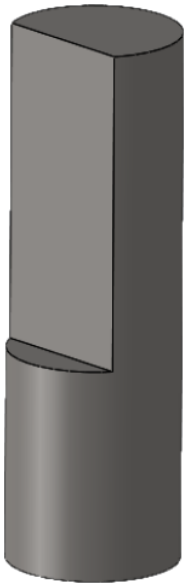

Figure 5.10: Shaft component

- **Blocks**

The blocks are used to give the Teflon tube in which the cable pass a 90° of curvature in order to provide the cable a tangential orientation with respect to the pulley.
They are inserted on the seats made into the base and their installation keep the torsional springs within their seats.

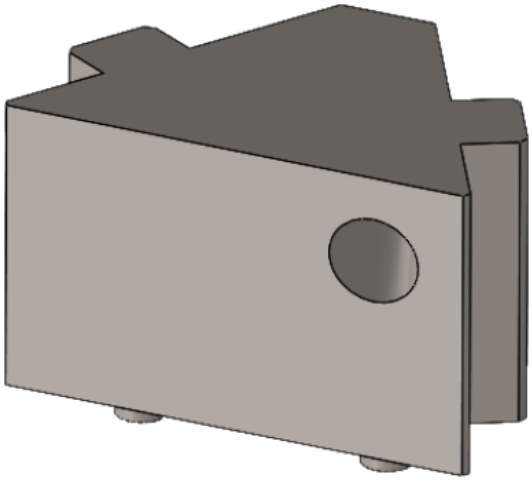

Figure 5.11: Block component

- **Baseplate**

This component accommodates the potentiometers and the wirings and is fixed to the base by mean of four screws.

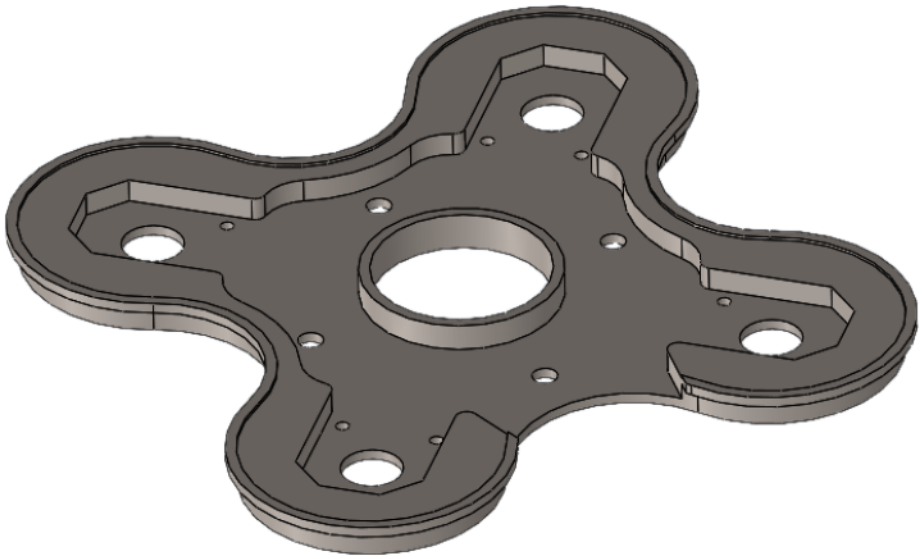

Figure 5.12: Baseplate component

- **Rotary potentiometers**

A potentiometer is a passive electronic component that works by varying the position of a sliding contact across a uniform resistance. In a potentiometer, the entire input voltage is applied across the whole length of the resistor, and the output voltage is the voltage drop between the fixed and sliding contact.
The rotary potentiometer has two terminal contacts between which a uniform resistance is placed in a semi-circular pattern. The device also has a middle terminal which is connected to the resistance through a sliding contact attached with a rotary rotor. By rotating, the rotor moves the sliding contact on the semi-circular resistance. The voltage is taken between a resistance end contact and the sliding contact. Figure 5.11 shown the rotary potentiometer construction, manufactured by muRata and used for the instrumented base.
This rotary potentiometer has a total resistance value of 10 ±30% kΩ and an effective rotational angle of 333,3°.

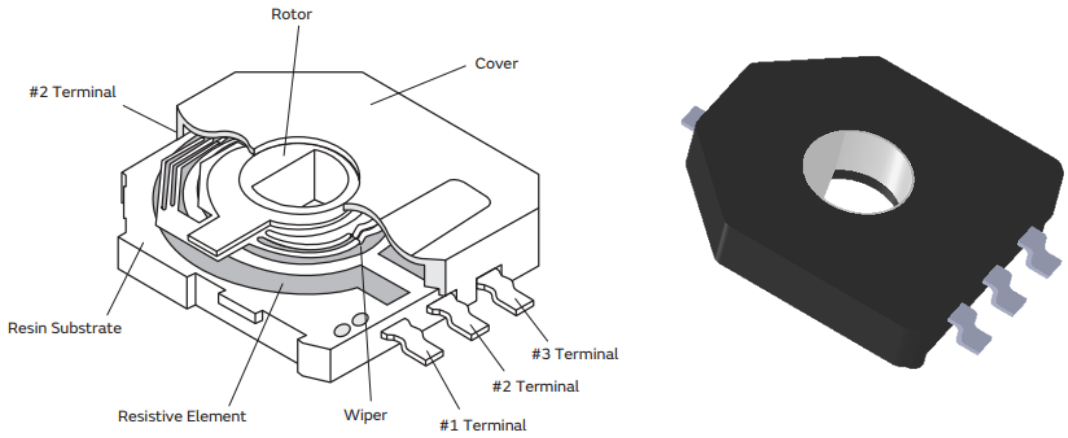


Figure 5.13: Rotary potentiometer construction and its CAD model

### 5.2.2 Assembly

A first prototype of the instrumented base has been manufactured. Base, lid, pulleys, baseplate and blocks components have been manufactured by 3D printing in Nylon PA12.
For the assembly of the instrumented base, the following steps have to be performed.

- Insert Teflon tubes into the block components.
- Insert the block components into the base.
- Fix the base to the BNP3.
- Pass the four cables through the holes of the neck (in this case for the cables a fishing line was used).
- Pass the extremity of the cable (base side) through the hole on the pulley side and glue it to the pulley surface.
- Insert the bearings into their seats.
- Mount the shafts on the bearings.
- For each pulley, install the torsional spring.

- Mount the pulleys with the torsional springs on the shafts. The torsional springs must remain within their seats.
- Apply a little glue to make the pulley stick to the shaft.
- With the help of a needle perform a winding of the cable around the pulley.
- Preload the springs by pulling the free extremity of the cables until the pulleys rotates about half turn (take the hole on the upper surface of the pulley as reference) and fixing the cables performing two turns of winding around the screws installed on the upper vertebra as shown in figure 5.13.
  The half turn of preload ensure to stay within the effective rotational angle of the potentiometer while the neck performs its movements.
- Mount and fix the baseplate with wired potentiometers on the base.
- Insert a piece of plastic as wedge between the shaft and the rotor of the potentiometer to remove the backlash between them as shown in figure 5.14.
- Close the base with the lid.

- *Unloaded configuration*
- *Loaded configuration*

Figure 5.14: On the top unloaded and loaded configuration of the instrumented base, on the bottom the upper vertebra where the four cables are fixed by winding them around the screws

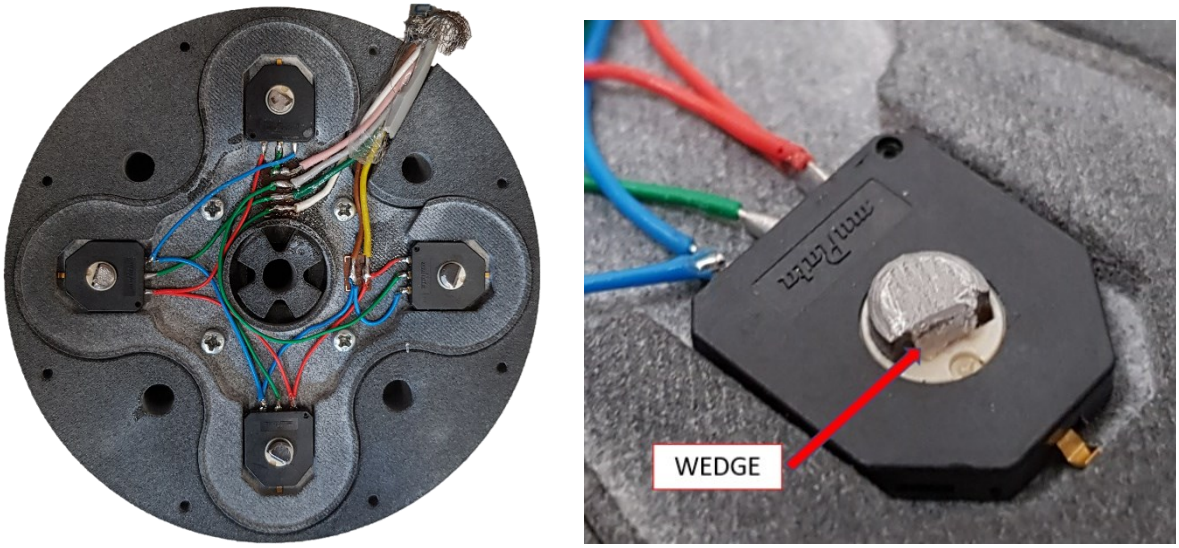


Figure 5.15: On the left the wired potentiometers installed on the base, on the right the wedge inserted between the shaft and the rotor of the potentiometer to remove the backlash

### 5.2.3 Calibration

The calibration of the instrumented base was performed by associating the neck bending angles while it performs flexion, extension and lateral bending movements, to the voltage signals from the rotary potentiometers of the base.
The calibration was done by applying known weights on a plate hanging on an extremity of the bar fixed on the upper vertebra of the neck as shown in figure 5.15.

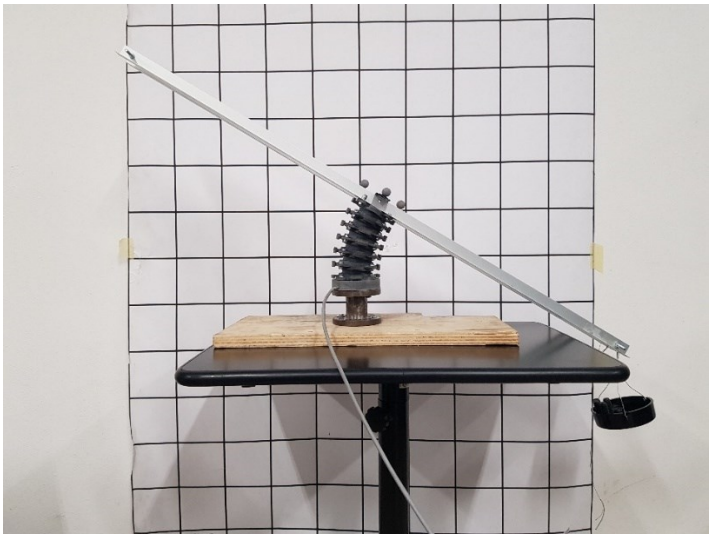

Figure 5.16: Setup for the calibration of the instrumented base

Each load steps involved the adding of four M12 screw (the same used in static tests in 4.1) on the plate. Six load steps (the first one is the plate installation) were followed by six unload steps.
Between two consecutive load steps, 7 seconds for stabilization were granted and the mean value of angles and potentiometers signals collected in this range were considered for the results.

A triad of markers were placed on the top of the neck to capture its rotation with the Motion Capture System “Vicon Bonita”.
Somat is the Data Acquisition System used to collect data from the potentiometers.
The bending moments generated with the loads were not acquired since they were not relevant for calibration.
To synchronize the data collected by the motion capture system with the ones collected by the data acquisition system, the neck has been perturbated as was done in damping tests in 4.2, in order to have a reference for the synchronization.
The first calibration test was run considering the BNP3 as it is without any stiffening component.
Both flexion-extension and lateral bending have been investigated.
Figure 5.15 shows the results obtained for this first test.
Flexion angles and right lateral bending angles were considered positive while extension angles and left lateral bending angles were considered negative.

- ***Flexion***

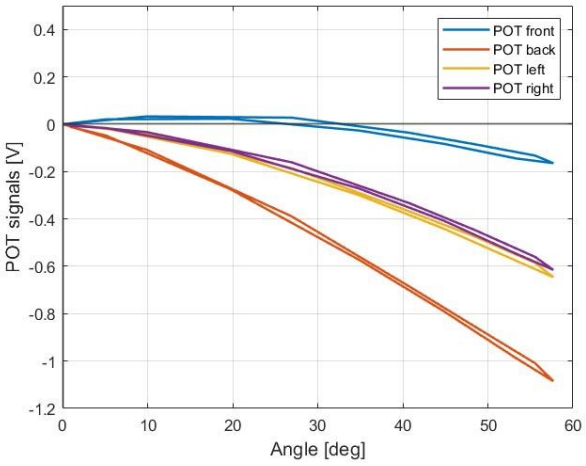


- ***Extension***

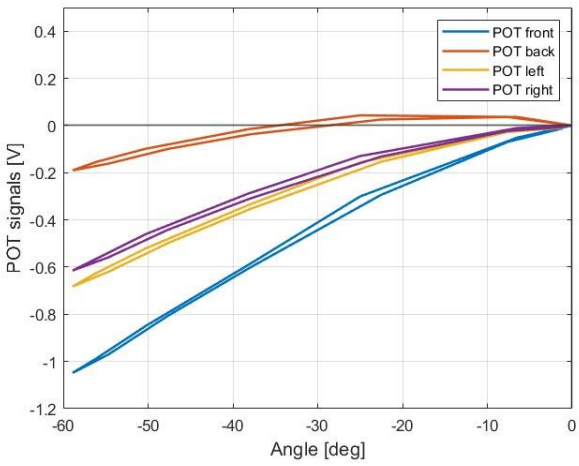


- ***Right lateral bending***

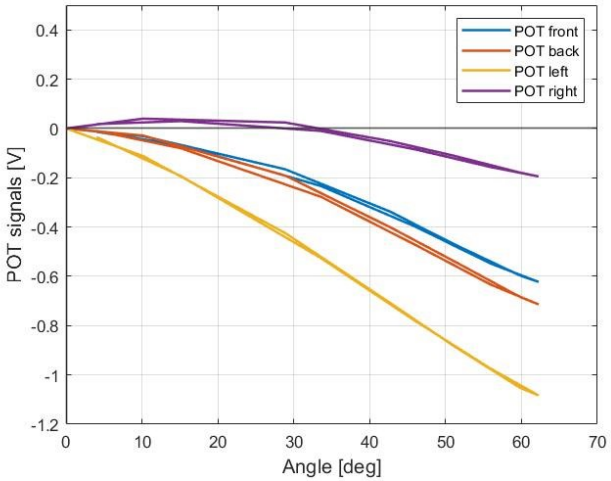


- ***Left lateral bending***

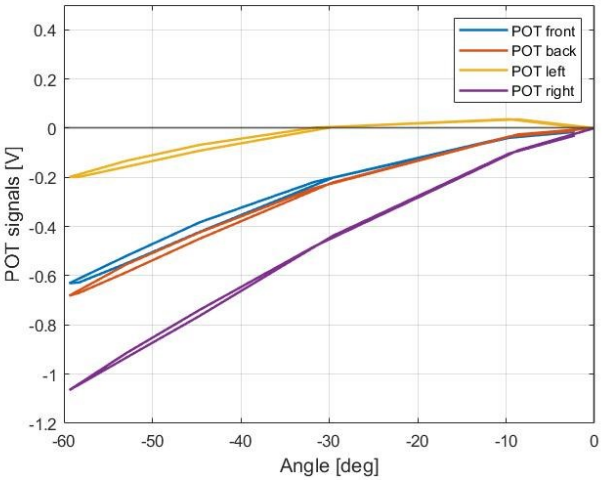


Figure 5.17: Correlation between bending angles and potentiometers signals in flexion, extension and lateral bending

An unexpected behavior of the instrumented base was observed.
In the flexion case, for example, the voltage relative to the frontal potentiometer should have a positive trend because the cable relative to the pulley connected to the front potentiometer should relax making the pulley rotate clock wise thanks to the action of the torsional spring. The plot in figure 5.16 shows instead a negative trend of the voltage after about 10° of flexion. This means that the front cable is stretched as the posterior one. The same consideration can be made considering the lateral potentiometers which relative cables should neither be stretched, nor relaxed while the neck performs a flexion movement and the potentiometers should give a constant signal of 0 V.
The same thing happens in extension and lateral bending with the inverted role of the potentiometers.
This behavior is due to the actual movement of the neck which is not a pure rotation but a combination of rotation and translation.
The translational component cause to stretch all the four cables as resulted from the plots on figure 5.16.
This behavior prevents to consider the single potentiometers to evaluate the angles in the four directions, the front potentiometer was to evaluate the flexion angles, the posterior potentiometer was to evaluate the extension angles, the left lateral potentiometer was to evaluate the left lateral bending angles and the right lateral potentiometer was to evaluate the right lateral bending angles.
Fortunately, it was observed that the differences between the signals from front and back potentiometers (for flexion and extension cases) and left lateral and right lateral potentiometers (for lateral bending cases) provided a linear trend which was used to define a calibration constant to correlate those differences of signals to the bending angles of the neck.
In figure 5.17 are reported the linear regression of the differences between the signals just mentioned.
For flexion and extension cases, the calibration constant was evaluated as the inverse of the slope of the linear regression of the difference between the front and back potentiometers signals, while for lateral bending cases the calibration constant was evaluated as the inverse of the slope of the linear regression of the difference between the right and left lateral potentiometers signals. Table 5.1 reports the results where K is the slope of the linear regressions, C is the calibration constant and R2 is the value for the assessment of the linear regressions.
The mean value of the calibration constants in flexion and extension cases was considered to evaluate the angles in flexion and extension, similarly was done for the lateral bending cases.
Finally figure 5.18 and 5.19 reports the comparison between the angles acquired by motion capture system with the ones evaluated by using the calibration constants just mentioned.
It is noted that the calibration constant in flexion case is less than the other cases; this is probably due to the fact that the previous tests, carried out for the characterization of the BNP3, were performed most of the time in flexion and this may have influenced the result.
The angles evaluated with the potentiometers signals follow quite well the angles acquired with the motion capture system. The instrumented base is not perfect especially for higher angles where a more pronounced difference between the two evaluation methods is observed but it responds well to dynamic impulses as shown in figure 5.20.

- ***Flexion***

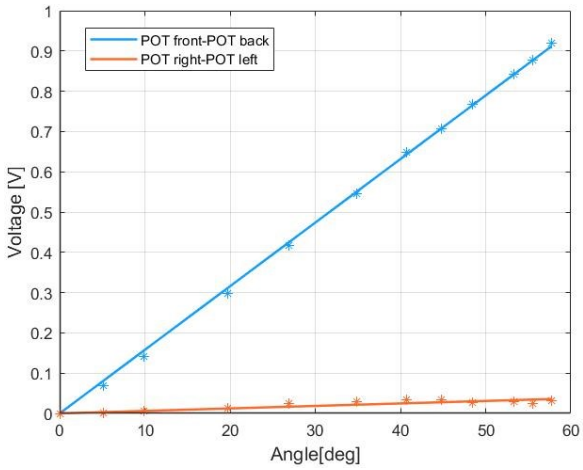


- ***Extension***

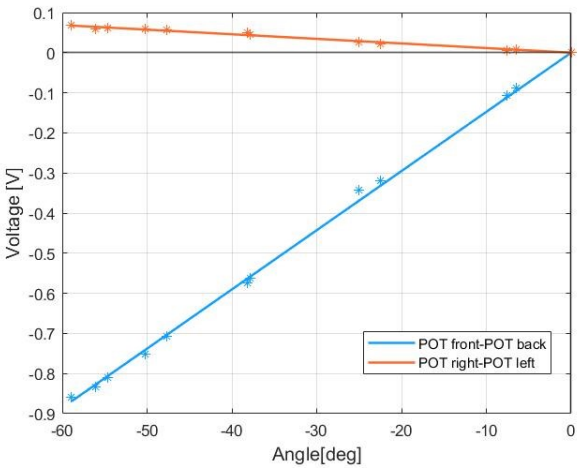


- ***Right lateral bending***

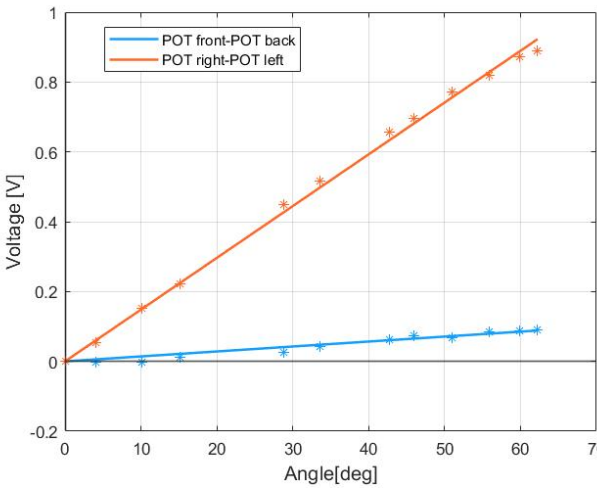


- ***Left lateral bending***

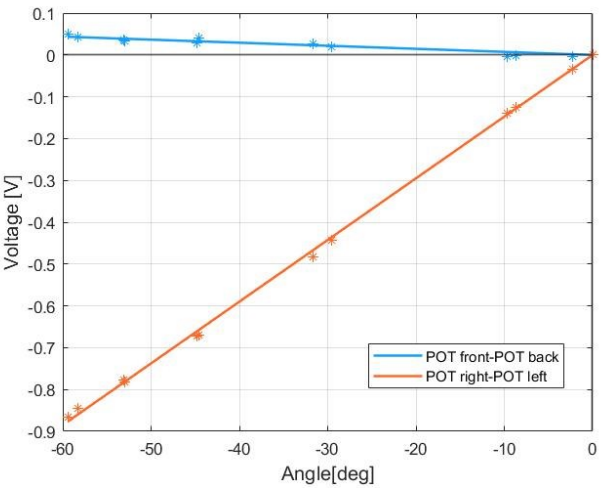


Figure 5.18: Linear regressions of the difference between the signals of front and back potentiometers and right and left lateral potentiometers

| | $R^2$ | K [V/°] | C [°/V] | $C_{Mean}$ [°/V] |
|---|---|---|---|---|
| **Flexion** | 0,999 | 0,0158 | 63,29 | 65,43 |
| **Extension** | 0,998 | 0,0148 | 67,57 | |
| **Right lateral bending** | 0,999 | 0,0147 | 68,03 | 67,8 |
| **Left lateral bending** | 0,997 | 0,0148 | 67,57 | |

Table 5.1: Results of the calibration of the instrumented base for the BNP3 without any stiffening component

- ***Flexion***

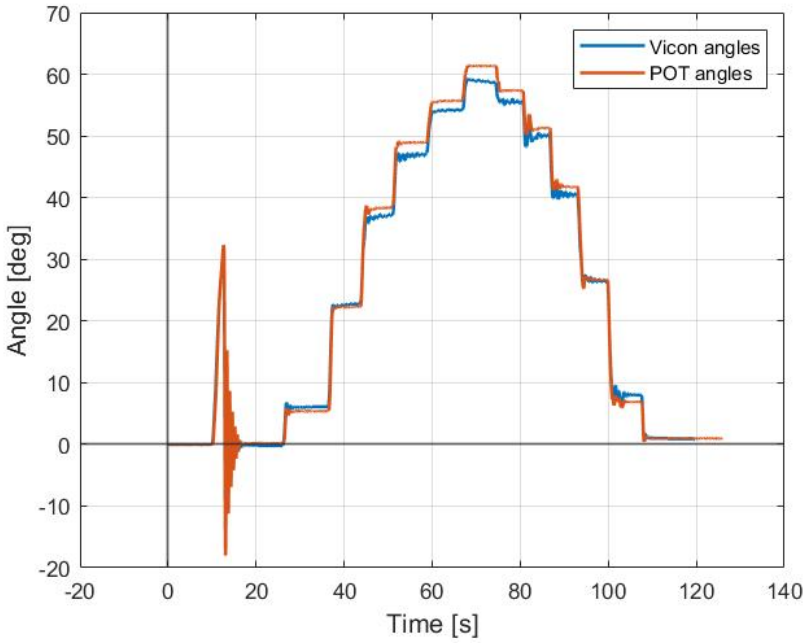


- ***Extension***

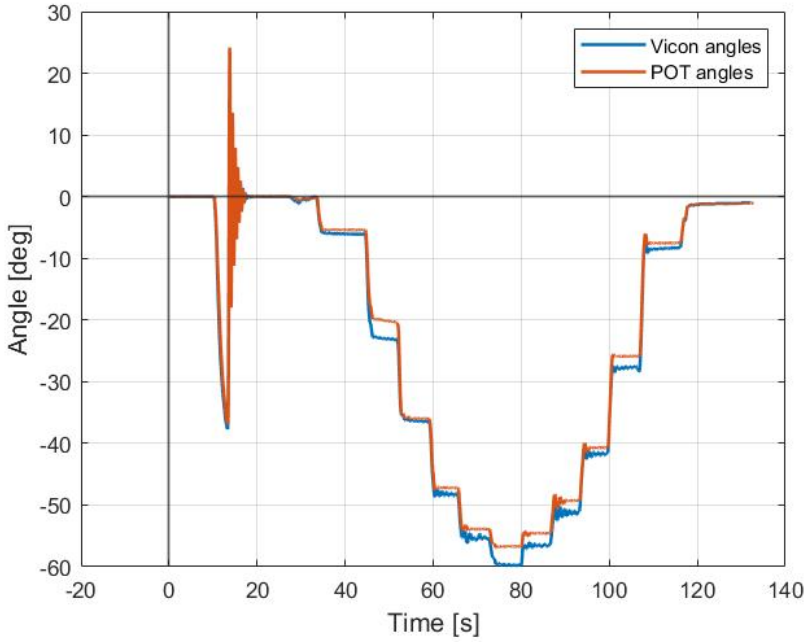


Figure 5.19: Comparison between the angles acquired by motion capture system and the angles evaluated with the potentiometers signals in flexion and extension

- ***Right lateral bending***

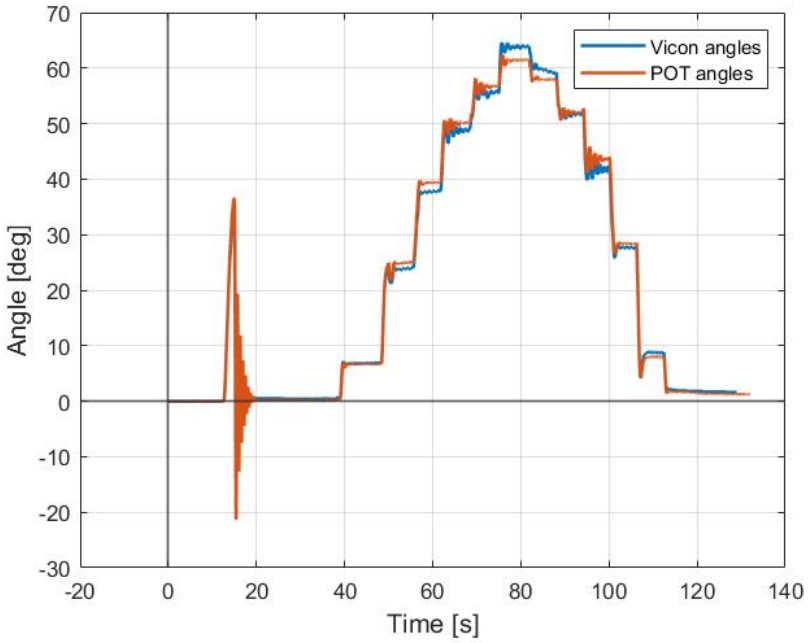


- ***Left lateral bending***

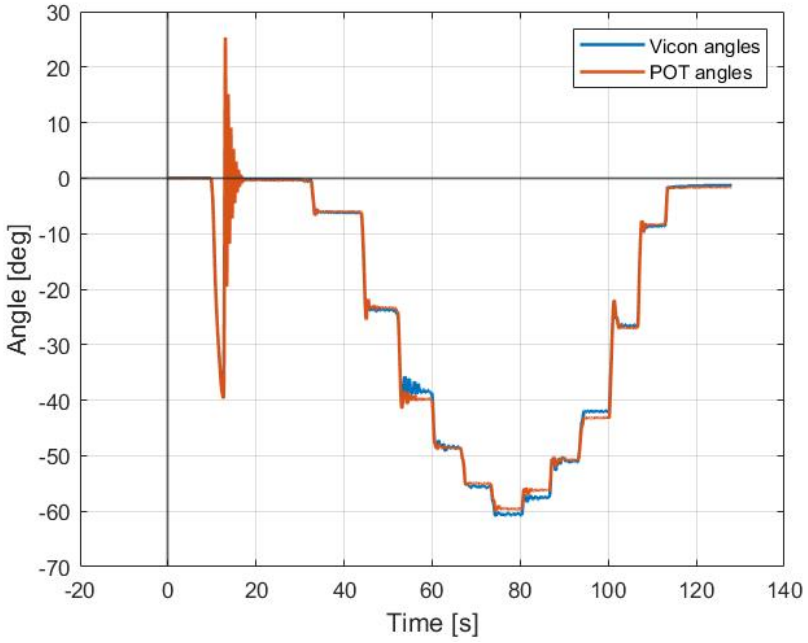


Figure 5.20: Comparison between the angles acquired by motion capture system and the angles evaluated with the potentiometers signals in lateral bending

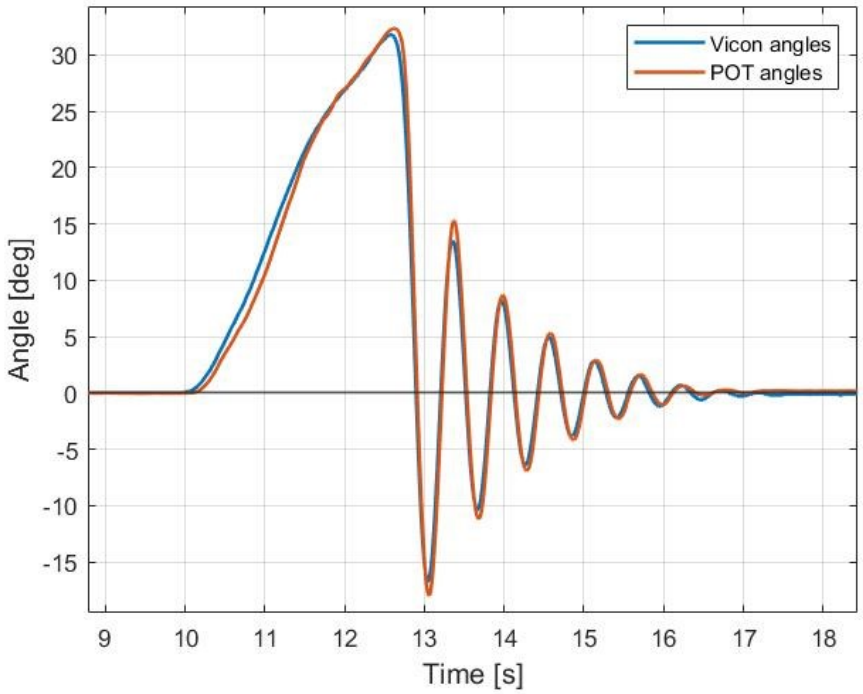


Figure 5.21: Comparison between the angles acquired by motion capture system and the angles evaluated with the potentiometers signals during the neck perturbation for the synchronization

A second calibration test was run considering the BNP3 with the Inner cable installed at one turns of the nut.
The effect of the translation of the neck during its bending movements observed in the first calibration test is much less marked when the Inner cable is installed, since the Inner cable forces the neck to perform a pure rotation since the translation is prevented.
If we consider the flexion case, figure 5.21 shows how the voltage relative to the frontal potentiometer has now a positive trend as we initially expected. And besides, the lateral potentiometers have now a trend closer to 0 V.
Even in this case, for flexion and extension cases, the calibration constant was evaluated as the inverse of the slope of the linear regression of the difference between the front and back potentiometers signals, while for lateral bending cases the calibration constant was evaluated as the inverse of the slope of the linear regression of the difference between the right and left lateral potentiometers signals.
Table 5.2 reports the results obtained while figure 5.23 and 5.24 report the comparison between the angles acquired by motion capture system and the angles evaluated with potentiometers signals.

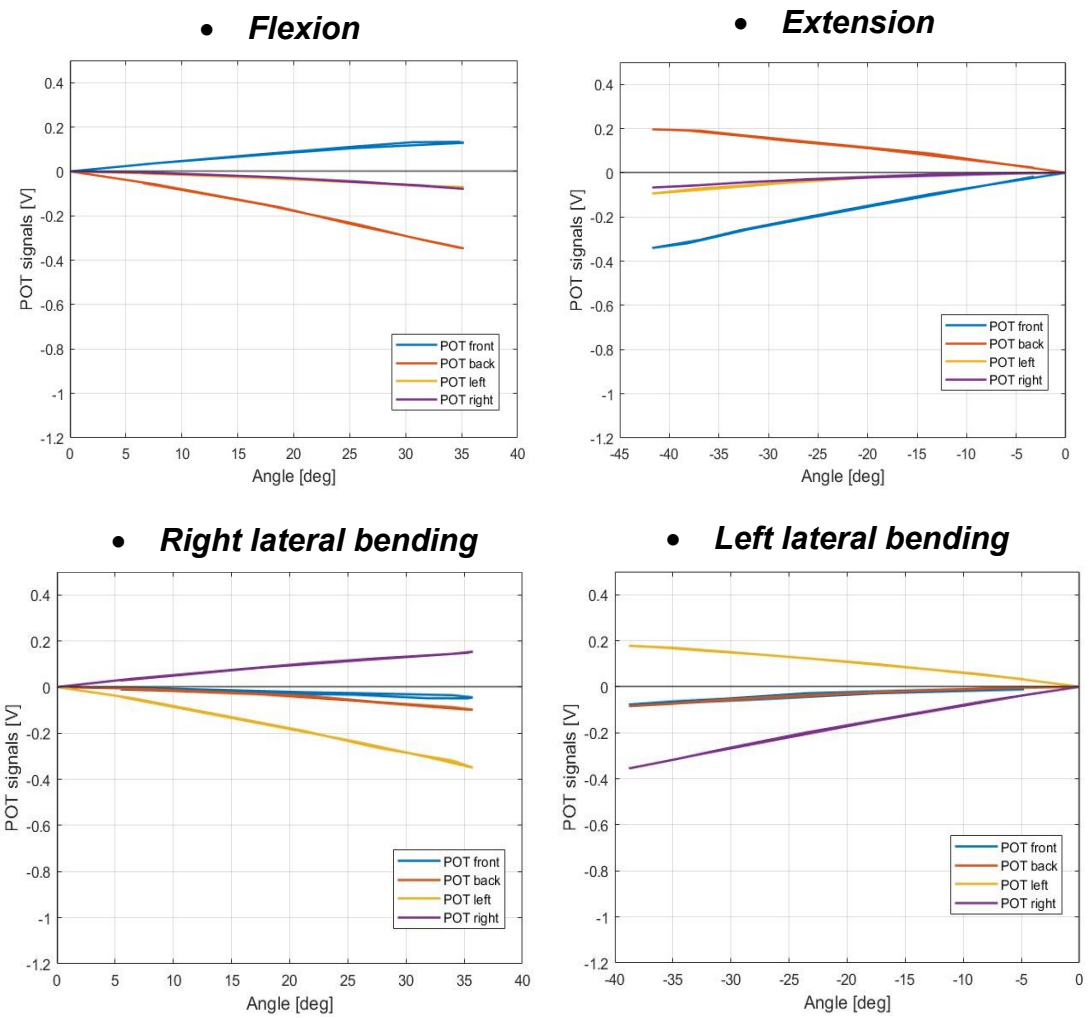


Figure 5.22: Correlation between bending angles and potentiometers signals in flexion, extension and lateral bending for the calibration with the Inner cable installed on the BNP3

- ***Flexion***

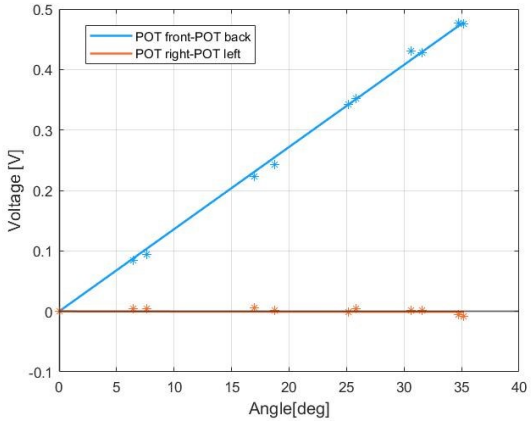


- ***Extension***

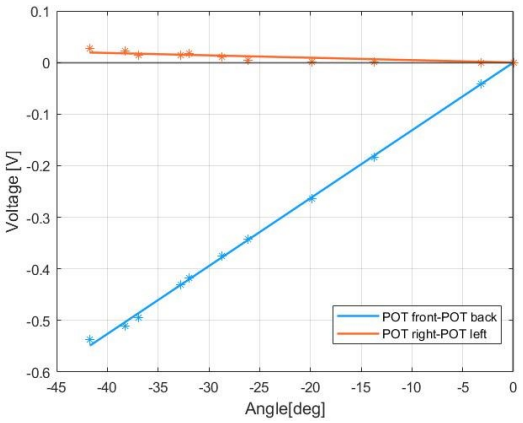


- ***Right lateral bending***

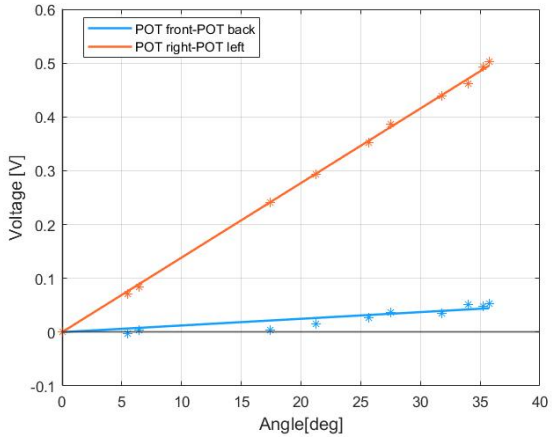


- ***Left lateral bending***

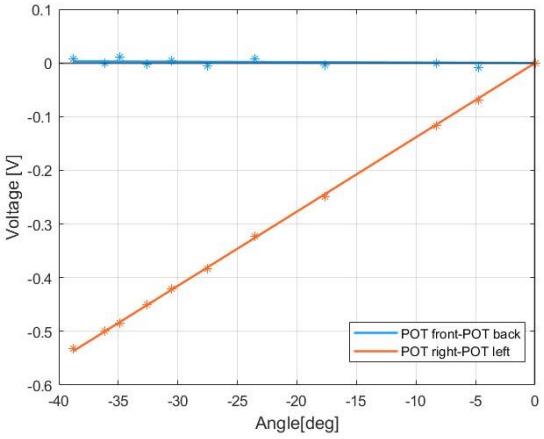


Figure 5.23: Linear regressions of the difference between the signals of front and back potentiometers and right and left lateral potentiometers for the calibration with the inner cable installed on the BNP3

| | $R^2$ | K [V/°] | C [°/V] | $C_{Mean}$ [°/V] |
|---|---|---|---|---|
| **Flexion** | 0,998 | 0,0136 | 73,53 | 74,64 |
| **Extension** | 0,999 | 0,0132 | 75,76 | |
| **Right lateral bending** | 0,999 | 0,0139 | 71,94 | 72,2 |
| **Left lateral bending** | 0,999 | 0,0138 | 72,46 | |

Table 5.2: Results of the calibration of the instrumented base with the Inner cable installed at one turn of the nut on the BNP3

- ***Flexion***

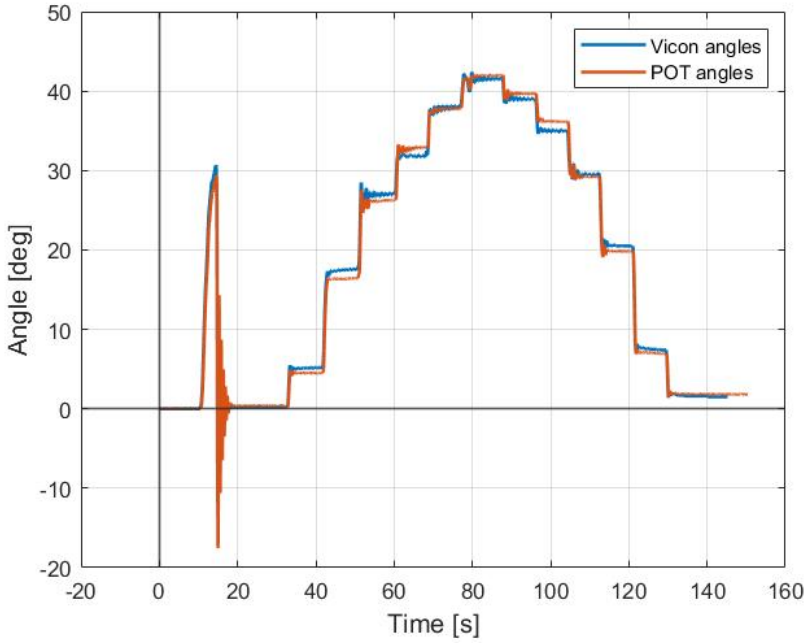


- ***Extension***

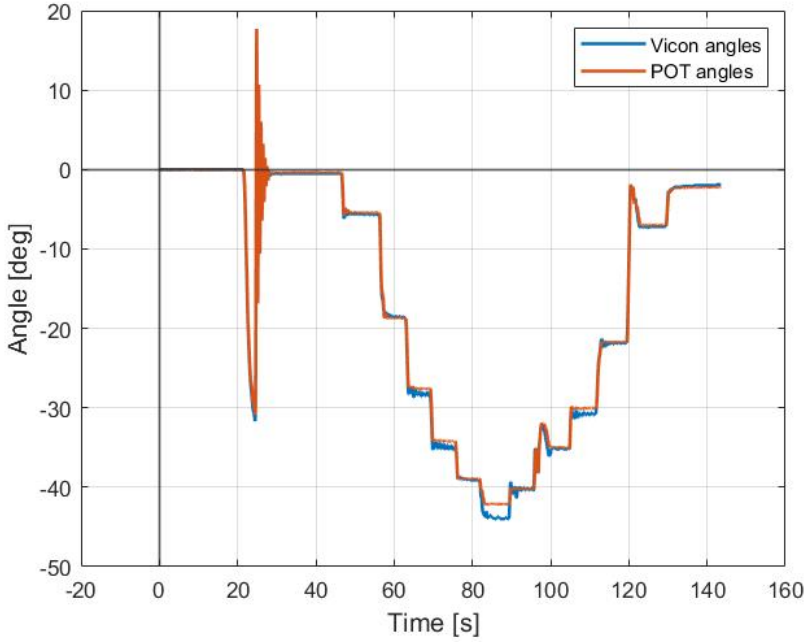


Figure 5.24: Comparison between the angles acquired by motion capture system and the angles evaluated with the potentiometers signals in flexion and extension for the calibration with the Inner cable installed on the BNP3

- ***Right lateral bending***

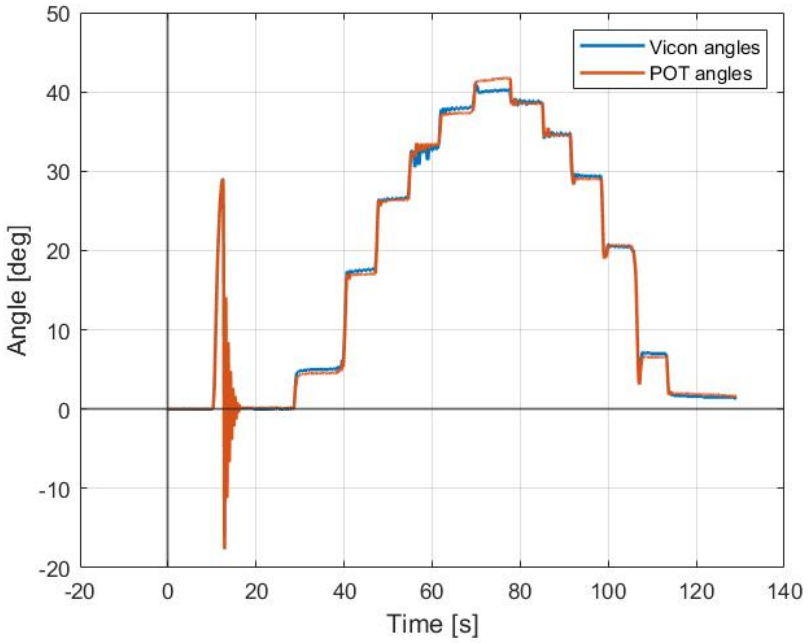


- ***Left lateral bending***

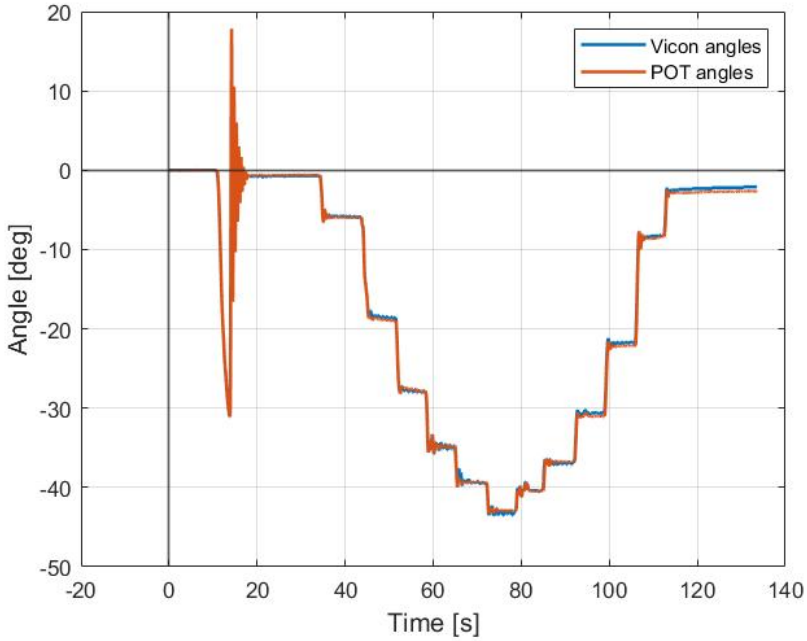


Figure 5.25: Comparison between the angles acquired by motion capture system and the angles evaluated with the potentiometers signals in lateral bending for the calibration with the Inner cable installed on the BNP3

With the Inner cable installed, we obtained similar results with respect to the previous case in terms of comparison between the angles acquired by motion capture system and the angles evaluated with the potentiometers signals indeed for higher angles a more pronounced difference between the two evaluation methods is observed in some cases.
The maximum angles reached are lower than the previous case since the neck configuration tested is stiffer while the loads applied are the same in the two cases.
The calibration constants obtained with the Inner cable installed on the neck are higher than previous case and that prevents to use a single general calibration constant for all neck configurations.
This calibration test was repeated (only in flexion) with the inner cable installed at 0, 3 and 6 turns of the nut in order to assess whether the number of turns affect the value of the calibration constant.
Table 5.3 reports the calibration constants obtained with these configurations.

| | $R^2$ | K [V/°] | C [°/V] |
|---|---|---|---|
| **BNP3-IC0** | 0,998 | 0,0135 | 74,07 |
| **BNP3-IC3** | 0,996 | 0,0132 | 75,76 |
| **BNP3-IC6** | 0,985 | 0,0128 | 78,12 |

Table 5.3: Calibration constants for different configuration of the neck in terms of turns of the nut of the Inner cable

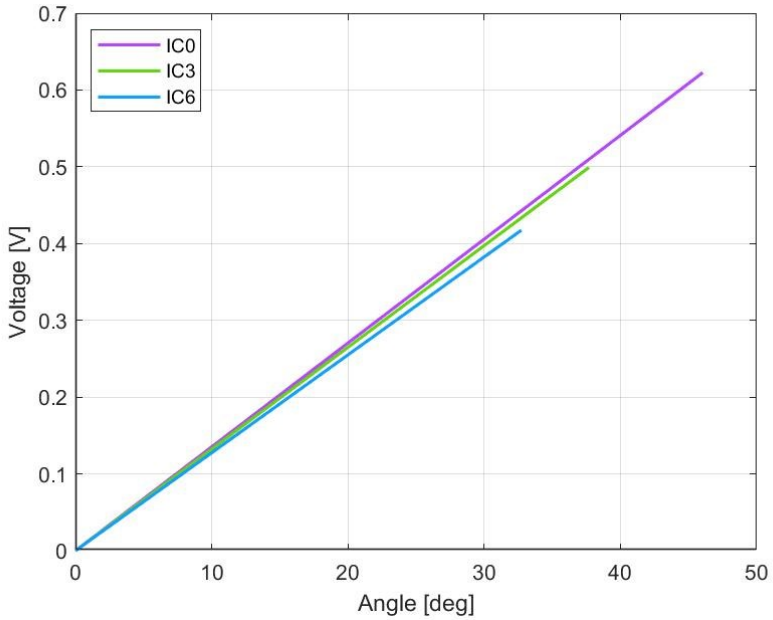


Figure 5.26: Linear regressions of the difference between the signals of front and back potentiometers for IC0, IC3 and IC6 neck configuration

The results showed in table 5.3 highlight how the number of turns of the nut doesn't influence so much the calibration constant, even if is noted that higher number of turns increase slightly this value.
To sum up, this instrumented base allows to estimate the bending angles of the neck along the sagittal and frontal plane.

If we want to estimate the flexion/extension angles, we have to multiply the difference between the signals of front and back potentiometers by the calibration constant evaluated for flexion-extension movements.
Positive values of angles will be associated to flexion movement of the neck while negative values of angles will be associated to extension movement.
Similarly, if we want to estimate lateral bending angles, we have to multiply the difference between the signals of right lateral and left lateral potentiometers by the calibration constant evaluated for the lateral bending movements.
Positive values of angles will be associated to right lateral movement of the neck while negative values of angles will be associated to left lateral movement.

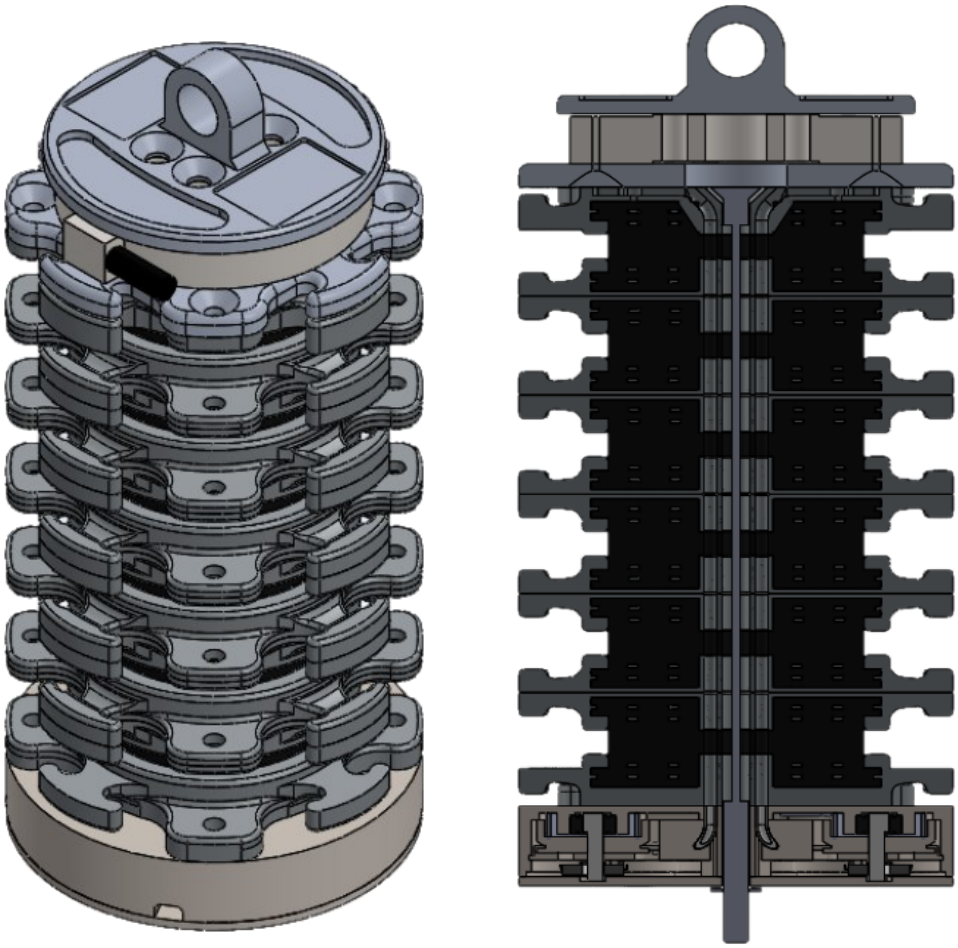

Figure 5.27: CAD model of the Instrumented BNP3

# CHAPTER 6

# 6 PILOT TESTS FOR THE ASSESSMENT OF NECK PROTECTORS

As introduced in chapter 1, neck injuries resulting from motorcycle accidents is a recurrent problem.
To prevent the injury risks, companies have started to develop specific personal protective equipment for the protection of the cervical spine.
Neck braces are part of PPE for neck protection developed to reduce the chance of neck injury by reducing range of motion and load on the neck.
However, the efficiency of these devices is still under discussion since a standardized test method for their assessment still doesn't exist.
In this chapter pilot tests with a pendulum were conducted to test neck protectors with two different neck surrogates: the Hybrid III neck and the BNP3.

## 6.1 NECK BRACE OPERATING PRINCIPLE

Neck braces are designed to be worn around the neck and interact with the underside rim of a properly fitted helmet limiting the overall movement of the head and neck and transferring the forces to adjacent body structures.
Figure 6.1 and 6.2 show how the movements of the head are restricted when the neck brace is worn. Table 6.1 reports the range of motion of the neck when a subject performs maximal flexion-extension and lateral bending movements with and without neck brace. Neck angles were acquired using the Motion Capture System (Vicon Bonita). Three markers were placed on the helmet and three on the subject's torso.
The angles were obtained from the relative rotation of the reference system defined by the three markers placed on the helmet with respect to the reference system defined by the three markers placed on the torso.
The neck brace worn in this test is the Bionic Neck Support Tech 2 (BNS) manufactured by Alpinestars. This neck protector is intended to reduce the chance of a rider sustaining a catastrophic neck injury when subject to compressive forces great enough to cause a fracture and possibly paralysis. The subject wore a protection jacket to simulate the clothing normally wear for riding.

*Extension* *Neutral* *Flexion*

Figure 6.2: On the top the ROM of the head in flexion and extension without neck brace, on the bottom the ROM of the head in flexion and extension with neck brace


*Right lateral* *Neutral* *Left lateral*

Figure 6.1: On the top the ROM of the head in lateral bending without neck brace, on the bottom the ROM of the head in lateral bending with neck brace

| | Flexion [deg] | Extension [deg] | Right lateral [deg] | Left lateral [deg] |
|---|---|---|---|---|
| **Without neck brace** | 61 | -60,5 | 40,7 | -42 |
| **With neck brace** | 32 | -35 | 25 | -28 |

Table 6.1: Range of motion of the head with and without neck brace

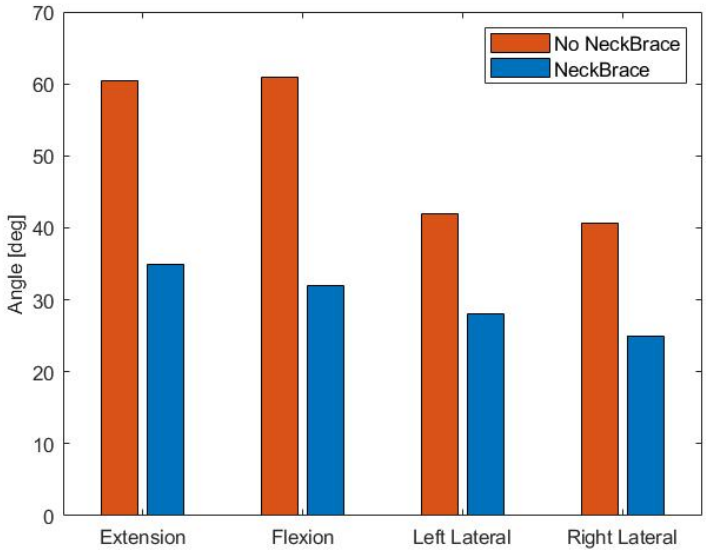


Figure 6.3: Comparison of head ROM with and without neck brace

## 6.2 IMPACT TEST

Test method here proposed consists on hitting a helmeted Hybrid III dummy on the head with a pendulum to induce a rotational motion of the neck.
The aim is to collect head kinematic data in order to evaluate neck range of motion with and without neck brace.

### 6.2.1 Test method

The helmeted Hybrid III dummy were placed seated in front of the pendulum.
The dummy trunk was fixed to the pendulum base frame with some belts while dummy shanks were removed to facilitated the dummy placement.
A motion capture system (Vicon Bonita) was used to records the kinematic of reflective markers placed on head (3), helmet (3), trunk (3), neck brace (3) (when worn) and pendulum (1).
From markers data head, helmet and trunk absolute angles and neck relative angles have been evaluated.
The impact energy was set by acting on the starting inclination of the pendulum.

Figure 6.4: Impact test setup

### 6.2.2 First tests session with Leatt neck brace

Preliminary tests were conducted to explore the method feasibility.
Different positions of the dummy were investigated at different impact energy with and without neck protector.
Positions investigated simulate frontal, back and side impact scenario.
The dummy was seated in a chair and fixed as mentioned above. In these tests the dummy wore a protection jacket and the neck brace tested was the Leatt GPX 6.5 model (Figure 6.5).

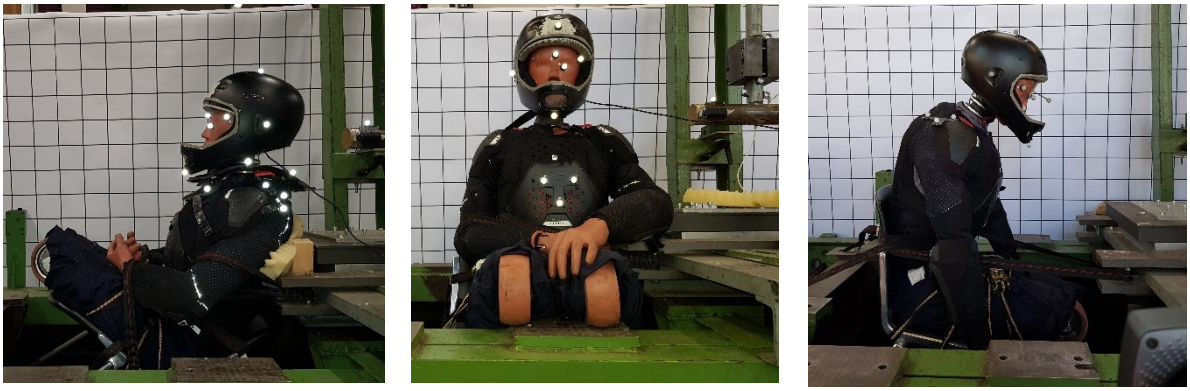

*Back impact* *Side impact* *Front impact*

Figure 6.5: Dummy position for back, side and front impact


Figure 6.6: Leatt GPX 6.5 neck brace model

For each impact scenario three run were performed changing the starting pendulum potential energy.
The potential energies were set acting on the inclination of the pendulum; by placing the pendulum at 45°, 60° and 90° the starting potential energy were respectively 54, 95 and 190 J.

### 6.2.3 First tests session results

Test results are reported below for back and side impact. Results are focused on the neck peak angle as a result of the impact. Data from front impact were not collected since the test was not feasible (the hammer interacted with the helmet mouthguard reducing the maximum excursion of the neck and influencing the test result as shown in figure 6.10).

- **Back impact**

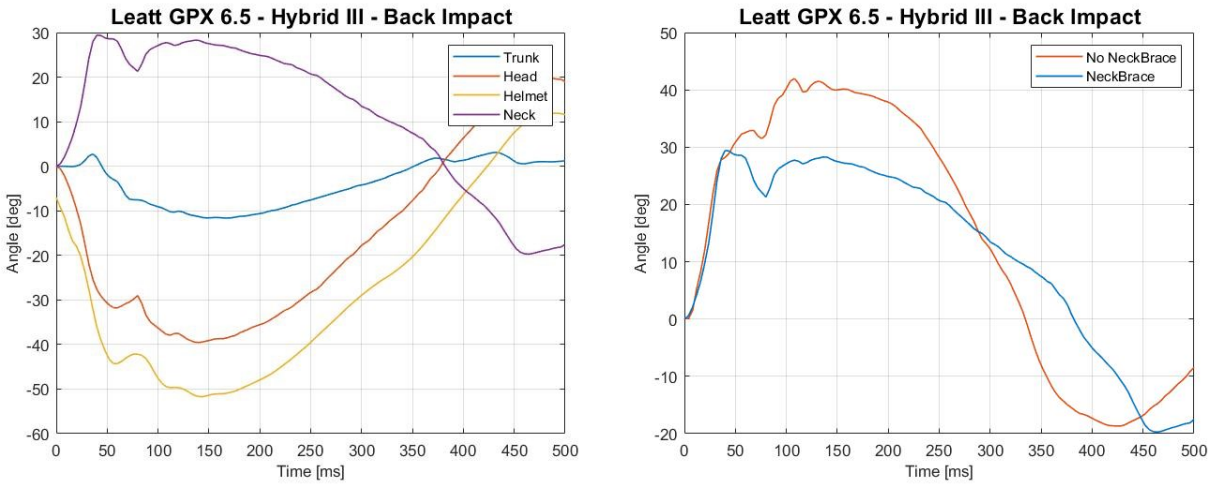


Figure 6.7: On the left example of trend of trunk, head, helmet and neck angles for 60 J back impact energy test with neck brace, on the right the comparison of neck relative angles with and without neck brace for 60 J back impact energy test

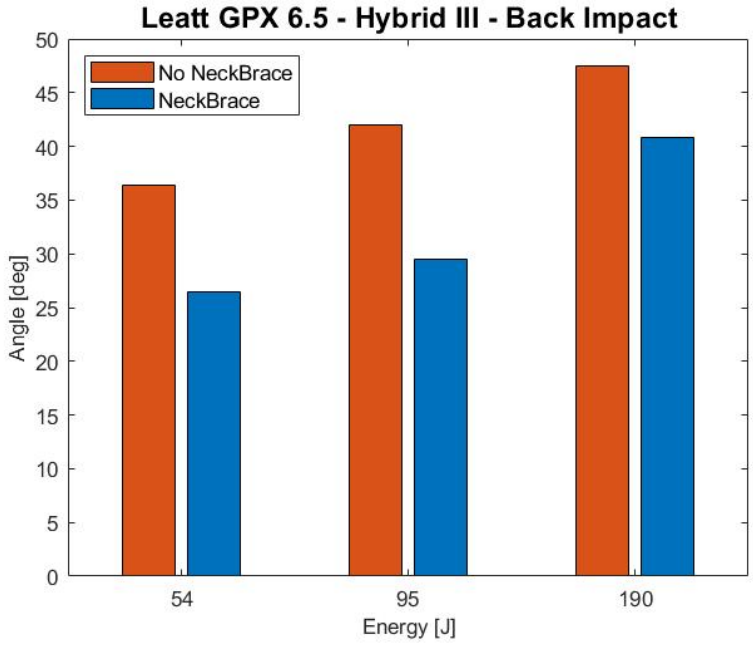


Figure 6.8: Comparison of neck peak angles with and without neck brace for different energies of back impact

| Impact energy [J] | Peak angle [deg] | | |
|---|---|---|---|
| | Without neck brace | With neck brace | Δθ [%] |
| **54** | 36,39 | 26,49 | 27,2 |
| **95** | 41,97 | 29,44 | 29,8 |
| **190** | 47,54 | 40,73 | 14,3 |

Table 6.2: Neck peak angles for back impact

- **Side impact**

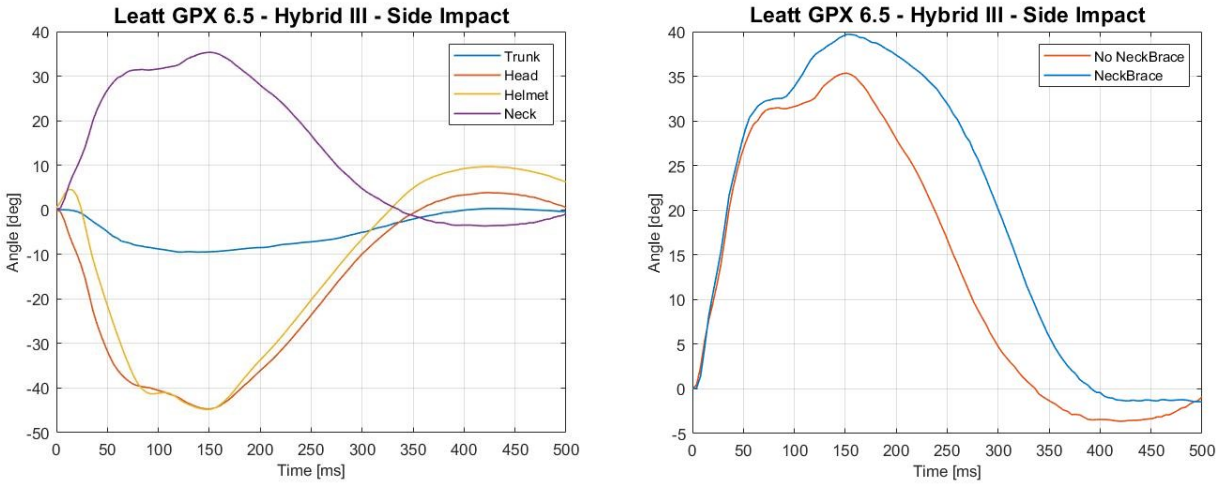


Figure 6.9: On the left example of trend of trunk, head, helmet and neck angles for 60 J side impact energy test with neck brace, on the right the comparison of neck relative angles with and without neck brace for 60 J side impact energy test

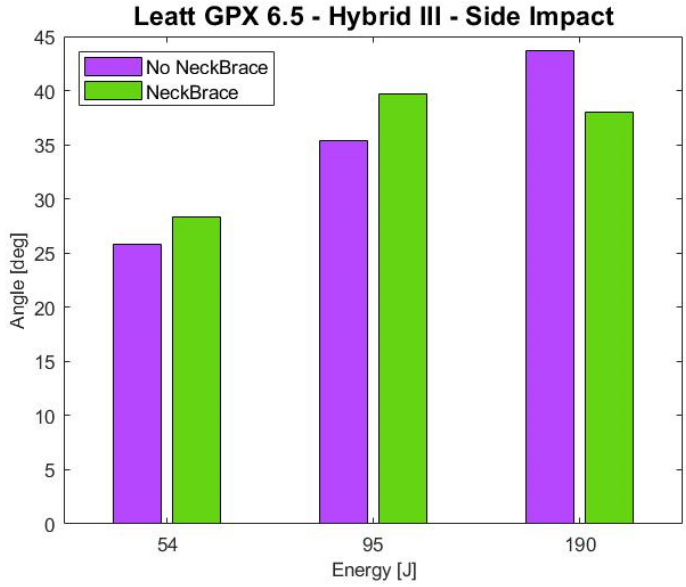


Figure 6.10: Comparison of neck peak angles with and without neck brace for different energies of side impact

| Impact energy [J] | Peak angle [deg] | | |
|---|---|---|---|
| | Without neck brace | With neck brace | Δθ [%] |
| **54** | 25,76 | 28,37 | -10,1 |
| **95** | 35,34 | 39,7 | -12,3 |
| **190** | 43,7 | 38,05 | 12,9 |

Table 6.3: Neck peak angles for side impact

- **Front impact**

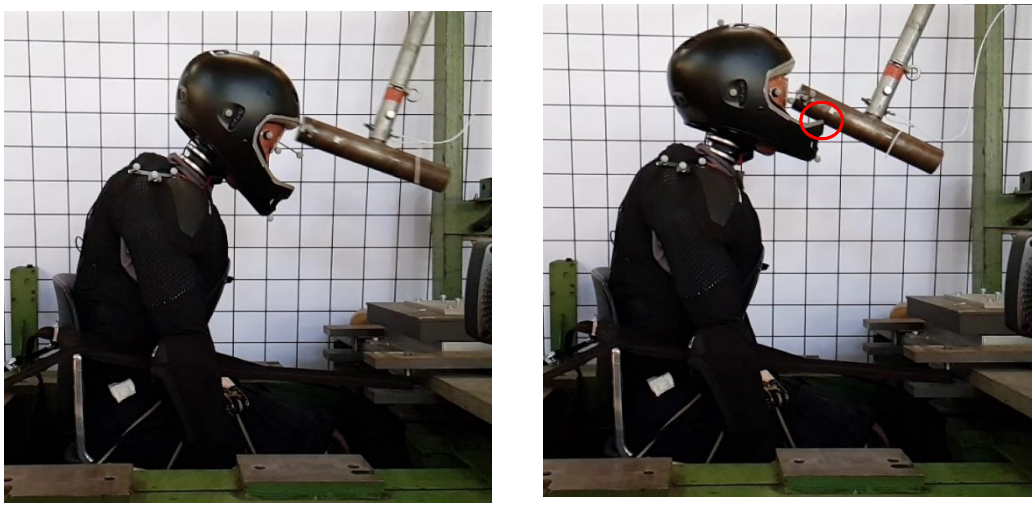

Figure 6.11: On the left the instant before the impact, on the right the interaction between the hammer and helmet after the impact

### 6.2.4 First tests session discussion

Figure 6.6 and 6.8 show different angles between head and helmet, highlighting a relative rotation resulting from the impact.
For this reason, neck relative angles were evaluated considering head absolute angles instead of helmet absolute angles.
Back impacts shown a reduction in the neck peak angle when the neck brace is worn suggesting an effective action of the neck protector. The reduction was maximum for the mid energy impact (29,8%) and decreased in the maximum impact energy (14,3%).
Unexpected results have been obtained for side impacts where the neck brace apparently increased the neck angle for the two lower energy tests while decreased the peak in the maximum energy test (13%); this could be attribute to the upward movement induced by the pendulum to the helmet influencing the contact mechanism between helmet and neck brace.

### 6.2.5 Second tests session with Alpinestar neck brace

In this session another neck brace model was tested.
The neck brace concerned is the BNS Tech 2 manufactured by Alpinestar and shown in figure 6.12.
The helmet used in previous tests was replaced as well in favor of helmet suitable to be use with this neck protector.
Besides, some tweaks have been made to setup.
The chair, in which the Hybrid III dummy was seated, was removed in favor of a simple booster seat that allowed to place the dummy in such a way that the helmet is hit when the pendulum kinetic energy is close to maximum.
In this case the dummy did not wear protective jacket.
Only back impact scenario was investigated since it has produced better results in previous tests.
The impact energies were limited to 50 and 100 J (higher values made the test unfeasible since the hammer tended to move forward passing the helmet after the impact instead of stopping and going back).

Figure 6.12: Improved test setup for back impact

Figure 6.13: BNS Tech 2 neck brace model

### 6.2.6 Second tests session results

Here are reported the results obtained in this test session.

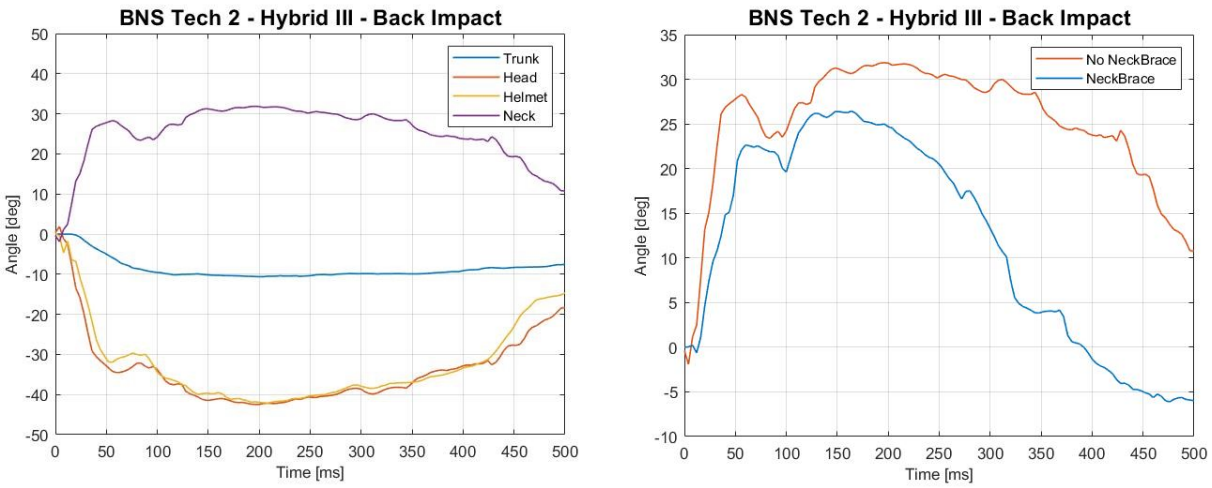


Figure 6.14: On the left example of trend of trunk, head, helmet and neck angles for 100 J impact energy test with neck brace, on the right the comparison of neck relative angles with and without neck brace for 100 J impact energy test

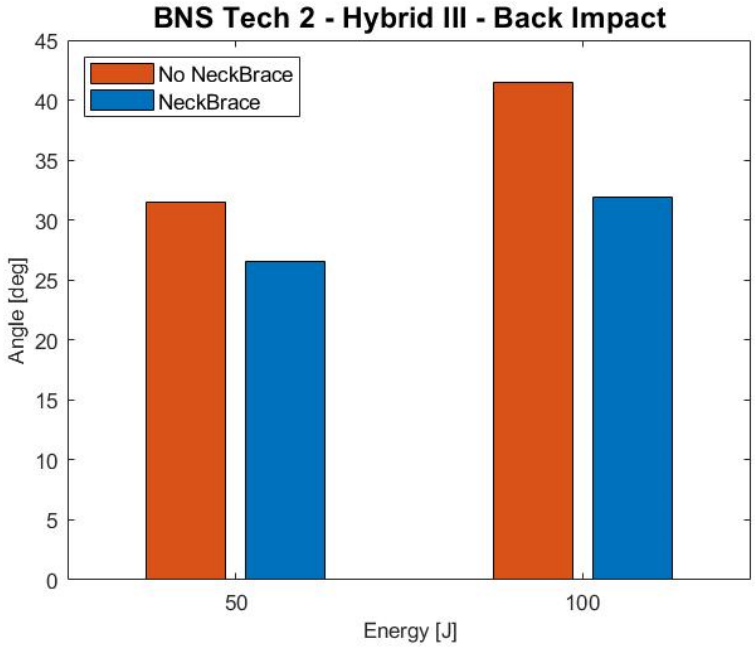


Figure 6.15: Comparison of neck peak angles with and without neck brace for different energies of back impact

| Impact energy [J] | Peak angle [deg] | | |
|---|---|---|---|
| | Without neck brace | With neck brace | Δθ [%] |
| **50** | 31,52 | 26,55 | 15,7 |
| **100** | 41,5 | 31,86 | 23,2 |

Table 6.4: Neck peak angles for back impact

### 6.2.7 Second tests session discussion

Also in this session, a reduction in the neck peak angle when the neck brace is worn was observed. Test conducted at 100 J impact energy presents higher reduction (23%) than test conducted at 50 J impact energy (16%). A comparison between the two neck protectors could not be made since the tests were conducted at different impact energy and with different test setup.

### 6.2.8 Third tests session with the BNP3

Finally, a last session of tests was carried out testing the BNS Tech 2 neck brace with the Hybrid III dummy mounting the new biofidelic neck surrogate developed in this thesis work.

The BNP3 allows to simulate a more realistic interaction between the helmet and the neck protector after a head impact but also to collect data of loads acting on neck as a result of the impact thanks to the six-axis load cell installed.

Moreover, the instrumented base was tested evaluating neck bending angles and making a comparison with the angles evaluated with motion capture system.

The setup used in this session is the same of the previous session with the only addition of the Data Acquisition System (Somat) to collect data from the load cell and the instrumented base implemented in BNP3.

To withstand the weight of helmet and Hybrid III head, “BNP3-OR-FB2L-IC6” neck configuration was used.

Tests were conducted at 10 and 20 J of back impact energy.

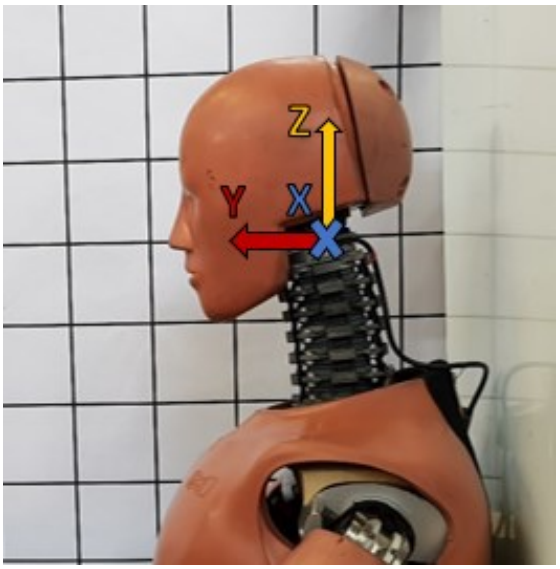


Figure 6.16: Hybrid III dummy with the new neck surrogate BNP3

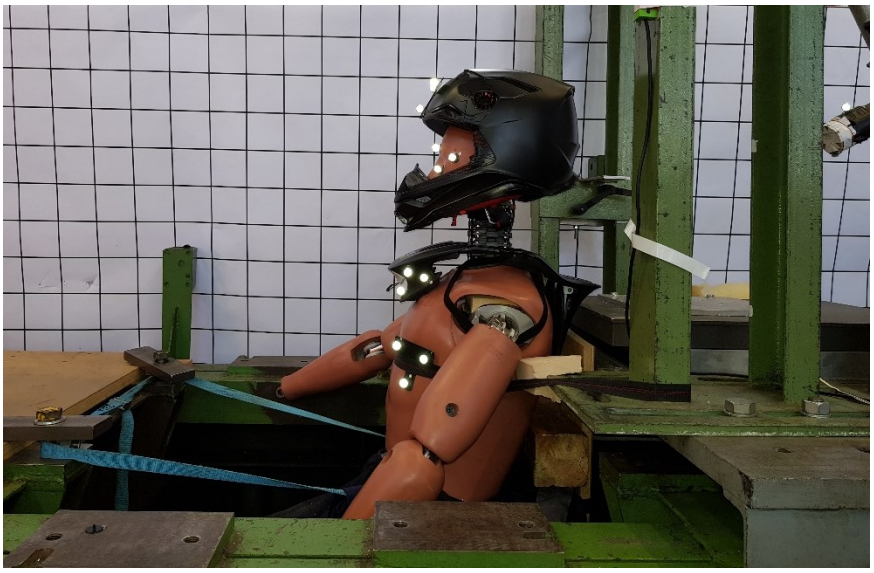

Figure 6.17: Setup for the last test session

### 6.2.9 Third tests session results

Below are reported the results of the last session tests.

Forces and moments reported in figure 6.18 are referred to a reference system integral to the load cell with z axis pointing upward, y axis pointing to left and x axis completing the triad with right hand rule.

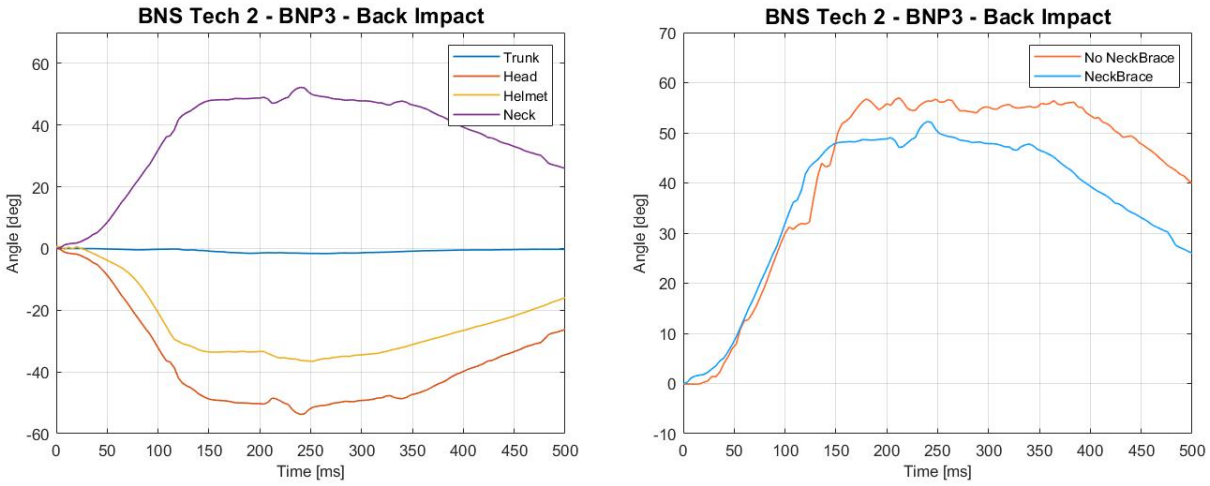


Figure 6.18: On the left example of trend of trunk, head, helmet and neck angles for 10 J impact energy test with neck brace, on the right the comparison of neck relative angles with and without neck brace for 10 J impact energy test

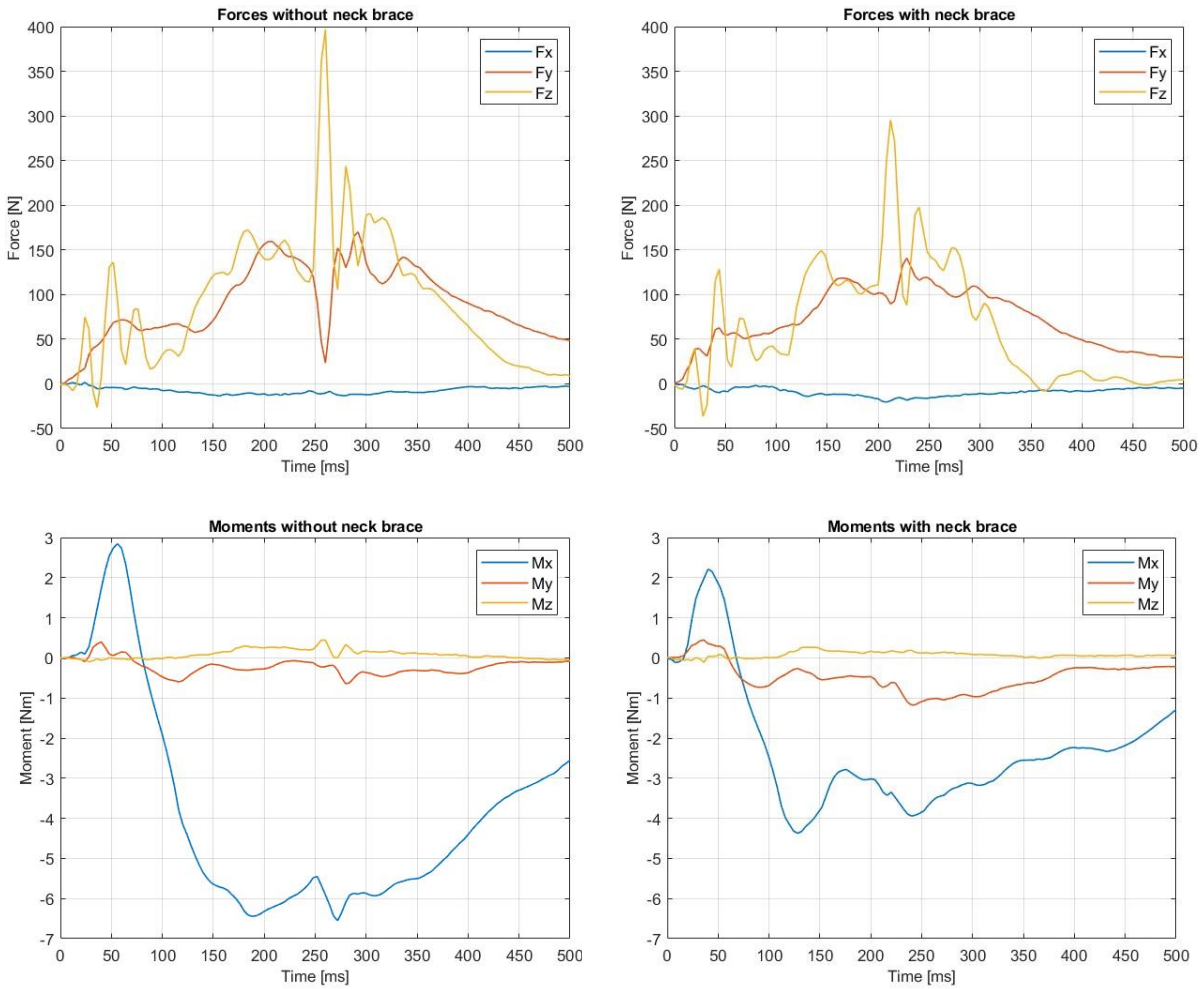


Figure 6.19: On the top, forces acquired by the load cell with and without neck brace for 10 J impact energy; on the bottom, moments acquired by load cell with and without neck brace for 10 J impact energy

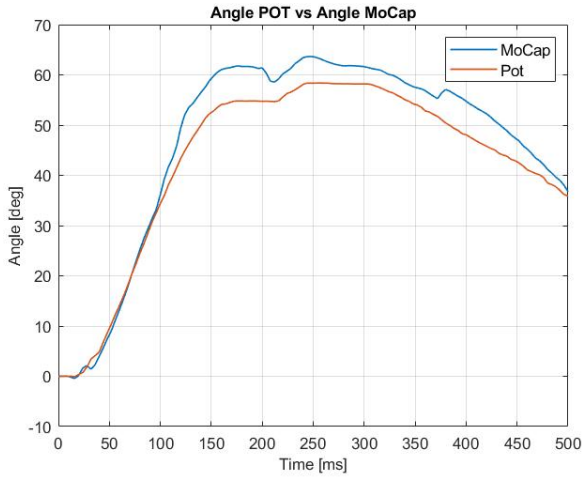


Figure 6.20: Comparison between angles evaluated with the motion capture system and angles evaluated with potentiometers signals

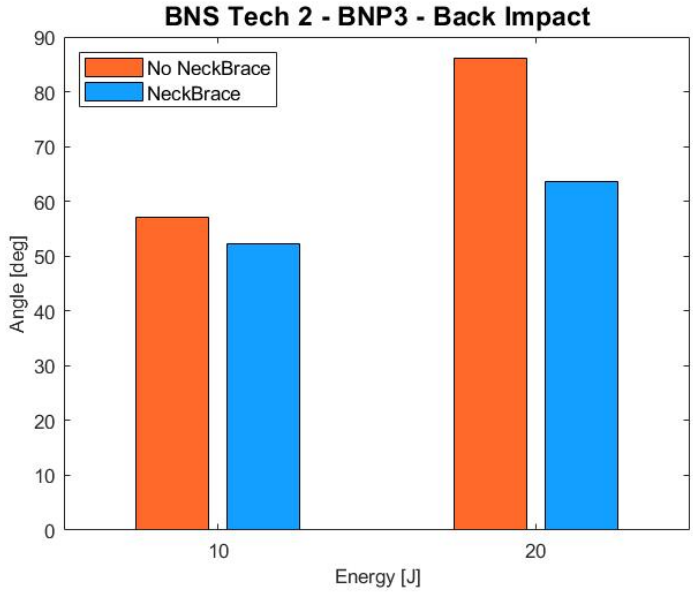


Figure 6.21: Comparison of neck peak angles with and without neck brace for different energies of back impact

| Impact energy [J] | Peak angle [deg] | | |
|---|---|---|---|
| | Without neck brace | With neck brace | $\Delta\theta$ [%] |
| **10** | 56,98 | 52,25 | 8,3 |
| **20** | 86,13 | 63,66 | 26 |

Table 6.5: Neck peak angles for back impact with BNP3 neck

### 6.2.10 Third tests session discussion

These results highlight how with a more biofidelic neck surrogate higher peak angles are reached with respect to the previous tests with the Hybrid III neck despite the lower energies impact at work (figure 6.21). It is also important to observe that the angles reached are close to the limit of 64° imposed for neck flexion.
The Hybrid III neck proves to be too stiff in fact it requires very high energies to reach a range of motion that engage the neck brace.
Peak angle of 86,13°, obtained in 20 J impact energy test without neck brace derives from a failure of the Inner cable and it should not be considered as a significative result but it was reported for the sake of completeness also to underline the fact that with neck brace the failure did not occur.
Figure 6.18 shows in fact that the force Fz, which is the tensile force that cause the failure of the cable, is reduced when the neck brace is worn; the same thing can be observed for Mx moment.
In general forces and moments values collected by the load cell are far from the limit loads that can cause neck injuries suggesting the need to perform tests with higher impact energies.
Unfortunately, the failure of the Inner cable establishes the limit of the new neck prototype which cannot be tested at higher energies impact.

A thicker Inner cable is needed to perform high energy impact tests, a thicker cable will also make the neck stiffer enough to make the system more stable (with the current neck configuration the system was unstable with the head and helmet supported by the neck only for precise positions of equilibrium).
As regards the instrumented base, figure 6.19 shows that the instrumented base underestimate the angles for high bending movements of the neck as already observed during the calibration procedure but it is still an encouraging result for the evaluation of neck angles without having to use a motion capture system which is high time demanding in terms of calibration procedure and needs a controlled environment to be feasible.

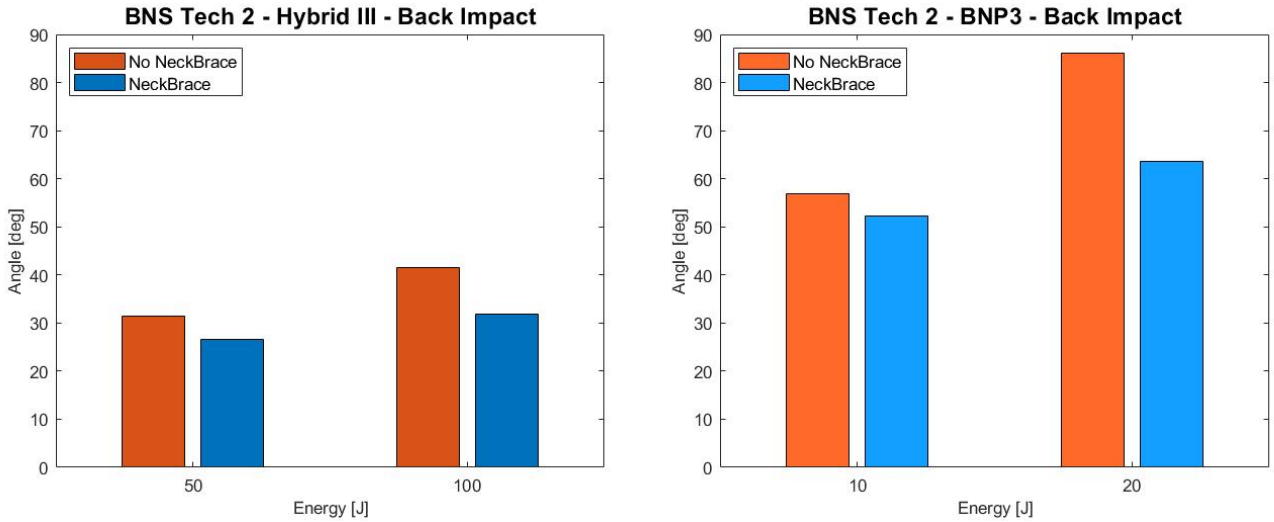


Figure 6.22: Comparison between tests conducted with Hybrid III neck and tests conducted with BNP3 neck

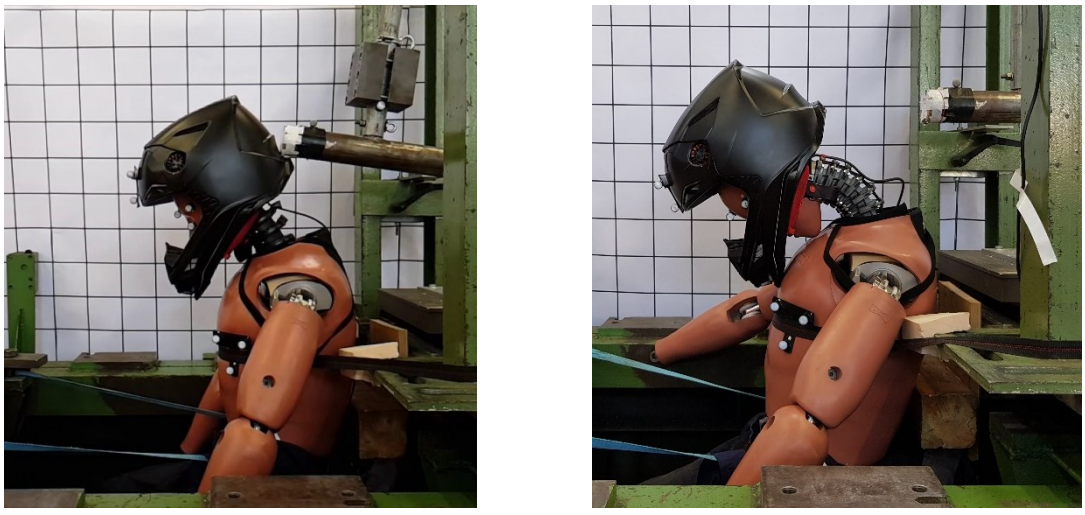

Figure 6.23: On the left the Hybrid III dummy with Hybrid III neck after being hit with 50 J of impact energy without neck brace, on the right the Hybrid III dummy with BNP3 neck after being hit with 20 J of impact energy without neck brace

It is clear that to perform meaningful tests a more robust neck is needed.
The BNP3 needs to be improved in terms of mechanical strength.
It's important to stress out that the Hybrid III dummy was used for the preliminary study of the test method.
Hybrid III shoulders and chin anthropometric features did not allow a proper fitting of the neck protector and fastening of the helmet which seems almost untied in figure 6.23.
A more biofidelic torso should be developed for a more correct evaluation of this personal protective device.
Despite that, the tests performed in this last session are a good starting point for future tests.
Test setup needs to be improved as well; an improved setup will allow to investigate different impact scenarios like side impacts and front impacts to have a more complete evaluation of neck braces functionality.

# CHAPTER 7

## 7 CONCLUSIONS

Neck braces are personal protective devices developed to prevent neck injuries.
The need to test these devices has led to the development of biofidelic neck surrogates to simulate a real interaction between the helmet and the neck brace after a head impact.
The University of Padua, in collaboration with the University of Mid-Sweden, has been developing a neck surrogate which has been constantly updated over the last few years
In this thesis work the new version this biofidelic neck surrogate has been develeped.
This new prototype aimed to improve the critical aspects of the previous necks surrogates in order to create a more biofidelic and more robust neck.
Starting from the first design proposed by Rango M. in a previous work, a first prototyping of the neck was made.
A deep characterization of the neck was done, performing static and dynamic tests to evaluate the mechanical properties.
Many configurations of the neck were investigated considering the stiffening components adopted to provide a modular stiffness to the neck.
Static flexion tests were performed to evaluate the behavior of the BNP3 in static flexion in order to have a comparison with the previous surrogates and to check how far is this new prototype from biofidelity.
The base configuration of the neck was shown to be similar to the previous prototype in terms of flexural stiffness and therefore this neck surrogate is still far from faithfully replicate the human neck behavior.
Damping tests were done to evaluate the damping property but also to evaluate the neck stiffness in bending and in torsion from a dynamic point of view.
This new neck surrogate was able to withstand dynamic tests without breaking down proving to be more resilient than the previous version. From these dynamic tests it was possible to define a dynamic stiffness of the neck in the sagittal plane.
A second goal of this work was the instrumentation of the new neck surrogate to measure bending movements and loads acting on the neck.
A redesign of some components of the first prototype allowed the employment of sensors in the neck.
Now a six-axis load cell can be installed between the upper vertebra and the nodding joint to measure loads that act at the Occipital condyles level.
The development of a device for the evaluation of the neck bending angles was a tough challenge.
Our efforts have led to the realization of the instrumented base. Initially designed to make the neck suitable to the assembly on the Hybrid III torso, it was exploit for the insertion of rotary potentiometers that allowed the evaluation of neck bending angles about frontal and sagittal plane.
Finally, pilot tests for the assessment of neck protectors were conducted using a pendulum to hit the helmeted Hybrid III dummy on the head.
Three sessions of tests were carried changing the setup and investigating different impact scenario to improve the method feasibility.

Final tests were conducted with both Hybrid III neck and the new more biofidelic neck surrogate to compare results.
Despite the experimental setup shown some criticalities, the results highlight the limits in using a very stiff neck surrogate like the Hybrid III neck to test neck braces and the need to use a more flexible and biofidelic neck surrogate instead.

## 7.1 FUTURE DEVELOPMENTS

Further developments of this study are proposed below.

Biofidelic neck surrogate:

- The BNP3 needs to be improved in terms of mechanical strength to perform significant impact tests. Plastic components of the current prototype could be made in aluminum to rise the overall structural strength.
- The biofidelity of the neck could be improved with a deeper investigation on the stiffening components adopted in this work by testing the neck in lateral bending, extension and torsion with non-symmetric configurations of the O-Rings.
- Test alternative solution to O-Rings.
- To improve the instrumented base by defining an algorithm to evaluate the neck bending angles on different planes.
- To implement a sensor to evaluate torsional neck angles.
- To increase the biofidelity of the neck with a solution that implements the Neutral Zone.
- To find a mechanical solution to reproduce the muscular system of the neck.
- To replicate the facets joint function.

Test method for the assessment of neck protectors:

- To improve the impact test setup to carry out different impact scenario.
- Test several models of neck brace.
- To investigate the helmet model influence on the neck braces effectiveness.
- To explore other method to test neck braces, taking advantage of servohydraulic cylinders or full dummy drop tests on traphole.

# APPENDIX

## PRODUCTS DATASHEETS

SCHEDA TECNICA MESCOLA 0170/1

MESCOLA: 0170 NBR 70 Nero MF 000601

CONDIZIONI DI VULCANIZZAZIONE:

Placchette 2 mm: 15' 160 °C Placchette 6 mm: 25' 160 °C

Tamboli 29 X 13: 30' 160 °C Post-cure: no

CAPITOLATO:

ASTM D 2000 M2 BG 714 A14 B14 E014 E034 F15 Z1=70h 100°C IRM903 d V=+/-10% Z2=70h 100°C acqua dV=+/-5

| | Norma | Unità | Richiesto | Misurato |
|---|---|---|---|---|
| **PROPRIETA' INIZIALI** | | | | |
| Durezza | ASTM D 2240 | SHA | 70 -3/+3 | 70,00 |
| Durezza | ISO 48 | IRHD | 70 -3/+3 | 70,00 |
| Densità | ASTM D 297 | GR/CM3 | 1,23 -0,02/+0,02 | 1,23 |
| Carico di rottura | ASTM D 412 C | MPA | > 14 | 16,20 |
| Allungamento a rottura | ASTM D 412 C | % | > 250 | 341,00 |
| Carico a lacerazione | ASTM D 624 B | KN/M | > 40 | 48,50 |
| Brittle point | ASTM D 2137 A | °C | < -25 | -26,60 |
| Tg midpoint | VDA 675 216 A | °C | < -20 | -24,00 |
| **COMPRESSION SET** | | | | |
| 22 h 100 °C | ASTM D 395 B | % | < 25 | 12,90 |
| **INVECCHIAMENTO IN acqua 70 h 100 °C** | | | | |
| Var Durezza | ASTM D 471 | SHA | -10 / 10 | -0,80 |
| Var Volume | ASTM D 471 | % | -5 / 5 | 2,60 |
| **INVECCHIAMENTO IN aria 70 h 100 °C** | | | | |
| Var Durezza | ASTM D 573 | SHA | < 15 | 5,80 |
| Var Carico rottura | ASTM D 573 | % | > -20 | 6,40 |
| Var Allungamento | ASTM D 573 | % | > -40 | -25,20 |
| **INVECCHIAMENTO IN ASTM 1 70 h 100 °C** | | | | |
| Var Durezza | ASTM D 471 | SHA | -5 / 10 | 3,50 |
| Var Carico rottura | ASTM D 471 | % | > -25 | 4,10 |
| Var Allungamento | ASTM D 471 | % | > -45 | -21,20 |
| Var Volume | ASTM D 471 | % | -10 / 5 | -5,40 |
| **INVECCHIAMENTO IN Fuel A 70 h 23 °C** | | | | |
| Var Durezza | ASTM D 471 | SHA | -10 / 10 | -2,20 |
| Var Carico rottura | ASTM D 471 | % | > -25 | -10,80 |
| Var Allungamento | ASTM D 471 | % | > -25 | -10,20 |
| Var Volume | ASTM D 471 | % | -5 / 10 | 3,60 |
| **INVECCHIAMENTO IN Fuel B 70 h 23 °C** | | | | |
| Var Durezza | ASTM D 471 | SHA | -30 / 0 | -14,40 |

% Segue

Figure A 1: O-Ring datasheet

## SCHEDA TECNICA MESCOLA 0170/1

MESCOLA: 0170 NBR 70 Nero MF 000601

CONDIZIONI DI VULCANIZZAZIONE:

Placchette 2 mm: 15' 160 °C Placchette 6 mm: 25' 160 °C

Tomboli 29 X 13: 30' 160 °C Post-cure: no

CAPITOLATO:

ASTM D 2000 M2 BG 714 A14 B14 EO14 EO34 F15 Z1=70h 100°C IRM903 d V=+/-10% Z2=70h 100°C acqua dV=+/-5

| | Norma | Unità | Richiesto | Misurato |
|---|---|---|---|---|
| **INVECCHIAMENTO IN Fuel B 70 h 23 °C** | | | | |
| Var Carico rottura | ASTM D 471 | % | > -60 | -52,30 |
| Var Allungamento | ASTM D 471 | % | > -60 | -39,30 |
| Var Volume | ASTM D 471 | % | 0 / 40 | 31,90 |
| **INVECCHIAMENTO IN IRM 903 70 h 100 °C** | | | | |
| Var Durezza | ASTM D 471 | SHA | -10 / 5 | -2,10 |
| Var Carico rottura | ASTM D 471 | % | > -45 | -5,40 |
| Var Allungamento | ASTM D 471 | % | > -45 | -15,40 |
| Var Volume | ASTM D 471 | % | -10 / 10 | 5,00 |

Note:

Figure A 2: O-Ring datasheet

# Rotary Position Sensors

## SMD/Lead Dust-proof Type 12mm Size SV01 Series

### Features

1. Excellent resistance materials and high reliability wiper achieves 1M cycles.
2. D formation thru-hole rotor enables selection of any kind of gear shape.
3. Ultra-thin size (2.1mm height)
4. Au plated terminals.
5. Operating Temperature: -40°C to +85°C
6. RoHS Compliant

SV01A

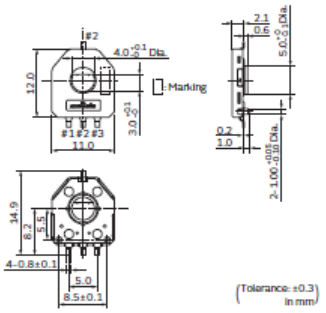


### Applications

1. Switch for white goods
2. Digital still camera
3. Switch for automotive
4. Car audio
5. Multi-function printer
6. Robot
7. Motor drive unit

| Part Number | Total Resistance Value (k ohm) | Linearity (%) | Effective Rotational Angle | Rotational Torque | Rotational Life | Rated Voltage |
|---|---|---|---|---|---|---|
| **SV01A103AEA01** | 10 ±30% | ±2 | 333.3° (Ref.) | 2mN.m (Ref.:21gf.cm) | 1M cycles | 5Vdc |

### Construction

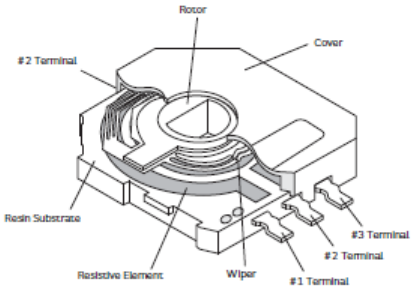


Figure A 3: Rotary potentiometer datasheet

## Standard Land Pattern

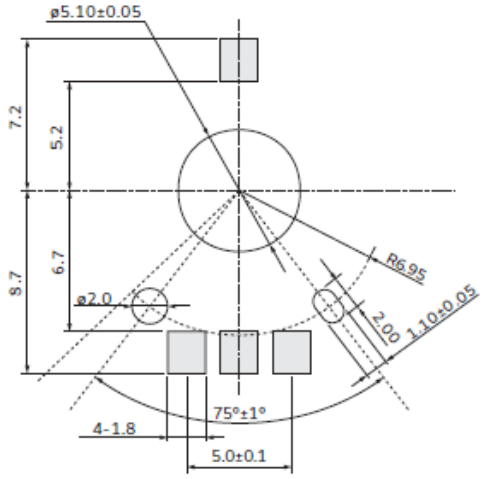


(Tolerance: ±0.1 In mm)

## Characteristics

| | |
|---|---|
| Temperature Cycle (Thermal Shock) | ΔTR : ±20%<br>Linearity: ±3% |
| Humidity | ΔTR : ±20%<br>Linearity: ±3% |
| Vibration | ΔTR : ±10%<br>Linearity: ±3% |
| Shock | ΔTR : ±10%<br>Linearity: ±3% |
| Humidity Load Life | ΔTR : ±20%<br>Linearity: ±3% |
| High Temperature Exposure | ΔTR : +5/-30%<br>Linearity: ±3% |
| Low Temperature Exposure | ΔTR : ±20%<br>Linearity: ±3% |
| Rotational Life | ΔTR : ±20%<br>Linearity: ±3% |

ΔTR: Total Resistance Change

Figure A 4: Rotary potentiometer datasheet

## SV01 Series Specifications and Test Methods

Tests and measurements should be conducted under the conditions of 15 to 35°C of temperature, 25 to 75% of relative humidity, and 86 to 106 kpa of atmospheric pressure unless otherwise specified. If questionable results occur that have been measured in accordance with the above-mentioned conditions, the tests and measurements should be conducted under the conditions of 25±2°C of temperature, 45 to 55% of relative humidity, and 86 to 106 kpa of atmospheric pressure. When the potentiometer is tested after soldering on PCB, it should be tested after being kept in a room (15 to 35°C, 25 to 75%RH) over 24 hours except "Resistance to soldering heat."

<table>
<tr><th>No.</th><th>Item</th><th>Test Methods</th></tr>
<tr><td>1</td><td>Linearity</td><td>Linearity should be specified a deviation with the below ideal straight line, between ±160° from the index point, which is 50% of output voltage.<br>The ideal straight line has 100%/333.3° as taper and pass the above index point.<br>Measurement is performed using the following measurement circuit, and the rotor should be rotated in a clockwise direction.<br> 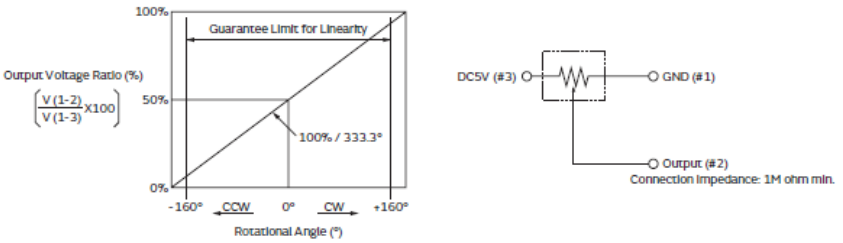
</td></tr>
<tr><td>2</td><td>Temperature Cycle (Thermal Shock)</td><td>The rotary position sensor should be subjected to Table 1 temperature for 5 cycles.<br>Then, the rotary position sensor should be kept in a dry box for 24 +8/-0 hrs.
<table>
<tr><th>Sequence</th><th>1</th><th>2</th><th>3</th><th>4</th></tr>
<tr><td>Temperature (°C)</td><td>-40±3</td><td>+25±2</td><td>+85±3</td><td>+25±2</td></tr>
<tr><td>Time (min.)</td><td>30</td><td>5 max.</td><td>30</td><td>5 max.</td></tr>
</table>
Table 1: One cycle of temperature cycle</td></tr>
<tr><td>3</td><td>Humidity</td><td>The rotary position sensor should be stored in a chamber at temperature of +60±2°C and relative humidity of 90-95% for 250±8 hrs. After removing from the chamber, the rotary position sensor should be kept in a dry box for 24 +8/-0 hours.</td></tr>
<tr><td>4</td><td>Vibration</td><td>The rotary position sensor should be tested under the condition of the amplitude of 1.5mm, the frequency range from 10 to 55Hz (should be traversed in approximately one minute) and 2 hours in each of 3 mutually perpendicular directions (total 6 hours). Then, the rotary position sensor should be kept in a dry box for 1-2 hrs.</td></tr>
<tr><td>5</td><td>Shock</td><td>The rotary position sensor should be tested under the condition of the peak acceleration 20G max. in half-sine wave and 5 shocks in each of 3 mutually perpendicular directions (total 15 shocks). Then, the rotary position sensor should be kept in a dry box for 1-2 hrs.</td></tr>
<tr><td>6</td><td>Humidity Load Life</td><td>Full rated continuous working voltage not exceeding 5Vdc should be applied intermittently between terminal #1 and terminal #3 of the rotary position sensor, 1.5 hours on and 0.5 hours off, for 96±4 hours in total in a chamber at a temperature of +40±2°C and relative humidity of 90-95%. After removing from the chamber, the rotary position sensor should be kept in a dry box for 24 +8/-0 hours.</td></tr>
<tr><td>7</td><td>High Temp. Exposure</td><td>The rotary position sensor should be stored in a chamber at the temperature of +85±3°C without loading for 250±8 hours. After removing from the chamber, the rotary position sensor should be kept in a dry box for 24 +8/-0 hours.</td></tr>
<tr><td>8</td><td>Low Temp. Exposure</td><td>The rotary position sensor should be stored in a chamber at the temperature of -40±3°C without loading for 168±4 hours. After removing from the chamber, the rotary position sensor should be kept in a dry box for 24 +8/-0 hours.</td></tr>
<tr><td>9</td><td>Rotational Life</td><td>The adjustment rotor should be continuously rotated within ±160° of effective electrical rotational angle, at the rate of one cycle for 6 seconds for 1 Million cycles under the condition of +25±2°C of temperature without loading.</td></tr>
</table>

Figure A 5: Rotary potentiometer datasheet

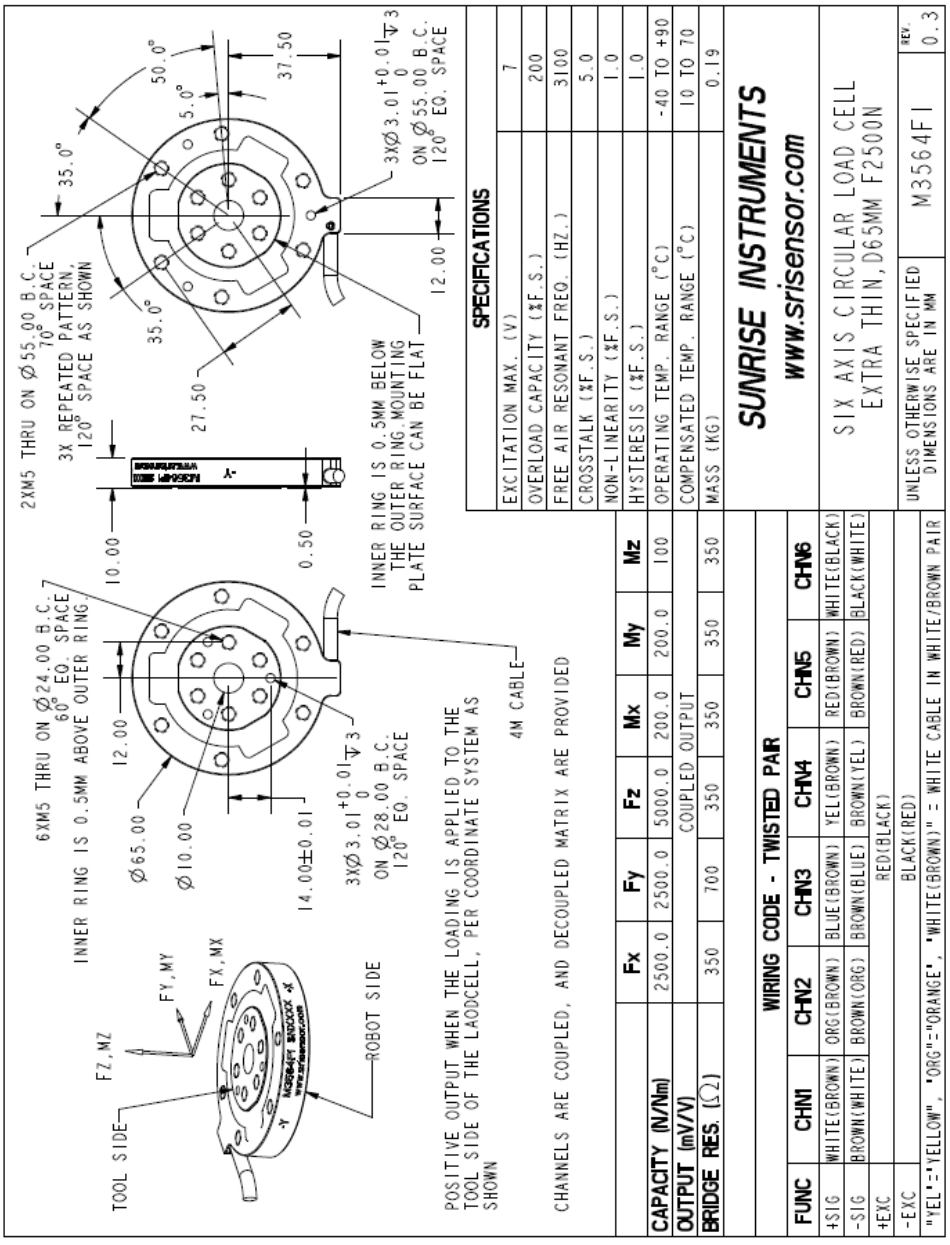


Figure A 6: Sunrise load cell

# RIASSUNTO IN ITALIANO

Le lesioni al collo a seguito di incidenti in moto sono un problema ricorrente.
Per prevenire il rischio di lesione, le aziende hanno iniziato a sviluppare dispositivi specifici per la protezione del collo.
I protettori per il collo fanno parte dei dispositivi di protezione personale progettati per ridurre la possibilità di lesione del collo limitando il suo movimento e riducendo i carichi a cui è sottoposto.
Tuttavia, l'efficacia di questi dispositivi è ancora oggi messa in discussione in quanto non è stato ancora definito un metodo standard per testarli.
Questo lavoro di tesi si focalizza sulla prototipazione e validazione di un surrogato di collo biofedele sensorizzato per la valutazione dei protettori del collo.
I componenti del nuovo collo biofedele sono stati ottenuti attraverso la tecnologia additiva Selective Laser Sintering (SLS) e le vertebre sono state realizzate colando una gomma siliconica nei componenti mediante l'utilizzo di uno stampo.
La rigidezza del collo può essere modulata con componenti di irrigidimento.
Sono stati eseguiti test statici e dinamici per valutare le proprietà meccaniche del nuovo collo e i risultati sono stati confrontati (quando possibile) con quelli ottenuti con i prototipi precedenti.
Un secondo obbiettivo di questo lavoro è stata la sensorizzazione del collo per misurare gli angoli di movimento e i carichi che agiscono su di esso.
Una cella di carico a sei assi è stata installata in cima al collo per misurare i carichi a livello dei condili occipitali.
É stata progettata una base sensorizzata per misurare gli angoli di piegamento del collo lungo il piano frontale e sagittale, inoltre questa base permette il fissaggio del collo sul busto del manichino Hybrid III.
Infine, sono stati eseguiti dei test di prova per valutare l'efficacia dei protettori per il collo.
Per eseguire le prove è stato utilizzato un pendolo per colpire la testa del manichino Hybrid III provocando la flessione del collo.
I test sono stati svolti con due diversi tipi di surrogati del collo: il rigido collo Hybrid III e il collo biofedele sensorizzato sviluppato in questa tesi.
Per confrontare i risultati dei test condotti con e senza protettore e con i due diversi surrogati del collo sono stati considerati gli angoli di picco raggiungi dal collo a seguito dell'impatto.
I risultati hanno evidenziato che le prove eseguite con il collo Hybrid III richiedono energie di impatto molto elevate per raggiungere angoli di flessione tali da impegnare il protettore, mentre le prove eseguite con il collo biofedele richiedono energie di impatto molto più basse.
Tuttavia, il collo biofedele si è dimostrato ancora troppo fragile per poter eseguire test d'impatto significativi.
Sviluppi futuri miglioreranno il prototipo realizzato in termini di biofedeltà e resistenza strutturale e ulteriori metodi di prova per testare i protettori per il collo saranno proposti.

# BIBLIOGRAPHY


[1] N. Yoganandan, F. Pintar, M. Haffner, J. Jentzen, D. Mainma, S. Weinshel, S. Larson, H. Nichols and A. Sances, "Epidemiology and Injury Biomechanics of Motor Vehicle Related Trauma to the Human Spine.," *Proceedings from the 33rd Stapp Car Crash Conference,* pp. 223-242, 1989.

[2] T. Pang, R. Radin Uma, A. Azhar and S. Harwant, "Fatal injuries in Malaysian motorcyclists," *International Medical Research Journal,* pp. 115-19, 1999.

[3] S. Ooi, S. Wong, R. Radin Umar, A. Azhar and M. ,. A. Megat, "Cervical spine injuries sustained by motorcyclists in road crashes in Malaysia," *International Journal of Crashworthiness,* p. 295–303, 2005.

[4] F. Shuaeib, A. Hamouda, R. R. Umar, M. Hamdan and M. Hashmi, "Motorcycle helmet-Part I: Biomechanics and computational issues," *Materials Processing Technology,* vol. 123, pp. 406-421, 2002.

[5] F. Shuaeib, A. Hamouda, M. Hamdan, R. R. Umar and M. Hashmi, "Motorcycle helmet-Part II: Materials and design issues," *Materials Processing Technology,* vol. 123, pp. 422-431, 2002.

[6] F. Fernandes and R. A. d. Sousa, "Motorcycle helmets-A state of art review," *Accident Analysis and Prevention,* vol. 56, pp. 1-21, 2013.

[7] M. Ghajari, S. Peldschus, U. Galvanetto and L. Iannucci, "Evaluation of the Effective Mass of the Body for Helmet Impacts," *International Journal of Crashworthiness,* vol. 16, pp. 621-631, 2011.

[8] A. Cernicchi, U. Galvanetto and L. Iannucci, "Virtual modelling of safety helmets: Practical problems," *International Journal of Crashworthiness,* vol. 13, pp. 451-467, 2008.

[9] B. Dowdell, G. Long, J. Ward and M. Griffiths, "A Study of Helmet Damage and Rider Head/Neck Injuries for Crash Involved Motorcyclists," *Road Safety Research Note 5/88,,* 1988.

[10] R. Ramlia, J. Oxleyc, F. Noord, N. Abdullahe, M. Mahmoode, A. Tajuddinf and R. McClure, "Fatal injuries among motorcyclists in Klang Valley, Malaysia," *Forensic & Legal Med,* vol. 26, pp. 39-45, 2014.

[11] J. Ouellet, D. Thom, T. Smith and H. Hurt, "Helmets and Neck Injuries in Fatal Motorcycle Crashes," in *International Motorcycle Safety Conference*, Orange County, 2013.

[12] M. Nasim, "Neck Protection Development and a Proposal of the Associated Standard for the Motorcyclists," 2018.

[13] S. V. Kushchayev, T. Glushko, M. Jarraya, K. H. Schuleri, M. C. Preul, M. L. Brooks and O. M. Teytelboym, "abcs of the degenerative spine," 2018.

[14] M. Panjabi, V. Goel and K. Takata, "Physiologic strains in the lumbar spinal ligaments. An in vitro biomechanical study 1981 Volvo Award in Biomechanics," *Spine,* vol. 7, pp. 192-203, 1982.

[15] H. Frank, S. Hendrik, K. Zdenek, C. Lutz and W. Hans-Joachim, "Stepwise reduction of functional spinal structures increase range of motion and change lordosis angle," *Journal of Biomechanics,* vol. 40, pp. 271-280, 2007.

[16] B. A. WINKELSTEIN and B. S. MYERS, "The biomechanics of cervical spine injury and implications for injury prevention," *Medicine & Science in Sports & Exercise,* vol. 29, pp. 246-255, 1997.

[17] R. Aranda, C. Deck, F. Meyer, W. Wei and R. Willinger, "Report on injury risk assessment procedures," PIONEERS, 2020.

[18] O. Boström, M. Svensson, B. Aldman, H. Hansson, Y. Häland, P. Lövsund, T. Seeman, A. Suneson, A. Säljö and T. Örtengren, "A NEW NECK INJURY CRITERION CANDIDATEBASED ON INJURY FINDINGS IN THE CERVICAL SPINAL GANGLIA AFTER EXPERIMENTAL NECK EXTENSION TRAUMA," in *Proceedings of the International Conference on the Biomechanics of Impact*, Dublin, 1996.

[19] C. R. ‘. Bass, L. Donnellan, R. Salzar, S. Lucas, B. Folk, M. Davis, K. Rafaels, C. Planchak, K. M. Ziemba and Adam, "A New Neck Injury Criterion in Combined Vertical/Frontal Crashes with Head Supported Mass," in *IRCOBI Conference*, Madrid (Spain), 2006.

[20] R. White, I. Kaleps and J. Whitestone, "Measurement of Hybrid III Dummy and Analytical Simulation Data Base Development," in *Armstrong Aerospace Medical Research Laboratory*, Ohio, 1988.

[21] E. Spittle, D. Miller and B. Shipley, "Hybrid II and Hybrid III Dummy Neck Properties for Computer Modeling," Interim Report, Ohio, 1992.

[22] D. J. Baughn, E. K. Spittle and G. Thompson, "a new technique for determining bending stiffness of mechanical necks," 1993.

[23] R. Nightingale, C. Chancey and D. Ottaviano, "Flexion and extension structural properties and strengths for male cervical spine segments," Duke University, 2007.

[24] R. Nightingale, A. Winkelstein and K. Knaub, "Comparative strengths and structural properties of the upper and lower cervical spine in flexion and extension," Duke University, 2002.

[25] M. Ogle, "Development and Validation of a Surrogate Mechanical Neck Prototype for use in Helmet Certification Applications," Department of Mechanical Engineering, University of Alberta, 2018.

[26] N. Tim S. and C. Peter A., "A New Biofidelic Sagittal Plane Surrogate Neck for Head-First Impacts," university of British Columbia, Canada, 2010.

[27] G. Fonseca, "Development of a Functional Spinal Unit for Evaluation of Sports and Automotive Protective Equipment," University of British Columbia, Canada, 2019/2020.

[28] A. M. and G. F., "Computational Design of a Dummy Neck for Head-First Impacts," Conference speech, BioMedIng, 2018.

[29] M. Abayazid and F. Ghajariand, "https://patentscope.wipo.int.," 2019. [Online].

[30] L. Marin, "Development of a biofidelic neck surrogate," Master Thesis, University of Padova, 2019.

[31] L. Riello, "Improvement of head and neck surrogates with sensor systems for the experimental investigation of traumatic brain injuries," Master Thesis, University of Padova, 2020.

[32] M. Rango, "Static and dynamic characterization of innovative biofidelic neck surrogates for head and neck impact testing," Master Thesis, University of Padova, 2020.

[33] "”http://www.matweb.com/search/propertysearch.aspx”," [Online].

[34] "https://en.wiktionary.org/wiki/Frankfurt_plane," [Online].

[35] N. Roger W., W. Beth A., K. Kurt E., R. William J., L. Jason F. and M. Barry S., "Comparative strengths and structural properties of the upper and lower cervical spine in flexion and extension," *Journal of Biomechanics,* vol. 35, pp. 725-732, 2002.

[36] M. M. Panjabi, J. J. Crisco, T. Oda, J. Cholewicki, K. Nibu and E. Shin, "Mechanical Properties of the Human Cervical Spine as Shown by Three-Dimensional Load–Displacement Curves," *Spine,* vol. 26, pp. 2692-2700, 2001.

[37] K. S. Saladin, Human Anatomy, McGraw-Hill, 2008.

[38] "https://www.nhtsa.gov/road-safety/motorcycles," [Online].